University of Innsbruck
Department for Experimental Physics
Photonics Group

Master Thesis

Parametric scattering in microcavities

Author:
Lukas Einkemmer

Advisors:
Dr. Gregor Weihs
Dr. Zoltán Vörös

Submitted to the Faculty of Mathematics, Computer Science and Physics of the University of Innsbruck
in partial fulfillment of the requirements for the degree of Master of Science.

March 10, 2013

Contents

1 Introduction

The study of excitons in quantum wells (i.e. in systems where the excitons are confined in single dimension) is well developed in the literature. In order to make the interaction between photon modes and the excitons strong enough for meaningful experiments to be performed, the quantum well is put in a microcavity that traps photons and thus increases the interaction strength between the excitons and photons. This is illustrated in Figure 1. The result is a new quantum state the so called (exciton) polaritons.

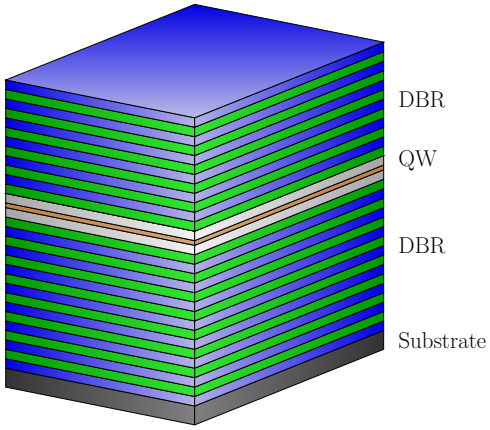

Figure 1: Schematic description of a (single) microcavity. Between the distributed Bragg reflectors a quantum well is placed. The excitons in the quantum well couple to the cavity modes producing a superposition state which we refer to as polaritons.

Such systems have a number of applications. They can, for example, be used for BEC (Bose Einstein condensate) generation and polariton lasing (see e.g. [4] or [5,7] for a review article). Recently, entanglement generation from such a system, both for frequency entanglement (see [2]) and polarization entanglement (see [15, 16]), has been discussed from a theoretical point of view. In both schemes polaritons are excited by (usually two) laser pumps and the photons resulting from the leaking of the polariton modes out of the cavity are picked up (this is illustrated in Figure 2).

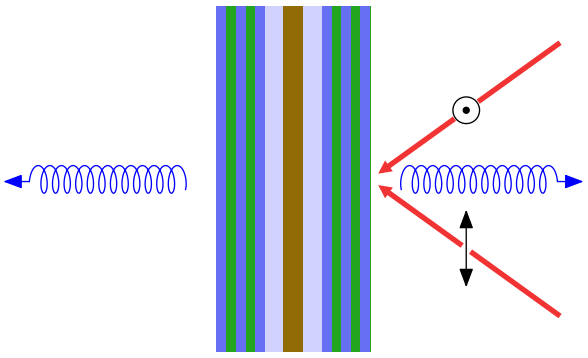

Figure 2: Schematic description of a pump scheme (the red lines illustrate an impinging laser beam). Entanglement is achieved between the two photons that leave to the front and back of the cavity, for example.

However, implementing such a scheme experimentally has proven difficult. Some difficulties, such as Rayleigh scattering, can be overcome by designing an appropriate scheme; this has been done in [15]. However, as

we will explain in more detail in the next section, pump-induced photoluminescence is the main concern, if we stay exclusively on the polariton state lowest in energy. If this assumption is violated additional noise is introduced; for example, the possibility of decay to the exciton reservoir.

In this thesis we will consider a double (see Figure 3) as well as triple cavity setup. We will demonstrate that such a structure can alleviate both problems mentioned above if an appropriately designed pump scheme is used. This is due to the fact that, as we will show, the double and triple cavity obey certain selection rules for single and double particle scattering processes.

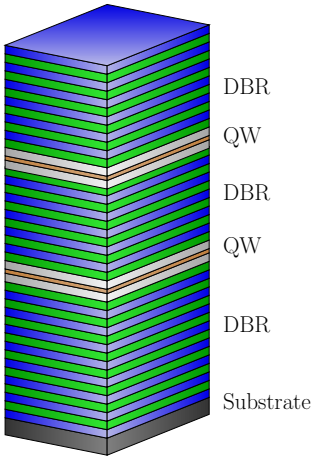

Figure 3: Schematic description of a double cavity. The distributed Bragg reflectors separate the two cavities; each includes a single quantum well.

In section 2 we will discuss the theoretical aspects of polaritons. This includes the dispersion relation in a two- and three-cavity setup as well as the derivation of the equations of motion in the quantum Langevin framework. In addition, we will discuss a steady state model that can be solved by analytical methods and derive an analytical expression for the coherent pump-induced polariton population. In section 3 we propose genuine double and triple cavity schemes that fulfill the selection rules derived in section 2, as well as discuss the protection from noise (such as pump-induced photoluminescence). In section 4 we will perform a number of numerical simulations in order to give a more quantitative account of the advantage of double cavity schemes; the figure of merit is chosen to be the entanglement of formation. In section 5 we will briefly discuss the current state of the experimental implementation of the schemes discussed in section 3. Finally, we conclude in section 6.

2 Theory

This section is devoted to the aspects of parametric scattering of polaritons in a microcavity that can be described analytically. First, we will describe the simple coupled oscillator model that is ubiquitous in the literature. In sections 2.2-2.5 we will derive the equations of motion in a single cavity, discuss how the resulting equations of motion give rise to entanglement, include noise in our treatment of parametric scattering using a quantum Langevin approach, and give a representation of the solution for both the populations and correlations in integral form (this is indeed the starting point of the numerical simulations conducted in section 4).

The integral representation of the solution can be solved analytically if a steady state pump is assumed and pump-induced photoluminescence is neglected. This is the content of section 2.6. We have chosen to present these results just after we introduced the single cavity case. Note, however, that this simplified model is applicable to the double and triple cavity case as well.

We then extend the single cavity model to the double (sections 2.7 and 2.8) and triple cavity (sections 2.9 and 2.10) case. Finally, the pump-induced polariton population is discussed for a steady state and a temporal Gaussian intensity profile in section 2.11.

2.1 An introduction to polaritons

In this section we describe the polaritons as a superposition of a cavity photon and an exciton (localized in a quantum well); this is done in the context of the coupled oscillator model. Such a treatment is quite common in the literature (see e.g. [1, 6, 7]). However, since this simple model forms the starting point for our discussion of parametric scattering we will reproduce the essential results here.

2.1.1 A single photon in a cavity

Let us first discuss the dispersion of a photon in a microcavity; due to the structure of the Bragg reflectors we can assume a resonance of wavelength λ_c at normal incidence. As the DBR confines the light in the z but not the x and y directions light entering the cavity at an angle θ (which also can be expressed as the wavevector parallel to the surface of the cavity $k_\parallel$) exhibits a resonance of energy

$$E_{\mathrm{c}}(k_\parallel) = \frac{\hbar c}{n_c}\sqrt{k_\perp^2 + k_\parallel^2}$$

with

$$k_\perp = n_c \frac{2\pi}{\lambda_c},$$

where n_c denotes the index of refraction inside the cavity.

2.1.2 A single exciton in a quantum well

In the microcavity described in the previous section a quantum well (a thin semiconductor that has a significantly smaller band gap than the cavity material) is placed inside the microcavity. Thus, excitons are confined in the z direction and can be described as bound states of electron hole pairs similar to a hydrogen atom. These quasiparticles are approximately bosons at low polariton intensities (they do not possess a definite statistics) and can be described by n (the excitation level of the bound state), $\boldsymbol{k}_\parallel$ (the wavevector in the unconfined parallel directions), and the spin σ. We will assume that only the $1s$ level (i.e. the lowest energy level) is occupied.

The exciton is a bound state of an electron (with spin either $\frac{1}{2}$ or $-\frac{1}{2}$) and a hole (which for heavy holes in GaAs cavities contributes a spin of $\frac{3}{2}$ or $-\frac{3}{2}$). Thus, there exist excitons with spin ± 1 and ± 2. The latter,

however, are not optically active and are thus called dark states. In the following we will only consider the optically active states with σ taking either the value 1 or -1. We can excite those states selectively by pumping with the corresponding circularly polarized light.

Finally, we have to specify the dispersion relation of the exciton. However, from a practical standpoint this is unnecessary as the effective mass of the cavity photon is given by (for small angles)

$$E_c \approx \frac{\hbar c}{n_c} k_\perp + \frac{\hbar^2 k_\parallel^2}{2 m_{c,\mathrm{eff}}}$$

with

$$m_{c,\mathrm{eff}} = \frac{\hbar n_c}{c} k_\perp \sim 7 \text{ eV/c}^2$$

at optical frequencies. This is five orders of magnitude smaller than the electron mass ($m_e \approx 0.51$ MeV/c^2) and still about four orders of magnitude smaller than the exciton mass as computed from the macroscopic theory (see e.g. [7]). Thus, we can assume an exciton dispersion relation that is independent of $k_\parallel$; the resulting value is then denoted by E_e.

2.1.3 The coupled oscillator model

Combining the ingredients discussed in the previous sections and neglecting the spin degree of freedom we get (in second quantization) the following Hamiltonian

$$H_s = \sum_{\boldsymbol{k}_\parallel} E_\mathrm{c}(\boldsymbol{k}_\parallel) a^\dagger_{\boldsymbol{k}_\parallel} a_{\boldsymbol{k}_\parallel} + E_e \sum_{\boldsymbol{k}_\parallel} B^\dagger_{\boldsymbol{k}_\parallel} B_{\boldsymbol{k}_\parallel} + \sum_{\boldsymbol{k}_\parallel} \hbar\Omega \left(a^\dagger_{\boldsymbol{k}_\parallel} B_{\boldsymbol{k}_\parallel} + a_{\boldsymbol{k}_\parallel} B^\dagger_{\boldsymbol{k}_\parallel} \right),$$

where Ω is the Rabi splitting resulting from the exciton-cavity coupling, $a_{\boldsymbol{k}_\parallel}$ is the photon annihilation operator, and $B^\dagger_{\boldsymbol{k}_\parallel}$ is the exciton creation operator (both energy and spin are fixed in this treatment and thus no additional subscripts are needed). If we fix the wavevector $\boldsymbol{k}_\parallel$ we can write the one particle subspace in matrix form by employing the basis $\{|\mathrm{X}\rangle, |\mathrm{P}\rangle\}$; the state $|\mathrm{X}\rangle$ represents a single exciton and the state $|\mathrm{P}\rangle$ a single cavity photon. The Hamilton is then given by the matrix

$$H_P = \begin{bmatrix} E_e & \hbar\Omega \\ \hbar\Omega & E_c \end{bmatrix}. \tag{1}$$

For obvious reasons this is called the coupled oscillator model. Proceeding in the usual manner we diagonalize the Hamiltonian and thus get two new quantum states with energy

$$\begin{aligned} E_1 &= \frac{1}{2}\left[E_e + E_c - \sqrt{4\left(\hbar\Omega\right)^2 + \left(\Delta E\right)^2} \right] \\ E_2 &= \frac{1}{2}\left[E_e + E_c + \sqrt{4\left(\hbar\Omega\right)^2 + \left(\Delta E\right)^2} \right], \end{aligned}$$

where $\Delta E := E_c - E_e$ is called the detuning. The corresponding eigenstates are

$$\begin{aligned} |\mathrm{P}_1\rangle &= X\,|\mathrm{X}\rangle + C\,|\mathrm{P}\rangle \\ |\mathrm{P}_2\rangle &= -C\,|\mathrm{X}\rangle + X\,|\mathrm{P}\rangle, \end{aligned}$$

where the Hopfield coefficients are given by

$$|X|^2 = \frac{1}{2}\left(1 + \frac{\Delta E}{\sqrt{(\Delta E)^2 + 4(\hbar\Omega)^2}}\right) \quad (2)$$

$$|C|^2 = \frac{1}{2}\left(1 - \frac{\Delta E}{\sqrt{(\Delta E)^2 + 4(\hbar\Omega)^2}}\right). \quad (3)$$

These coefficients satisfy the normalizing condition $|X|^2 + |C|^2 = 1$ as a simple calculation shows.

For a fixed $k_\parallel$ the detuning ΔE is a characteristic of the cavity . That is, by tuning the cavity off resonance with respect to the excitons this value can be changed. We will discuss this in more detail in the next section.

2.1.4 Detuning

The exciton energy E_e is a parameter that is determined by the physical characteristics of the quantum well. In GaAs cavities the energy of the exciton can be changed by adjusting the width of the quantum well. In InGaAs quantum wells, in addition, the Indium content can be varied to change the exciton energy.

The wavelength of the photon resonance λ_c can be engineered with relative ease by changing the length of the cavity. Due to the way the samples are grown the thickness (i.e. the length of the cavity) varies monotonically as a function of the radius of the wafer. Therefore, we can adjust the detuning by pointing our excitation laser to a different spot on the sample.

If we consider ΔE as a function of both $\boldsymbol{k}_\parallel$ and the length of the cavity we will often employ the detuning parameter δ that is given by

$$\delta = E_c(0) - E_e.$$

If $\delta > 0$, i.e. if the cavity resonance is higher in energy than that of the exciton we speak of blue detuning (the opposite case is called red detuning). In the case of blue detuning the lower polariton component has an increased exciton component which results in a longer lifetime. The Hopfield coefficients (see equations (2) and (3)) are illustrated for $\delta = 0$ as well as blue and red detuning in Figure 4.

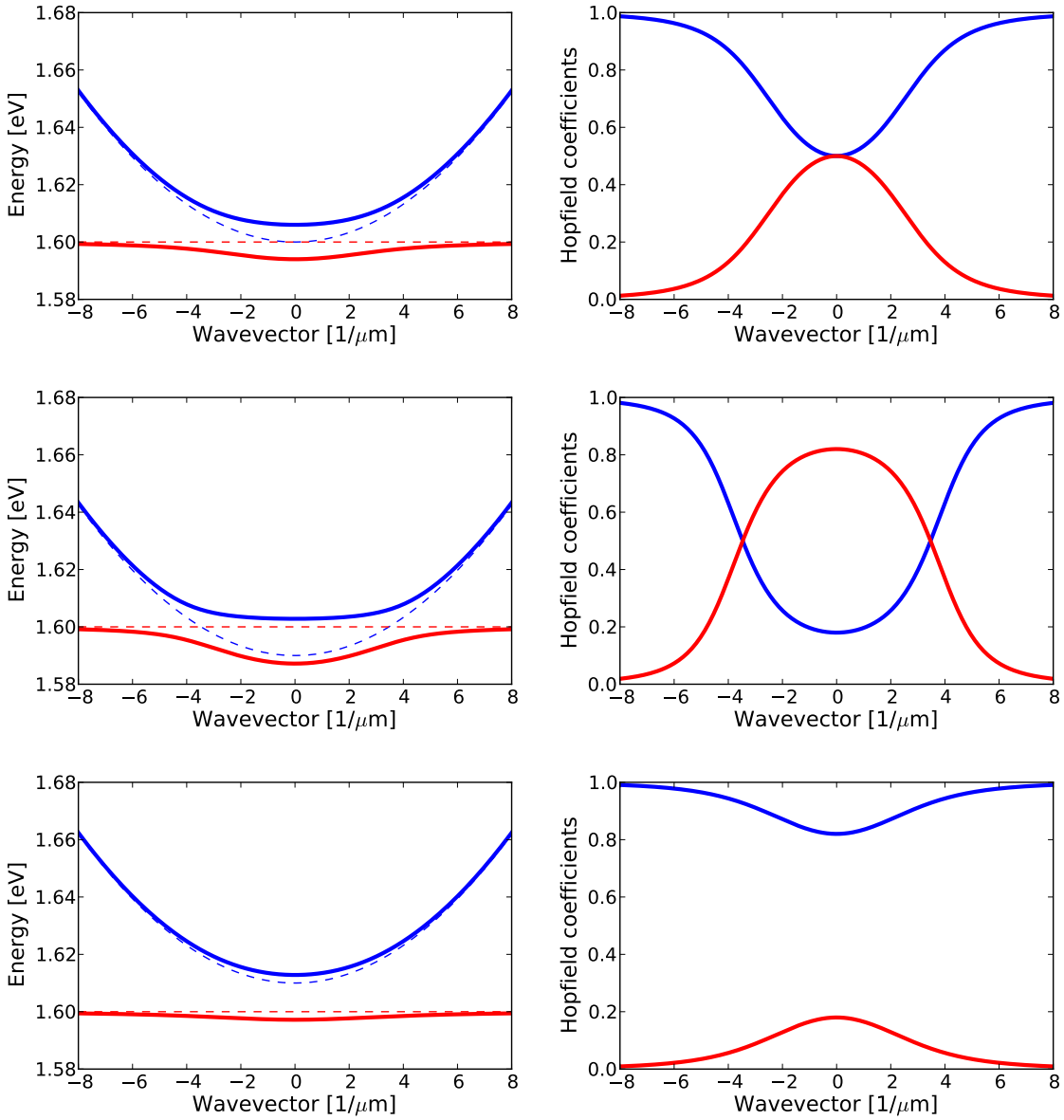

Figure 4: On the left the lower polariton dispersion (red) and the upper polariton dispersion (blue) are shown together with the exciton dispersion (red dashed) and the photon dispersion (blue dashed) for $\delta = 0$ (top), blue detuning (middle) and red detuning (bottom). On the right the exciton content $|X|^2$ (red) and the photon content (blue) are shown for the same three detunings.

2.1.5 The strong coupling regime

So far we have treated the cavity mirrors as perfect (i.e. neglecting losses that result from photons leaking out of the cavity) and assumed that there is no decay mechanism for the excitons. None of these assumptions are attainable in experiments. In a purely phenomenological approach we can add exciton and photon decay rates (i.e. the rate at which excitons/photons leak out of the cavity) that are denoted by γ_e and γ_c respectively. Typical values are $\gamma_c = \hbar/(1 \ldots 10 \text{ ps}) \approx 0.066 \ldots 0.66$ meV and $\gamma_e \approx \hbar/(1 \text{ ns}) \approx 0.66$ μeV

(see [7]). Thus, the lifetime of the polariton is determined largely by the lifetime of the photon and thus by the quality of the cavity.

Let us include this effect into our coupled oscillator model by modifying the dispersion appropriately. This yields a modified polariton dispersion

$$E_1 = \frac{1}{2}\left[E_e + E_c + i(\gamma_c - \gamma_e) - \sqrt{4\left(\hbar\Omega\right)^2 + \left(E_e - E_c + i(\gamma_e - \gamma_c)\right)^2}\right] \tag{4}$$

$$E_2 = \frac{1}{2}\left[E_e + E_c + i(\gamma_c - \gamma_e) + \sqrt{4\left(\hbar\Omega\right)^2 + \left(E_e - E_c + i(\gamma_e - \gamma_c)\right)^2}\right]. \tag{5}$$

In this case it is not sufficient to simply have an energy difference between the lower and upper polariton. Instead the energy difference must be larger than the linewidth in order to be able to speak unambiguously about lower and upper polaritons. If the latter condition is satisfied, i.e. if (note that $\gamma_c - \gamma_e$ and not $\gamma_c + \gamma_e$ represents the linewidth of the polaritons)

$$\mathrm{Re}\left(E_1 - E_2\right) \gg \gamma_c - \gamma_e,$$

we say that the system is in the **strong coupling regime** (or that it exhibits **anticrossing**). If we examine the condition more closely we have

$$\mathrm{Re}\left(E_1 - E_2\right) = \mathrm{Re}\sqrt{4\left(\hbar\Omega\right)^2 + \left(E_e - E_c + i(\gamma_e - \gamma_c)\right)^2} \approx 2\hbar\Omega \gg \gamma_c - \gamma_e,$$

which follows from the fact that the Rabi splitting $\hbar\Omega$ is on the order of meV and comparable to the detuning. The condition now simply requires that

$$\hbar\Omega \gg \frac{\gamma_e - \gamma_c}{2}.$$

We will take this inequality as the definition of strong coupling and employ it whenever needed.

2.1.6 Polariton decay

Finally, let us conclude this section by discussing the decay rate of the polaritons. We will consider a cavity where $\gamma_e \ll \gamma_c \ll \hbar\Omega$. Now since a polariton is a superposition of an exciton and photon the decay width of the lower polariton is given by

$$\gamma_1 = |X|^2\gamma_e + |C|^2\gamma_c \approx |C|^2\gamma_c$$

and that of the upper polariton by

$$\gamma_2 = |C|^2\gamma_e + |X|^2\gamma_c \approx |X|^2\gamma_c.$$

As discussed before the decay time is mainly determined by the leakage out of the cavity. The decay results in a photon leaving the cavity where energy, the in-plane momentum, the spin, and the phase are conserved. Thus, we can conveniently access the polariton state (which is uniquely determined by energy, in-plane momentum, and spin) by collecting the light emitted in an experimental setup.

2.2 Nonlinear equations of motion in a single cavity

The treatment in section 2.1 introduces polaritons in a simplified model. However, even though such a model elucidates many aspects of the polariton state, physically speaking it is not very interesting. It is thus our goal to derive an equation of motion that includes parametric scattering effects and a less ad-hoc

model of polariton decay; more precisely speaking we will employ a quantum Langevin approach based on phonon-scattering.

In the literature there are two competing approaches to incorporate parametric scattering in the single cavity case. First, Ciuti introduced a method based on a Hamiltonian that has been derived from scattering rates using Fermi's golden rule (see e.g. [2]). In this method we assume that polaritons are bosons (that is in line with the coupled oscillator model but strictly speaking it is only a valid approximation for low polariton densities).

Second, Portolan (see e.g. [14]) introduced a method based on the excitonic equations of motion that are derived from a microscopic theory of excitons in a quantum well. No bosonization is used and as such the scheme is expected to more closely match experimental data. Nevertheless, it is our opinion that due to the explicitly available Hamiltonian and the more straightforward extension to the double cavity case it is useful to consider Ciuti's model as well.

The work of Portolan and Ciuti also differ in the way noise is incorporated. In Portolan's work a phonon induced noise term is introduced via the quantum Langevin approach while in Ciuti's work polariton decay is only included phenomenologically. However, a supplementation of Ciuti's model with a quantum Langevin noise term is easily achieved.

In this section, we will show that both models lead to an equation that is of the form

$$\frac{d}{dt}p_{j\boldsymbol{k}} = -i\tilde{\omega}_{\boldsymbol{k}}p_{j\boldsymbol{k}} - i\sum_{\boldsymbol{k}_1\boldsymbol{k}_2 j_1 j_2 j_3} g_{jj_1j_2j_3\boldsymbol{k}\boldsymbol{k}_1\boldsymbol{k}_2}p_{j_1\boldsymbol{k}_1}p_{j_2\boldsymbol{k}_2}p^\dagger_{j_3\boldsymbol{k}_i} + S_{\boldsymbol{k}}, \tag{6}$$

where $p_{j\boldsymbol{k}}$ is the polariton annihilation operator with in-plane momentum $\boldsymbol{k}$ and branch index j and $S_{\boldsymbol{k}}$ is an appropriate source term. We will call $g_{j_1j_2j_3\boldsymbol{k}\boldsymbol{k}_1\boldsymbol{k}_2}$ the (non-linear) scattering rate and the idler wavevector is determined by the condition that $\boldsymbol{k}_i = \boldsymbol{k}_1 + \boldsymbol{k}_2 - \boldsymbol{k}$.

This is the sought equation describing parametric scattering. We will discuss in section 2.3 how such an equation of motion gives rise to entangled polariton pairs (and thus entangled photon pairs that leave the cavity) and extend the equations of motion by a phonon induced noise term by using the quantum Langevin approach in section 2.4.

It should also be duly noted that the only difference between Ciuti's and Portolan's scheme will concern the scattering rate g. Apart from this the equations of motion are identical in both models.

2.2.1 Ciuti's model in a single cavity

Hamiltonian So far we have only treated the, relatively simple, coupled oscillator model where in addition to the dispersion relation of the excitons and cavity photons a simple photon-exciton coupling was introduced. We will now include additional interaction effects. First, a purely exciton-exciton scattering channel is introduced. Let us denote the exciton annihilation operator with in-plane momentum $\boldsymbol{k}$ by $B_{\boldsymbol{k}}$ and the corresponding photon annihilation operator by $a_{\boldsymbol{k}}$. Then the Hamiltonian is given by

$$H_{XX} = \frac{1}{2}\sum \frac{\lambda_x^2}{A}\frac{6e^2}{\epsilon\lambda_x}B^\dagger_{\boldsymbol{k}+\boldsymbol{q}}B^\dagger_{\boldsymbol{k}'-\boldsymbol{q}}B_{\boldsymbol{k}}B_{\boldsymbol{k}'}$$

with ϵ the dielectric constant of the semiconductor (in the quantum well), A the area of quantization, and λ_x is the two-dimensional Bohr radius of the exciton. This effective Hamiltonian is derived from the Coulomb electron-hole Hamiltonian under the assumption that $q \ll \lambda_x^{-1}$(as described in [5]).

Second, due to the composite nature of the polariton quasi-particle a saturation effect must be included (see e.g. [4]). The Hamiltonian is given by

$$H^{sat}_{XC} = -\sum \frac{\hbar\Omega}{n_{sat}A}a^\dagger_{\boldsymbol{k}+\boldsymbol{q}}B^\dagger_{\boldsymbol{k}'-\boldsymbol{q}}B_{\boldsymbol{k}}B_{\boldsymbol{k}'} + h.c.$$

with

$$n_{sat} = \frac{7}{16\pi\lambda_x^2}$$

and represents the decay of two excitons into an exciton and a photon. The same model is used in [2] and a derivation of the scattering rates can be found in [19]. More detailed information is given, for example, in [3] .

In order to simplify matters we will use the notation of [14], i.e.

$$V = \frac{\hbar\Omega}{A}$$
$$V_{xx} = \frac{6e^2}{\pi\epsilon\lambda_x},$$

where we have chosen the area A such that $A = \pi\lambda_x^2$. Note that this fixes the energy for the Hamiltonian at the expense of the pump induced polariton occupation (as we will discuss in some detail in section 4.2).

Then the Hamiltonian reads

$$H_{XX} = \sum \frac{V_{xx}}{2} B^\dagger_{\boldsymbol{k}+\boldsymbol{q}} B^\dagger_{\boldsymbol{k}'-\boldsymbol{q}} B_{\boldsymbol{k}} B_{\boldsymbol{k}'}$$
$$H^{sat}_{XC} = \sum \frac{-V}{n_{sat}} a^\dagger_{\boldsymbol{k}+\boldsymbol{q}} B^\dagger_{\boldsymbol{k}'-\boldsymbol{q}} B_{\boldsymbol{k}} B_{\boldsymbol{k}'} + h.c.$$

Now we will transform the full Hamiltonian, i.e.

$$H = H_P + H_{XX} + H^{sat}_{XC},$$

to the polariton basis (i.e. to the eigenbasis of the Hamiltonian H_P given by the coupled oscillator model). In section 2.1.3 we already derived the relation that gives a representation of the polariton operators in terms of the exciton and photon operators; this relation is given by

$$\begin{bmatrix} p^\dagger_{1\boldsymbol{k}} \\ p^\dagger_{2\boldsymbol{k}} \end{bmatrix} = \begin{bmatrix} c_{1\boldsymbol{k}} & c_{2\boldsymbol{k}} \\ -c_{2\boldsymbol{k}} & c_{1\boldsymbol{k}} \end{bmatrix} \begin{bmatrix} B^\dagger_{\boldsymbol{k}} \\ a^\dagger_{\boldsymbol{k}} \end{bmatrix}. \tag{7}$$

The astute reader might have immediately recognized that the notation in the above representation is slightly different to what has been used in section 2.1.3 (more specifically we used $c_{1\boldsymbol{k}} = X_{\boldsymbol{k}}$ and $c_{2\boldsymbol{k}} = C_{\boldsymbol{k}}$). The new notation is less suggestive; however, it has a number of advantages. First, it enables us to represent both the lower and upper polariton by still referring to only one set of Hopfield coefficients. Second, it will enable us to make a more straightforward comparison with the double cavity case.

Inverting the relation above we get

$$\begin{bmatrix} B^\dagger_{\boldsymbol{k}} \\ a^\dagger_{\boldsymbol{k}} \end{bmatrix} = \begin{bmatrix} c_{1\boldsymbol{k}} & -c_{2\boldsymbol{k}} \\ c_{2\boldsymbol{k}} & c_{1\boldsymbol{k}} \end{bmatrix} \begin{bmatrix} p^\dagger_{1\boldsymbol{k}} \\ p^\dagger_{2\boldsymbol{k}} \end{bmatrix}. \tag{8}$$

Now using this relation we can rewrite the Hamiltonian for the exciton-exciton interaction in terms of the polariton operators as

$$\begin{aligned} H_{XX} = \sum \frac{V_{xx}}{2} &\left(c_{1\boldsymbol{k}+\boldsymbol{q}} p^\dagger_{1\boldsymbol{k}+\boldsymbol{q}} - c_{2\boldsymbol{k}+\boldsymbol{q}} p^\dagger_{2\boldsymbol{k}+\boldsymbol{q}}\right)\left(c_{1\boldsymbol{k}'-\boldsymbol{q}} p^\dagger_{1\boldsymbol{k}'-\boldsymbol{q}} - c_{2\boldsymbol{k}'-\boldsymbol{q}} p^\dagger_{2\boldsymbol{k}'-\boldsymbol{q}}\right) \\ &\left(c_{1\boldsymbol{k}} p_{1\boldsymbol{k}} - c_{2\boldsymbol{k}} p_{2\boldsymbol{k}}\right)\left(c_{1\boldsymbol{k}'} p_{1\boldsymbol{k}'} - c_{2\boldsymbol{k}'} p_{2\boldsymbol{k}'}\right) \\ = \sum &\overline{V}^{j_1 j_2 j_3 j_4}_{\boldsymbol{k}\boldsymbol{k}'\boldsymbol{q}} p^\dagger_{j_1\boldsymbol{k}+\boldsymbol{q}} p^\dagger_{j_2\boldsymbol{k}'-\boldsymbol{q}} p_{j_3\boldsymbol{k}} p_{j_4\boldsymbol{k}'} \end{aligned}$$

with

$$\overline{V}^{j_1 j_2 j_3 j_4}_{\boldsymbol{k}\boldsymbol{k}'\boldsymbol{q}} = \frac{V_{xx}}{2}(-1)^{\sum_i j_i} c_{j_1\boldsymbol{k}+\boldsymbol{q}} c_{j_2\boldsymbol{k}'-\boldsymbol{q}} c_{j_3\boldsymbol{k}} c_{j_4\boldsymbol{k}'}. \tag{9}$$

The same procedure is then conducted with the saturation Hamiltonian resulting in

$$H^{sat}_{XC} = \sum \underline{V}^{j_1 j_2 j_3 j_4}_{\boldsymbol{k}\boldsymbol{k}'\boldsymbol{q}} p^\dagger_{j_1\boldsymbol{k}+\boldsymbol{q}} p^\dagger_{j_2\boldsymbol{k}'-\boldsymbol{q}} p_{j_3\boldsymbol{k}} p_{j_4\boldsymbol{k}'},$$

where

$$\underline{V}^{j_1 j_2 j_3 j_4}_{\boldsymbol{k}\boldsymbol{k}'\boldsymbol{q}} = \frac{-V}{n_{sat}} \left((-1)^{j_2+j_3+j_4} c_{3-j_1\boldsymbol{k}+\boldsymbol{q}} c_{j_2\boldsymbol{k}'-\boldsymbol{q}} c_{j_3\boldsymbol{k}} c_{j_4\boldsymbol{k}'} + (-1)^{j_1+j_2+j_3} c_{j_1\boldsymbol{k}+\boldsymbol{q}} c_{j_2\boldsymbol{k}'-\boldsymbol{q}} c_{j_3\boldsymbol{k}} c_{3-j_4\boldsymbol{k}'} \right). \tag{10}$$

Finally, we can rewrite the polariton-polariton interaction Hamiltonian as

$$H_{PP} = \sum V^{j_1 j_2 j_3 j_4}_{\boldsymbol{k}\boldsymbol{k}'\boldsymbol{q}} p^\dagger_{j_1\boldsymbol{k}+\boldsymbol{q}} p^\dagger_{j_2\boldsymbol{k}'-\boldsymbol{q}} p_{j_3\boldsymbol{k}} p_{j_4\boldsymbol{k}'},$$

where

$$V^{j_1 j_2 j_3 j_4}_{\boldsymbol{k}\boldsymbol{k}'\boldsymbol{q}} = \underline{V}^{j_1 j_2 j_3 j_4}_{\boldsymbol{k}\boldsymbol{k}'\boldsymbol{q}} + \overline{V}^{j_1 j_2 j_3 j_4}_{\boldsymbol{k}\boldsymbol{k}'\boldsymbol{q}}. \tag{11}$$

Equations of motion To derive an equation of motion we employ the Heisenberg equation, i.e.

$$\frac{dp_{j\boldsymbol{p}}}{dt} = \frac{i}{\hbar} \left[H_{PP}, p_{j\boldsymbol{p}} \right].$$

The right hand side can then be rewritten as

$$\left[H_{PP}, p_{j\boldsymbol{p}} \right] = \sum V^{j_1 j_2 j_3 j_4}_{\boldsymbol{k}\boldsymbol{k}'\boldsymbol{q}} \left[p^\dagger_{j_1\boldsymbol{k}+\boldsymbol{q}} p^\dagger_{j_2\boldsymbol{k}'-\boldsymbol{q}} p_{j_3\boldsymbol{k}} p_{j_4\boldsymbol{k}'}, p_{j\boldsymbol{p}} \right]$$

and by using

$$\begin{aligned}
[ABCD, E] &= ABC\,[D, E] + [ABC, E]\,D \\
&= ABC\,[D, E] + AB\,[C, E]\,D + [AB, E]\,CD \\
&= ABC\,[D, E] + AB\,[C, E]\,D + A\,[B, E]\,CD + [A, E]\,BCD
\end{aligned}$$

we get

$$\begin{aligned}
\left[p^\dagger_{j_1\boldsymbol{k}+\boldsymbol{q}} p^\dagger_{j_2\boldsymbol{k}'-\boldsymbol{q}} p_{j_3\boldsymbol{k}} p_{j_4\boldsymbol{k}'}, p_{j\boldsymbol{p}} \right] &= p^\dagger_{j_1\boldsymbol{k}+\boldsymbol{q}} p^\dagger_{j_2\boldsymbol{k}'-\boldsymbol{q}} p_{j_3\boldsymbol{k}} \left[p_{j_4\boldsymbol{k}}, p_{j\boldsymbol{p}} \right] + p^\dagger_{j_1\boldsymbol{k}+\boldsymbol{q}} p^\dagger_{j_2\boldsymbol{k}'-\boldsymbol{q}} \left[p_{j_3\boldsymbol{k}}, p_{j\boldsymbol{p}} \right] p_{j_4\boldsymbol{k}'} \\
&\quad + p^\dagger_{j_1\boldsymbol{k}+\boldsymbol{q}} \left[p^\dagger_{j_2\boldsymbol{k}'-\boldsymbol{q}}, p_{j\boldsymbol{p}} \right] p_{j_3\boldsymbol{k}} p_{j_4\boldsymbol{k}'} + \left[p^\dagger_{j_1\boldsymbol{k}+\boldsymbol{q}}, p_{j\boldsymbol{p}} \right] p^\dagger_{j_2\boldsymbol{k}'-\boldsymbol{q}} p_{j_3\boldsymbol{k}} p_{j_4\boldsymbol{k}'} \\
&= -p^\dagger_{j_1\boldsymbol{k}+\boldsymbol{q}} p_{j_3\boldsymbol{k}} p_{j_4\boldsymbol{k}'} \delta_{\boldsymbol{k}'-\boldsymbol{q},\boldsymbol{p}} \delta_{j_2,j} - p^\dagger_{j_2\boldsymbol{k}'-\boldsymbol{q}} p_{j_3\boldsymbol{k}} p_{j_4\boldsymbol{k}'} \delta_{\boldsymbol{k}+\boldsymbol{q},\boldsymbol{p}} \delta_{j_1,j}.
\end{aligned}$$

Now we have to employ the bosonization of the polariton operator (i.e. we assume that $\left[p_{j\boldsymbol{k}}, p^\dagger_{k\boldsymbol{p}} \right] = \delta_{jk}\delta_{\boldsymbol{k}\boldsymbol{p}}$). If in addition we include a phenomenological damping term and an appropriate source term, that we denote by $S_{\boldsymbol{k}}$ below and discuss in more detail in section 2.11, we arrive at the equations of motion (we use $E_{j\boldsymbol{p}}$ to denote the energy of an polariton on the j-th branch with momentum $\boldsymbol{p}$)

$$\frac{dp_{j\boldsymbol{p}}}{dt} = -i(E_{j\boldsymbol{p}} + i\gamma)p_{j\boldsymbol{p}} - i \sum_{j_1 j_3 j_4 \boldsymbol{k}\boldsymbol{k}'} \left(V^{j_1 j j_3 j_4}_{\boldsymbol{k}\boldsymbol{k}',\boldsymbol{k}'-\boldsymbol{p}} + V^{j j_1 j_3 j_4}_{\boldsymbol{k}\boldsymbol{k}',\boldsymbol{p}-\boldsymbol{k}} \right) p^\dagger_{j_1\boldsymbol{k}+\boldsymbol{k}'-\boldsymbol{p}} p_{j_3\boldsymbol{k}} p_{j_4\boldsymbol{k}'} + S_{\boldsymbol{k}} \tag{12}$$

that have the form stated in equation (6).

2.2.2 Portolan's model in a single cavity

Let us now repeat the derivation of the equations of motion we conducted in the previous section with the method of Portolan (see [12, 15, 17]). We proceed from the equations of motion for the exciton that are derived directly from the microscopic theory of the exciton as a bound state of electron-hole pairs in a semiconductor. The cavity-photon is added by employing once again the coupled oscillator model that is coupled to a classical external light field $\mathscr{E}^{in}_{\boldsymbol{k}}$. These equations of motion have the following form (see [13])

$$\partial_t B_{\boldsymbol{k}} = -iE_{\boldsymbol{k}} B_{\boldsymbol{k}} - i\hbar\Omega a_{\boldsymbol{k}} - iR^{NL}_{\boldsymbol{k}}, \tag{13}$$

$$\partial_t a_{\boldsymbol{k}} = -iE^c_{\boldsymbol{k}} a_{\boldsymbol{k}} - i\hbar\Omega B_{\boldsymbol{k}} + t_c \mathscr{E}^{in}_{\boldsymbol{k}}, \tag{14}$$

where t_c is the transmission coefficient of the cavity and the nonlinearity is given by

$$\begin{aligned} R^{NL}_{\boldsymbol{k}} &= R^{xx}_{\boldsymbol{k}} + R^{sat}_{\boldsymbol{k}} \\ R^{xx}_{\boldsymbol{k}} &= V_{xx} \sum_{\boldsymbol{k}_1 \boldsymbol{k}_2} B^\dagger_{\boldsymbol{k}_1+\boldsymbol{k}_2-\boldsymbol{k}} B_{\boldsymbol{k}_1} B_{\boldsymbol{k}_2} \\ R^{sat}_{\boldsymbol{k}} &= \frac{V}{n_{sat}} \sum_{\boldsymbol{k}_1 \boldsymbol{k}_2} B^\dagger_{\boldsymbol{k}_1+\boldsymbol{k}_2-\boldsymbol{k}} B_{\boldsymbol{k}_1} a_{\boldsymbol{k}_2}, \end{aligned}$$

Note that compared to [13] we have made additional simplifications. The shift term (denoted $s_{\boldsymbol{k}}$ in the before mentioned paper) has been omitted as it induces only a renormalization of the exciton dispersion relation. In addition, the spin indices have not been written out (spin effects are discussed in some detail in section 2.3).

Let us rewrite (13) and (14) in matrix form; this gives

$$\frac{d}{dt}\mathcal{B}_{\boldsymbol{k}} = -i\boldsymbol{\Omega}^{xc}_{\boldsymbol{k}} \mathcal{B}_{\boldsymbol{k}} + \mathcal{E}^{in}_{\boldsymbol{k}} - i\mathcal{R}^{NL}_{\boldsymbol{k}},$$

$$\mathcal{B}_{\boldsymbol{k}} = \begin{bmatrix} B_{\boldsymbol{k}} \\ a_{\boldsymbol{k}} \end{bmatrix}, \qquad \boldsymbol{\Omega}^{xc}_{\boldsymbol{k}} = \begin{bmatrix} E_{\boldsymbol{k}} & \hbar\Omega \\ \hbar\Omega & E^c_{\boldsymbol{k}} \end{bmatrix}, \qquad \mathcal{E}^{in}_{\boldsymbol{k}} = \begin{bmatrix} 0 \\ t_c \mathscr{E}^{in}_{\boldsymbol{k}} \end{bmatrix}, \qquad \mathcal{R}^{NL}_{\boldsymbol{k}} = \begin{bmatrix} R^{NL}_{\boldsymbol{k}} \\ 0 \end{bmatrix}.$$

It is apparent that the linear part is generated by the Hamiltonian of the coupled oscillator model. Thus, we employ the transformation to the polariton basis already investigated in section 2.2.1 (i.e. by using the relations in equation (7) and (8)). After some simple algebra we arrive at the equations of motion in the polariton basis given by

$$\frac{d}{dt} p_{1\boldsymbol{k}} = -i\omega_{1\boldsymbol{k}} p_{1\boldsymbol{k}} + \tilde{\mathscr{E}}^{in}_{1\boldsymbol{k}} - i\tilde{R}^{NL}_{1\boldsymbol{k}} \tag{15}$$

$$\frac{d}{dt} p_{2\boldsymbol{k}} = -i\omega_{1\boldsymbol{k}} p_{2\boldsymbol{k}} + \tilde{\mathscr{E}}^{in}_{2\boldsymbol{k}} - i\tilde{R}^{NL}_{2\boldsymbol{k}}, \tag{16}$$

where

$$\tilde{R}^{NL}_{i\boldsymbol{k}} = c_{i\boldsymbol{k}} R^{NL}_{\boldsymbol{k}}, \qquad \tilde{\mathscr{E}}^{in}_{i\boldsymbol{k}} = (-1)^i c_{3-i\boldsymbol{k}} t_c \mathscr{E}^{in}_{\boldsymbol{k}}.$$

It is still necessary to transform $R^{NL}_{\boldsymbol{k}}$ to the polariton basis. To that end we use once more equation (7) to express the exciton and photon operators in the polariton basis

$$\begin{aligned} B_{\boldsymbol{k}} &= c_{1\boldsymbol{k}} p_{1\boldsymbol{k}} - c_{2\boldsymbol{k}} p_{2\boldsymbol{k}} \\ a_{\boldsymbol{k}} &= c_{2\boldsymbol{k}} p_{1\boldsymbol{k}} + c_{1\boldsymbol{k}} p_{2\boldsymbol{k}}. \end{aligned}$$

From this relation we get

$$\begin{aligned}
R^{xx}_{\boldsymbol{k}} &= V_{xx}\sum_{\boldsymbol{k}_1\boldsymbol{k}_2} B^\dagger_{\boldsymbol{k}_1+\boldsymbol{k}_2-\boldsymbol{k}} B_{\boldsymbol{k}_1} B_{\boldsymbol{k}_2} \\
&= V_{xx}\sum_{\boldsymbol{k}_1\boldsymbol{k}_2}\left(c_{1\boldsymbol{k}_1+\boldsymbol{k}_2-\boldsymbol{k}} p^\dagger_{1\boldsymbol{k}_1+\boldsymbol{k}_2-\boldsymbol{k}} - c_{2\boldsymbol{k}_1+\boldsymbol{k}_2-\boldsymbol{k}} p^\dagger_{2\boldsymbol{k}_1+\boldsymbol{k}_2-\boldsymbol{k}}\right)\left(c_{1\boldsymbol{k}_1} p_{1\boldsymbol{k}_1} - c_{2\boldsymbol{k}_1} p_{2\boldsymbol{k}_1}\right)\left(c_{1\boldsymbol{k}_2} p_{1\boldsymbol{k}_2} - c_{2\boldsymbol{k}_2} p_{2\boldsymbol{k}_2}\right) \\
&= -V_{xx}\sum_{\boldsymbol{k}_1\boldsymbol{k}_2 j j_1 j_2} (-1)^{j+j_1+j_2} c_{j\boldsymbol{k}_1+\boldsymbol{k}_2-\boldsymbol{k}} c_{j_1\boldsymbol{k}_1} c_{j_2\boldsymbol{k}_2} p^\dagger_{j\boldsymbol{k}_1+\boldsymbol{k}_2-\boldsymbol{k}} p_{j_1\boldsymbol{k}_1} p_{j_2\boldsymbol{k}_2}
\end{aligned}$$

and

$$\begin{aligned}
R^{sat}_{\boldsymbol{k}} &= \frac{V}{n_{sat}}\sum_{\boldsymbol{k}_1\boldsymbol{k}_2} B^\dagger_{\boldsymbol{k}_1+\boldsymbol{k}_2-\boldsymbol{k}} B_{\boldsymbol{k}_1} a_{\boldsymbol{k}_2} \\
&= \frac{V}{n_{sat}}\sum_{\boldsymbol{k}_1\boldsymbol{k}_2 j j_1 j_2} (-1)^{j+j_1} c_{j\boldsymbol{k}_1+\boldsymbol{k}_2-\boldsymbol{k}} c_{j_1\boldsymbol{k}_1} c_{3-j_2\boldsymbol{k}_2} p^\dagger_{j\boldsymbol{k}_1+\boldsymbol{k}_2-\boldsymbol{k}} p_{j_1\boldsymbol{k}_1} p_{j_2\boldsymbol{k}_2}.
\end{aligned}$$

Finally, let us introduce a phenomenological decay rate γ as well as rewrite equations (15) and (16) in a form comparable to equation (12) in the previous section. This yields,

$$\frac{d}{dt}p_{m\boldsymbol{p}} = -i(\omega_{m\boldsymbol{k}} + i\gamma)p_{m\boldsymbol{p}} - ic_{m\boldsymbol{p}}\sum\left(\overline{V}^{jj_1j_2}_{\boldsymbol{k}_1\boldsymbol{k}_2\boldsymbol{p}} + \underline{V}^{jj_1j_2}_{\boldsymbol{k}_1\boldsymbol{k}_2\boldsymbol{p}}\right) p^\dagger_{j\boldsymbol{k}_1+\boldsymbol{k}_2-\boldsymbol{p}} p_{j_1\boldsymbol{k}_1} p_{j_2\boldsymbol{k}_2} + (-1)^m c_{3-m\boldsymbol{p}} t_c E^{in}_{\boldsymbol{p}}. \quad (17)$$

with

$$\overline{V}^{jj_1j_2}_{\boldsymbol{k}_1\boldsymbol{k}_2\boldsymbol{p}} = -V_{xx}(-1)^{j+j_1+j_2} c_{j_1\boldsymbol{k}_1+\boldsymbol{k}_2-\boldsymbol{p}} c_{j_2\boldsymbol{k}_1} c_{j_3\boldsymbol{k}_2} \quad (18)$$

and

$$\underline{V}^{jj_1j_2}_{\boldsymbol{k}_1\boldsymbol{k}_2\boldsymbol{p}} = \frac{V}{n_{sat}}(-1)^{j+j_1} c_{j\boldsymbol{k}_1+\boldsymbol{k}_2-\boldsymbol{k}} c_{j_1\boldsymbol{k}_1} c_{3-j_2\boldsymbol{k}_2}. \quad (19)$$

We notice that this is not the same result that we derived in the previous section using Ciuti's model. This, however, is entirely expected as different assumptions are made in the respective models. Once we have discussed the double and triple cavity case we will revisit this point in more detail (see section 3).

2.3 Parametric scattering and entanglement

The equations of motion derived in the previous sections are quite general in that scattering processes from any point in $\boldsymbol{k}$ space to any other point in $\boldsymbol{k}$ space are considered. In fact, as we have not narrowed down which processes we are interested in, both equation (12) and (17) couple an infinite number of degrees of freedom. We will now investigate parametric scattering where we pump at two points in $\boldsymbol{k}$ space (the branch indices and wavevectors are denoted by $(j_{p_1}, \boldsymbol{k}_{p_1})$ and $(j_{p_2}, \boldsymbol{k}_{p_2})$ respectively) and consider scattering processes that satisfy the phase matching condition (i.e. energy and momentum conservation). We specifically choose to omit scattering processes that are not directly pump induced. This is a good approximation for the purpose of entanglement generation since in contrast to the pump the signal and idler (i.e. which possibly result in entangled photons) are only microscopically populated.

This still leaves one wavevector undefined which we are free to choose. We will call this wavevector the **signal** and denote it by $\boldsymbol{k}$. The corresponding wavevector satisfying momentum conservation is called the **idler** and is then given by $\boldsymbol{k}_i = \boldsymbol{k}_{p_1} + \boldsymbol{k}_{p_2} - \boldsymbol{k}$. Note that we can also consider the case where signal and idler are on different branches, i.e. the signal can be on branch j while the idler is, in general, on a different branch j_i.

The advantage of quantum well polaritons is that the in-plane wavevectors/spin of the signal and idler polaritons can be directly mapped to the angle of emission/polarization of the corresponding photons. Thus, an entanglement of the polaritons, either in the in-plane momentum or the spin, is mapped to an entanglement in the corresponding degree of freedom for the emitted photons.

2.3.1 Entanglement with respect to the branch index

That such a scattering process can create entanglement between a polariton with wavevector $\boldsymbol{k}$ and $\boldsymbol{k}_i$ is most easily seen by considering the polariton-polariton interaction Hamiltonian (see section 2.2.1)

$$H_{PP} = \frac{1}{2}\sum_{\boldsymbol{k}\boldsymbol{k}'} \frac{\lambda_x^2}{A} V^{j_1 j_2 j_3 j_4}_{\boldsymbol{k}\boldsymbol{k}'\boldsymbol{q}} p^\dagger_{j_1\boldsymbol{k}+\boldsymbol{q}} p^\dagger_{j_2\boldsymbol{k}'-\boldsymbol{q}} p_{j_3\boldsymbol{k}} p_{j_4\boldsymbol{k}'}\,.$$

As discussed in the introduction let us only consider scattering processes that are a direct result of two pump polaritons. In addition, we fix the signal wavevector at $\boldsymbol{k}$. Then the Hamiltonian reads

$$H_{PP} = \frac{1}{2}\frac{\lambda_x^2}{A}\sum_{j_1 j_2} V^{j_1 j_2 j_{p_1} j_{p_2}}_{\boldsymbol{k}_{p_1}\boldsymbol{k}_{p_2}\boldsymbol{k}-\boldsymbol{k}_{p_1}} p^\dagger_{j_1\boldsymbol{k}} p^\dagger_{j_2\boldsymbol{k}_i} p_{j_{p_1}\boldsymbol{k}_{p_1}} p_{j_{p_1}\boldsymbol{k}_{p_2}}\,.$$

We can easily deduce from equations (11), (10), and (9) that $V^{j_1 j_2 j_{p_1} j_{p_2}}_{\boldsymbol{k}_{p_1}\boldsymbol{k}_{p_2}\boldsymbol{k}-\boldsymbol{k}_{p_1}} = V^{j_2 j_1 j_{p_1} j_{p_2}}_{\boldsymbol{k}_{p_1}\boldsymbol{k}_{p_2}\boldsymbol{k}-\boldsymbol{k}_{p_1}}$, i.e. the matrix element is invariant with respect to the interchange of the signal and idler branch indices. Moreover, as energy conservation implies that $j_1 \neq j_2$ if the two pumps are on the second branch (i.e. $j_{p_1}, j_{p_2} = 2$ as in [2]) we get (an illustration of this scheme is given in Figure 16 section 3.2.2)

$$H_{PP} = \frac{1}{2}\frac{\lambda_X^2}{A} V^{j j_i j_{p_1} j_{p_2}}_{\boldsymbol{k}_{p_1}\boldsymbol{k}_{p_2}\boldsymbol{k}-\boldsymbol{k}_{p_1}} \left(p^\dagger_{1\boldsymbol{k}} p^\dagger_{2\boldsymbol{k}_i} + p^\dagger_{2\boldsymbol{k}} p^\dagger_{1\boldsymbol{k}_i}\right) p_{2\boldsymbol{k}_{p_1}} p_{2\boldsymbol{k}_{p_2}}\,.$$

Employing a straightforward argument using Fermi's golden rule, the scattering induced by this Hamiltonian results in two polaritons that are entangled with respect to the branch index, i.e.

$$|\psi\rangle \propto |12\rangle + |21\rangle\,.$$

If these two polaritons decay the result is a pair of photons that are entangled in frequency (as the branch index is mapped to the corresponding energy of the photon given by the dispersion of the polariton). The scheme described here has been suggested in [2].

To measure frequency entangled photon pairs in this setup is not straightforward. Since a photon with a given energy can exit the cavity either to the left or to the right (or to be more precise either at $\boldsymbol{k}$ or $-\boldsymbol{k}$) we have to mix the two path at some point in our measurement setup. An example of how such an experiment can be conducted is shown in Figure 5.

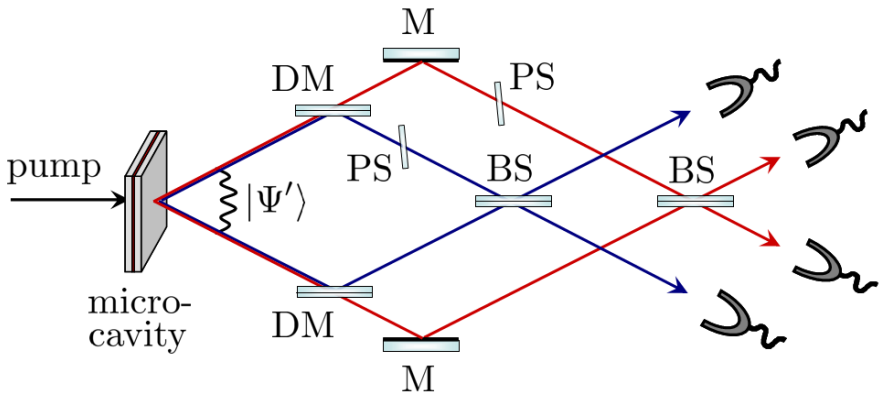

Figure 5: Setup to measure entanglement in frequency of photon pairs. Two dichroic mirrors (DM) are used to separate the photons by frequency and two beam splitters (BM) are used to superimpose paths of the same color. Mirrors are labeled by M and phase shifter plates by PS. The illustration is taken from [6].

2.3.2 Entanglement with respect to the spin degree of freedom

Although frequency entangled photons have a number of applications (for example, in quantum-optical coherence tomography as demonstrated in [10]) we are more interested in entanglement in the spin degree of freedom; such an entanglement would result in two photons which are entangled in polarization leaving the cavity.

That this is indeed possible is a consequence of the fact that if signal and idler are on the same branch we still have indistinguishability with respect to the polarization degree of freedom. Since we can excite polaritons of a specific spin with circularly polarized light (see section 1), this gives us an additional possibility of creating entanglement in our setting.

In [11] spin based entanglement is investigated in some detail in the context of the framework developed in [15]. However, we can understand the entanglement properties using the Hamiltonian approach (that is in essentially the same way as we did in case of the branch entanglement in the previous section). Fortunately, we can assume that the main scattering channel is insensitive to polarization (see [15]) and it is thus easy to put the corresponding indices with respect to spin back into the Hamiltonian (we will use $+$ to denote a spin of 1 and $-$ to denote a spin of -1). Let us discuss schemes were we pump with left and right circularly polarized light, i.e. we consider a Hamiltonian of the form

$$H_{PP} = \frac{\lambda_X^2}{A} V^{jj_ij_{p_1}j_{p_2}}_{\boldsymbol{k}_{p_1}\boldsymbol{k}_{p_2}\boldsymbol{k}-\boldsymbol{k}_{p_1}} \left[\left(p^\dagger_{+j\boldsymbol{k}} p^\dagger_{-j_i\boldsymbol{k}_i} + p^\dagger_{-j\boldsymbol{k}} p^\dagger_{+j_i\boldsymbol{k}_i} \right) p_{+j_{p_1}\boldsymbol{k}_{p_1}} p_{-j_{p_1}\boldsymbol{k}_{p_2}} \right]$$

which once again results in an entangled state of the form

$$|\psi\rangle \propto |{+}{-}\rangle + |{-}{+}\rangle \,.$$

However, in reality the situation is more complicated. A number of four-particle channels (bound biexcitons, for example) tend to diminish the entanglement. To remedy this in [15] it is suggested that we pump with linearly cross-polarized light. In this case we pump with a quantum superposition of circularly polarized light, i.e.

$$\begin{aligned} p_{\theta j_{p_1}\boldsymbol{k}_{p_1}} &= \frac{1}{\sqrt{2}} \left(e^{-i\theta} p_{+j_{p_1}\boldsymbol{k}_{p_1}} + e^{+i\theta} p_{-j_{p_1}\boldsymbol{k}_{p_1}} \right) \\ p_{\theta+\frac{\pi}{2} j_{p_2}\boldsymbol{k}_{p_2}} &= \frac{i}{\sqrt{2}} \left(e^{-i\theta} p_{+j_{p_2}\boldsymbol{k}_{p_2}} - e^{+i\theta} p_{-j_{p_2}\boldsymbol{k}_{p_2}} \right) \end{aligned}$$

and thus

$$p_{\theta j_{p_1}\boldsymbol{k}_{p_1}} p_{\theta+\frac{\pi}{2} j_{p_2}\boldsymbol{k}_{p_2}} = \frac{1}{2} i e^{-i2\theta} \left(p_{+j_{p_1}\boldsymbol{k}_{p_1}} p_{+j_{p_2}\boldsymbol{k}_{p_2}} - e^{4i\theta} p_{-j_{p_1}\boldsymbol{k}_{p_1}} p_{-j_{p_2}\boldsymbol{k}_{p_2}} \right).$$

Now the resulting Hamiltonian can be written as

$$H_{PP} = \frac{\lambda_X^2}{A} V^{jjj_{p_1}j_{p_2}}_{\boldsymbol{k}_{p_1}\boldsymbol{k}_{p_2}\boldsymbol{k}-\boldsymbol{k}_{p_1}} \left[\left(p^\dagger_{+j\boldsymbol{k}} p^\dagger_{+j_i\boldsymbol{k}_i} p_{+j_{p_1}\boldsymbol{k}_{p_1}} p_{+j_{p_1}\boldsymbol{k}_{p_2}} - e^{4i\theta} p^\dagger_{-j_i\boldsymbol{k}} p^\dagger_{-j\boldsymbol{k}_i} p_{-j_{p_1}\boldsymbol{k}_{p_1}} p_{-j_{p_1}\boldsymbol{k}_{p_2}} \right) \right]. \tag{20}$$

Therefore it is evident that this approach cancels out the $+-$ channel (counter-circular channel) and we are left with just the $++$ and the $--$ channel (co-circular channel). The polarization angle θ will be important later when we compute density matrices. However, the resulting entangled state

$$|\psi\rangle \propto |{+}{+}\rangle - e^{-4i\theta} |{-}{-}\rangle \,,$$

as symmetry suggests, is maximally entangled for any value of θ.

2.4 The quantum Langevin approach

Until now we have not incorporated noise resulting from additional polariton-polariton scattering (such as pump induced photoluminescence). We will introduce the quantum Langevin approach to add such effects in this section. This was done for Portolans's model in [14]; however, the approach is equally applicable to Ciuti's model.

The fundamental idea of the Heisenberg-Langevin approach is that we derive equations that give the partial trace over the reservoir of some system operator in the Heisenberg picture and extend them to the full system. Thus, if we assume that $\{a_\mu\}$ are a number of system operators that satisfy the following equation

$$\frac{d}{dt}\mathrm{tr}_R a_\mu = \mathrm{tr}_R A_\mu(\boldsymbol{a})$$

we can promote them to equations for the the system and reservoir as follows

$$\frac{d}{dt}a_\mu = A_\mu(\boldsymbol{a}) + F_\mu(\boldsymbol{a}, t),$$

where $F_\mu(\boldsymbol{a}, t)$ are called Langevin noise source operators. These operators satisfy $\mathrm{tr}_R F_\mu(\boldsymbol{a}, t) = 0$. If we assume the Markov approximation we can represent the correlations of the noise term as

$$\mathrm{tr}_R F_\mu(t) F_\nu(t') = 2\delta(t - t')\mathrm{tr}_R D_{\mu\nu}$$

with diffusion coefficients $D_{\mu\nu}$. In our case we will assume that the equation of motion can be written as a set of two equations (coupling signal and idler) in the form

$$\begin{aligned}
\frac{d}{dt}\mathrm{tr}_R p_{j\boldsymbol{k}} &= -i\tilde{\omega}_{\boldsymbol{k}}\mathrm{tr}_R p_{j\boldsymbol{k}} + g_{\boldsymbol{k}}\mathcal{P}_{\boldsymbol{k}_{p_1}}\mathcal{P}_{\boldsymbol{k}_{p_2}}\mathrm{tr}_R p_{j\boldsymbol{k}_i} \\
\frac{d}{dt}\mathrm{tr}_R p^\dagger_{j_i\boldsymbol{k}_i} &= i\tilde{\omega}_{\boldsymbol{k}_i}\mathrm{tr}_R p_{j_i\boldsymbol{k}_i} + ig^*_{\boldsymbol{k}}\mathcal{P}_{\boldsymbol{k}_{p_1}}\mathcal{P}_{\boldsymbol{k}_{p_2}}\mathrm{tr}_R p_{j\boldsymbol{k}}.
\end{aligned}$$

We have written $\mathcal{P}$ instead of p to emphasize that we assume a coherent pump (i.e. $\mathcal{P}_{\boldsymbol{k}} = \langle p_{\boldsymbol{k}}\rangle$). It is clear that such a treatment is possible for both the methods discussed in the previous sections; note that we assume that signal and idler are sufficiently far away from both pumps such that there is no source term in the equation above.

Now we can apply the procedure outlined and promote these two equations to the desired Heisenberg-Langevin equations (for convenience we have chosen to index the Heisenberg noise source operator with the corresponding system operators)

$$\frac{d}{dt}p_{j\boldsymbol{k}} = -i\tilde{\omega}_{\boldsymbol{k}}p_{j\boldsymbol{k}} + g_{\boldsymbol{k}}\mathcal{P}_{\boldsymbol{k}_{p_1}}\mathcal{P}_{\boldsymbol{k}_{p_2}}p_{j\boldsymbol{k}_i} + F_{p_{\boldsymbol{k}}} \tag{21}$$

$$\frac{d}{dt}p^\dagger_{j_i\boldsymbol{k}_i} = i\tilde{\omega}_{\boldsymbol{k}_i}p_{j_i\boldsymbol{k}_i} + g^*_{\boldsymbol{k}}\mathcal{P}_{\boldsymbol{k}_{p_1}}\mathcal{P}_{\boldsymbol{k}_{p_2}}p_{j\boldsymbol{k}} + F^\dagger_{p_{\boldsymbol{k}_i}}. \tag{22}$$

In order to close the equations we still need to compute some representation of the Langevin noise source operators. Even though no direct formula for $F_{p_{\boldsymbol{k}}}$ is derived in [17] the second moments are computed to be

$$\begin{aligned}
2\mathrm{tr}_R D_{p^\dagger_{j\boldsymbol{k}}p_{j\boldsymbol{k}}} &= \sum_{\boldsymbol{k}'} W_{\boldsymbol{k},\boldsymbol{k}'}\langle p^\dagger_{j\boldsymbol{k}}p_{j\boldsymbol{k}}\rangle_{PL} \\
2\mathrm{tr}_R D_{p_{j\boldsymbol{k}}p^\dagger_{j\boldsymbol{k}}} &= \sum_{\boldsymbol{k}'}\left[W_{\boldsymbol{k},\boldsymbol{k}'}\left(\langle p^\dagger_{j\boldsymbol{k}}p_{j\boldsymbol{k}}\rangle_{PL} + 1\right) + \gamma^c_{\boldsymbol{k}}\right],
\end{aligned}$$

where $W_{\boldsymbol{k},\boldsymbol{k}'}$ are the scattering rates from a polariton with wavevector $\boldsymbol{k}$ to a polariton with wavevector $\boldsymbol{k}'$. We use the term $\langle p^\dagger_{j\boldsymbol{k}} p_{j\boldsymbol{k}}\rangle_{PL}$ to denote the population due to pump induced photoluminescence. The simulations we conduct will use pump induced phonon scattering (as described in [14]) which is the dominant channel for decoherence.

In the next section we will discover that the knowledge of $\langle p^\dagger_{j\boldsymbol{k}} p_{j\boldsymbol{k}}\rangle_{PL}$ is sufficient for computing the density matrix resulting from the equations of motion.

2.5 Solution of the equations of motion

Our starting point of the present discussion are the Heisenberg-Langevin equations given in (21) and (22). For a given wavevector $\boldsymbol{k}$ and the corresponding idler $\boldsymbol{k}_i$ these equations are a set of coupled differential equations of order 1. For notational simplicity we will use a subscript s and i to denote the signal and idler respectively. Then we can write the two equation in matrix form as

$$\frac{d}{dt}\begin{bmatrix} p_s \\ p_i^\dagger \end{bmatrix} = \mathcal{M}(t)\begin{bmatrix} p_s \\ p_i^\dagger \end{bmatrix} + \begin{bmatrix} F_s \\ F_i \end{bmatrix},$$

with

$$\mathcal{M}(t) = -i\begin{bmatrix} -i\tilde{\omega}_s & -i\Delta(t) \\ i\Delta^*(t) & i\tilde{\omega}_i^* \end{bmatrix},$$

where

$$\Delta(t) = g_{\boldsymbol{k}}\mathcal{P}_{\boldsymbol{k}_{p_1}}(t)\mathcal{P}_{\boldsymbol{k}_{p_2}}(t)e^{-i\left(\omega_{\boldsymbol{k}_{p_1}}+\omega_{\boldsymbol{k}_{p_2}}\right)}.$$

Formally we can write the solution as

$$\begin{bmatrix} p_s(t) \\ p_i^\dagger(t) \end{bmatrix} = e^{\int_0^t dt'\,\mathcal{M}(t')}\begin{bmatrix} p_s(0) \\ p_i^\dagger(0) \end{bmatrix} + \int_0^t dt'\, e^{\int_{t'}^t dt''\,\mathcal{M}(t'')}\begin{bmatrix} F_s(t') \\ F_i(t') \end{bmatrix},$$

where this expression is exact if $[\mathcal{M}(t_1),\mathcal{M}(t_2)] = 0$ for all times t_1 and t_2. However, in line with [15] we proceed with the above expression.

Computing the matrix exponentials and forming the corresponding population averages we get (see [14])

$$\begin{aligned} N_s(t) = {} & |c_1^s(0,t)|^2 N_s(0) + |c_2^s(0,t)|^2\,(N_i(0)+1) \\ & + \int_0^t d\tau\,|c_1^s(\tau,t)|^2 \sum_{\boldsymbol{k}'} W_{s,\boldsymbol{k}'} N^{PL}_{\boldsymbol{k}'}(\tau) \\ & + \int_0^t d\tau\,|c_2^s(\tau,t)|^2 \left(\sum_{\boldsymbol{k}'} W_{i,\boldsymbol{k}'} N^{PL}_{\boldsymbol{k}'}(\tau) + \gamma_i^{(c)}\right) \end{aligned} \tag{23}$$

and for the correlations

$$\begin{aligned} \langle P_s^\dagger(t_1)P_i^\dagger(t_2)\rangle = {} & c_1^s(0,t_1)^* c_2^i(0,t_2) N_s(0) + c_2^s(0,t_1)^* c_1^i(0,t_2)\,(N_i(0)+1) \\ & + \int_0^{\min(t_1,t_2)} du\, c_1^s(u,t_1) c_2^i(u,t_2)^* \left(\sum_{\boldsymbol{k}'} W_{s,\boldsymbol{k}'}\left(N^{PL}_{\boldsymbol{k}'}(u)+1\right) + \gamma_s^{(c)}\right) \\ & + \int_0^{\min(t_1,t_2)} du\, c_2^s(u,t_1) c_1^i(u,t_2)^* \sum_{\boldsymbol{k}'} N^{PL}_{\boldsymbol{k}'}(u) \end{aligned} \tag{24}$$

with

$$c_1^s(t_1,t_2) = \alpha_1(t_1,t_2)\int_{t_1}^{t_2} d\tau\,(-i\tilde{\omega}_s) + \alpha_0(t_1,t_2)$$
$$c_2^s(t_1,t_2) = \alpha_1(t_1,t_2)\int_{t_1}^{t_2} d\tau\,\Delta(s,\tau)$$

and

$$\alpha_0(t_1,t_2) = \frac{\Lambda_+(t_1,t_2)e^{\Lambda_-(t_1,t_2)} - \Lambda_-(t_1,t_2)e^{\Lambda_+(t_1,t_2)}}{\Lambda_+(t_1,t_2) - \Lambda_-(t_1,t_2)}$$
$$\alpha_1(t_1,t_2) = \frac{e^{\Lambda_+(t_1,t_2)} - e^{\Lambda_-(t_1,t_2)}}{\Lambda_+(t_1,t_2) - \Lambda_-(t_1,t_2)}$$
$$\Lambda_\pm(t_1,t_2) = \int_{t_1}^{t_2} \lambda_\pm(\tau)\,d\tau$$
$$\lambda_\pm(\tau) = \omega^+ \pm \sqrt{(\omega^-)^2 + |\Delta(\tau)|^2}$$
$$\omega^\pm = \frac{\overline{\omega}_{\boldsymbol{k}} \pm \overline{\omega}^*_{\boldsymbol{k}_i}}{2}.$$

Now in the actual experiment we want to measure the coincidence (from which for example the entanglement of formation can be computed). In the canonical $\{|+\rangle, |-\rangle\}$ basis this is equivalent to the two-particle density matrix

$$\rho_{\sigma\tilde{\sigma},\sigma'\tilde{\sigma}'} = \frac{1}{\mathcal{N}}\int_{T_d} \mathrm{d}t_1 \int_{T_d} \mathrm{d}t_2\,\langle P^\dagger_{s\sigma}(t_1)P^\dagger_{i\tilde{\sigma}}(t_2)P_{i\tilde{\sigma}'}(t_2)P_{s\sigma'}(t_1)\rangle, \tag{25}$$

where T_d is the detector window and we have used the shorthand $P_{s\sigma} = P_{\boldsymbol{k}\sigma}$ and $P_{i\sigma} = P_{\boldsymbol{k}_i\sigma}$. We employ the Wick factorization for bosons to compute the integrand in equation (25); this results in the following expression

$$\begin{aligned}\langle P^\dagger_{s\sigma}(t_1)P^\dagger_{i\tilde{\sigma}}(t_2)P_{i\tilde{\sigma}'}(t_2)P_{s\sigma'}(t_1)\rangle &= \langle P^\dagger_{s\sigma}(t_1)P_{s\sigma'}(t_1)\rangle\langle P^\dagger_{i\tilde{\sigma}}(t_2)P_{i\tilde{\sigma}'}(t_2)\rangle - \langle P^\dagger_{s\sigma}(t_1)P_{i\tilde{\sigma}'}(t_2)\rangle\langle P^\dagger_{i\tilde{\sigma}}(t_2)P_{s\sigma'}(t_1)\rangle \\ &\quad + \langle P^\dagger_{s\sigma}(t_1)P^\dagger_{i\tilde{\sigma}}(t_2)\rangle\langle P_{i\tilde{\sigma}'}(t_2)P_{s\sigma'}(t_1)\rangle \\ &= \langle P^\dagger_{s\sigma}(t_1)P_{s\sigma'}(t_1)\rangle\langle P^\dagger_{i\tilde{\sigma}}(t_2)P_{i\tilde{\sigma}'}(t_2)\rangle + \langle P^\dagger_{s\sigma}(t_1)P^\dagger_{i\tilde{\sigma}}(t_2)\rangle\langle P_{i\tilde{\sigma}'}(t_2)P_{s\sigma'}(t_1)\rangle.\end{aligned}$$

Since a parametric scattering process conserves spin it is evident that not all matrix elements are different from zero. In fact, we get a non-zero value if and only if

$$(\sigma = \tilde{\sigma}) \wedge (\sigma' = \tilde{\sigma}')$$

or

$$(\sigma = \sigma') \wedge (\tilde{\sigma} = \tilde{\sigma}')\,.$$

This gives a total of 6 combinations (since $\sigma, \tilde{\sigma}, \sigma', \tilde{\sigma}' = +$ and $\sigma, \tilde{\sigma}, \sigma', \tilde{\sigma}' = -$ satisfy both conditions, i.e. we have $8 - 2 = 6$ combinations). If we employ the cross-linearly polarized pump scheme described in section (2.3.2), we can deduce from the Hamiltonian given in equation (20) that

$$\langle P^\dagger_{s+}(t_1)P^\dagger_{i+}(t_2)\rangle = -e^{4i\theta}\langle P^\dagger_{s-}(t_1)P^\dagger_{i-}(t_2)\rangle$$
$$\langle P^\dagger_{s+}(t_1)P^\dagger_{i-}(t_2)\rangle = \langle P^\dagger_{s-}(t_1)P^\dagger_{i+}(t_2)\rangle.$$

In addition, the populations of spin up and spin down polaritons are equal. Thus we get three additional relations between the entries in the density matrix

$$\begin{aligned}\rho_{++,++} &= \rho_{--,--}\\ \rho_{+-,+-} &= \rho_{-+,-+}\\ \rho_{++,--} &= \rho^*_{--,++}\end{aligned}$$

which leaves a total of 3 parameters that are to be determined. Those can be conveniently represented by the population and correlations

$$\begin{aligned}\rho_{++,++} &= \frac{1}{\mathcal{N}}\int_{T_d}\mathrm{d}t_1\int_{T_d}\mathrm{d}t_2\,\left[N_s(t_1)N_i(t_2)+\langle P^\dagger_{s+}(t_1)P^\dagger_{i+}(t_2)\rangle\langle P_{s+}(t_1)P_{i+}(t_2)\rangle\right]\\ \rho_{+-,+-} &= \frac{1}{\mathcal{N}}\int_{T_d}\mathrm{d}t_1\int_{T_d}\mathrm{d}t_2\,N_s(t_1)N_i(t_2)\\ \rho_{++,--} &= \frac{1}{\mathcal{N}}\int_{T_d}\mathrm{d}t_1\int_{T_d}\mathrm{d}t_2\,\langle P^\dagger_{s+}(t_1)P^\dagger_{i+}(t_2)\rangle\langle P_{s-}(t_1)P_{i-}(t_2)\rangle,\end{aligned}$$

where the normalization constant is given by summing the diagonal terms; that is

$$\mathcal{N}=\int_{T_d}\mathrm{d}t_1\int_{T_d}\mathrm{d}t_2\,\left[4N_s(t_1)N_i(t_2)+2\langle P^\dagger_{s+}(t_1)P^\dagger_{i+}(t_2)\rangle\langle P_{s+}(t_1)P_{i+}(t_2)\rangle\right].$$

Finally, writing out the density matrix explicitly gives

$$\rho=\frac{1}{\mathcal{N}}\begin{bmatrix}\rho_{++,++} & 0 & 0 & \rho^*_{++,--}\\ 0 & \rho_{+-,+-} & 0 & 0\\ 0 & 0 & \rho_{-+,-+} & 0\\ \rho_{++,--} & 0 & 0 & \rho_{--,--}\end{bmatrix}.$$

Thus, we have succeeded to give a complete description of the system under consideration. However, equations (23) and (24) can, in general, not be solved analytically.

2.6 A steady state calculation

The explicit solutions of the populations (23) and correlations (24) can be used to calculate the density matrix. However, an analytic solution is only available if a sufficiently simple model is used to determine the photoluminescence $N^{PL}_{\boldsymbol{k}'}(\tau)$. For example, if we include pump induced photoluminescence, i.e. noise from polaritons that are created by the pump and diffuse by phonon scattering, the only viable approach is to solve the equations numerically.

However, if we assume a uniform noise background we can compute an analytic solution for the steady state. A steady state obviously requires that we pump at a constant intensity for some time. This is obviously not desirable in an experimental setup since pump induced photoluminescence (which is neglected in this section) would destroy the entanglement. Nevertheless, the analytic result derived here is interesting as it can be seen as the zero temperature case where the uniform noise background models detector noise and other imperfections in the experimental setup that are essentially independent of the pump and signal/idler wavevector. Note that a similar model has been considered in [18].

We will denote the value of the uniform background population by n; that is, we set $\langle F^\dagger_k(t_1)F_k(t_2)\rangle = \Gamma n\delta(t_1-t_2)$ and $\langle F_k(t_1)F^\dagger_k(t_2)\rangle=\Gamma(n+1)\delta(t_1-t_2))$, where Γ is the decay width (which is also assumed to be independent of the wavevector). Putting all assumptions together we get (from equations (23) and (24))

for the population

$$\begin{aligned} N_s(t) = |c_1^s(0,t)|^2 N_s(0) + |c_2^s(0,t)|^2 \left(N_i(0)+1\right) \\ + \Gamma n \int_0^t d\tau \, |c_1^s(\tau,t)|^2 \\ + \Gamma \left(n+1\right) \int_0^t d\tau \, |c_2^s(\tau,t)|^2 \end{aligned}$$

and for the correlation

$$\begin{aligned} \langle P_s^\dagger(t_1) P_i^\dagger(t_2)\rangle = c_1^s(0,t_1)^* c_2^i(0,t_2) N_s(0) + c_2^s(0,t_1)^* c_1^i(0,t_2)\left(N_i(0)+1\right) \\ + \Gamma n \int_0^{\min(t_1,t_2)} du \, c_1^s(u,t_1) c_2^i(u,t_2)^* \\ + \Gamma(n+1) \int_0^{\min(t_1,t_2)} du \, c_2^s(u,t_1) c_1^i(u,t_2)^*, \end{aligned}$$

where

$$\begin{aligned} c_1(t_1,t_2) &= e^{\left(-i\omega - \frac{\Gamma}{2}\right)(t_2-t_1)} \cosh\left(\Delta(t_2-t_1)\right) \\ c_2(t_1,t_2) &= e^{\left(-i\omega - \frac{\Gamma}{2}\right)(t_2-t_1)} \sinh\left(\Delta(t_2-t_1)\right). \end{aligned}$$

The pump as well as the coupling strength enters into those equations via the Δ parameter which is given by

$$\Delta = g\mathcal{P}_1\mathcal{P}_2,$$

where $\mathcal{P}_1, \mathcal{P}_2$ are the pump-induced polariton populations (and are thus constant in time).

Note that this discussion implies that the solution of the steady state only depends on three parameters. Thus, any system can be characterized by specifying the decay width Γ, the noise background n, and Δ which combines the pump and coupling strength. However, this is a clear sign of the insufficiency of the model as there is no way to make a determination of the merit of a given scheme. Thus, the formulas derived in this section are equally applicable to the double cavity case for example (which we will see in the subsequent discussion has some advantages over the single cavity if phonon induced photoluminescence is considered).

Let us now (in line with the steady state assumption) take the limit of $t \to \infty$. Then the explicit expressions for the population and correlation (assuming that $N_s(0) = N_i(0) = 0$) are given by

$$\begin{aligned} N_s(t) = N_i(t) &= \frac{n\Gamma^2 + 2\Delta^2}{\Gamma^2 - 4\Delta^2} \\ \langle P_s^\dagger(t_1) P_s^\dagger(t_2)\rangle = \langle P_s^\dagger(t_1) P_s^\dagger(t_2)\rangle &= \frac{(1+2n)\Gamma\Delta}{\Gamma^2 - 4\Delta^2}. \end{aligned}$$

From this we get an analytic expression of the density matrix

$$\rho = \frac{1}{16\Delta^4 + 4\Gamma^4 n^2 + 2\Gamma^2\Delta^2(4n(n+3)+1)} \cdot \begin{bmatrix} 4\Delta^4 + \Gamma^4 n^2 + \Gamma^2\Delta^2(4n(n+2)+1) & 0 & 0 & \Gamma^2\Delta^2 e^{-4i\theta}(2n+1)^2 \\ 0 & \left(2\Delta^2 + \Gamma^2 n\right)^2 & 0 & 0 \\ 0 & 0 & \left(2\Delta^2 + \Gamma^2 n\right)^2 & 0 \\ \Gamma^2\Delta^2 e^{4i\theta}(2n+1)^2 & 0 & 0 & 4\Delta^4 + \Gamma^4 n^2 + \Gamma^2\Delta^2(4n(n+2)+1) \end{bmatrix}.$$

If we fix the timescale by setting $\Gamma = 1$ we are left with two parameters and the angle θ. The parameter Δ is then understood as the pump/coupling parameter divided by Γ. As expected the parameter Δ is now

unitless as gP_1P_2 has units of s^{-1}. The density matrix is then given by

$$\rho = \frac{1}{16\Delta^4 + 2(4n(n+3)+1)\Delta^2 + 4n^2} \cdot \begin{bmatrix} 4\Delta^4 + (4n(n+2)+1)\Delta^2 + n^2 & 0 & 0 & e^{-4i\theta}(2n\Delta + \Delta)^2 \\ 0 & \left(2\Delta^2 + n\right)^2 & 0 & 0 \\ 0 & 0 & \left(2\Delta^2 + n\right)^2 & 0 \\ e^{4i\theta}(2n\Delta + \Delta)^2 & 0 & 0 & 4\Delta^4 + (4n(n+2)+1)\Delta^2 + n^2 \end{bmatrix}.$$

To measure the degree of entanglement we chose the entanglement of formation. Even though it would be, in principle, possible to diagonalize the above-mentioned matrix (this is necessary to compute the entanglement of formation) this still results in a formula that is complicated at best. However, the essential results are readily accessible, if we plot the entanglement of formation (which is independent of θ) as a function of n and Δ (see Figure (6)). The formula for computing the entanglement of formation is given in appendix (A).

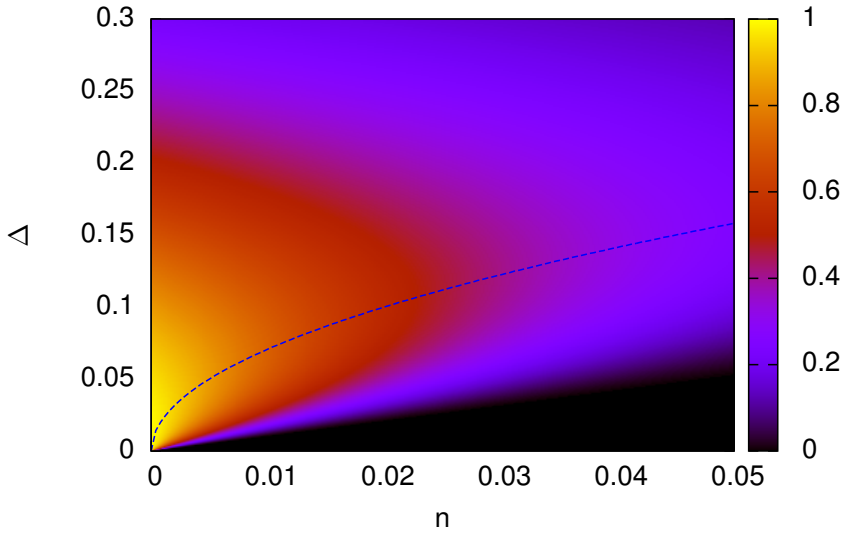

Figure 6: The entanglement of formation as a function of the background noise n and the pump/coupling strength Δ is shown. The blue dashed line gives the necessary pump intensity such that the the entanglement of formation is maximized for a fixed noise background.

It is no surprise that the higher the noise background the harder we have to pump and that the maximal achievable entanglement of formation decreases with increasing noise background. It should, however, be noted that even though no photoluminescence (and thus no temperature effects) is included in this model the entanglement is already significantly reduced not only for moderate values of n but also for moderate values of the pump intensity. Also the pump intensity that is needed to achieve the maximal entanglement of formation for a fixed noise background is not a linear function of n.

The reduction in entanglement for increasing pump intensities can also be observed if we consider the case $n = 0$, i.e. no background noise is present. In this case the density matrix simplifies to

$$\rho = \frac{1}{8\Delta^2 + 1} \begin{bmatrix} \frac{1}{2} + 4\Delta^2 & 0 & 0 & \frac{1}{2}e^{-4i\theta} \\ 0 & 2\Delta^2 & 0 & 0 \\ 0 & 0 & 2\Delta^2 & 0 \\ \frac{1}{2}e^{4i\theta} & 0 & 0 & \frac{1}{2} + 4\Delta^2 \end{bmatrix}.$$

In Figure 7 the entanglement of formation computed from this density matrix is shown as a function of Δ. Although this looks like an exponential decay, the rate for $\Delta \to \infty$ is only quadratic. Nevertheless, after initially (low pump intensities) a high degree of entanglement is observed it diminishes quite rapidly with increasing Δ; this is primarily due to the creation of multiple pairs in the same mode. If we add a background noise this will also set a lower bound on the possible pump intensity as expected. This is illustrated in Figure 7.

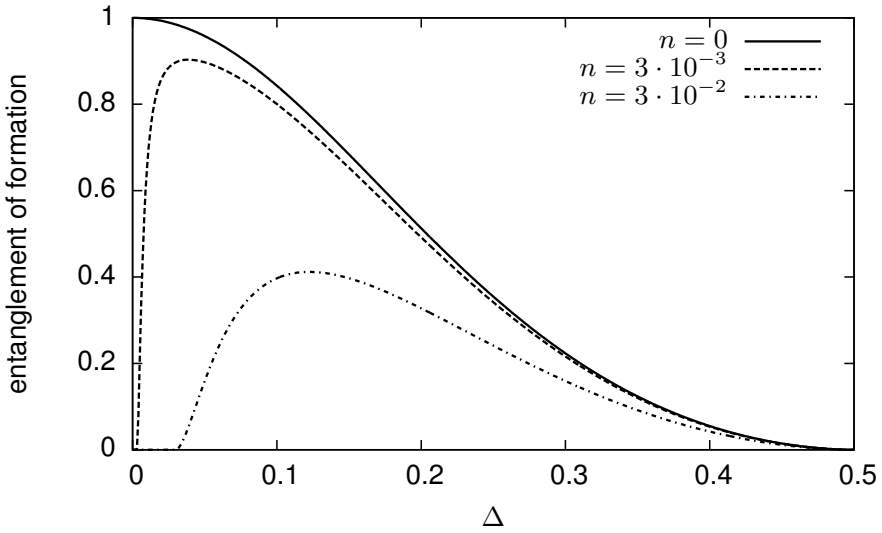

Figure 7: The entanglement of formation is shown as a function of the pump intensity for different (but fixed) levels of background noise.

Figure 6 and 7 already show the interesting features of the steady state model discussed in this section. However, an analytic formula would be quite useful in some circumstance. Since we are mainly interested in systems where the background noise is small (both compared to the pump intensity and in absolute magnitude) one might be tempted to expand the exact formula for the entanglement of formation in a Taylor series at $n = 0$, for example. A good approximation for a fixed Δ and $n \in [0, 0.01]$ already requires a polynomial of degree 5 in n. However, such a procedure is not sufficient as the resulting coefficients are still quite complicated functions of Δ.

Therefore, let us try a different approach. The computation the concurrence $C(\rho)$ as given in Appendix A is relatively straightforward and $C(\rho)$ is given by

$$C(\rho) = \begin{cases} 0 & \Delta \leq n \\ \frac{\left(4\Delta^2-1\right)(n-\Delta)(\Delta+n)}{8\Delta^4+2n^2+\Delta^2(4n(n+3)+1)} & \text{otherwise} \end{cases}.$$

The quantity $C(\rho)$ is a measure of entanglement of its own (see e.g. [20]). To get the entanglement of formation we have to compute

$$h\left(\frac{1-\sqrt{1-C(\rho)^2}}{2}\right),$$

where

$$h(x) = -x \log_2 x - (1-x)\log_2(1-x).$$

Now, if we consider

$$h\left(\frac{1-\sqrt{1-x}}{2}\right)$$

as a function in x we deduce from Figure 8 that, besides for small values of entanglement, it can be approximated to good agreement by a polynomial of degree one[1].

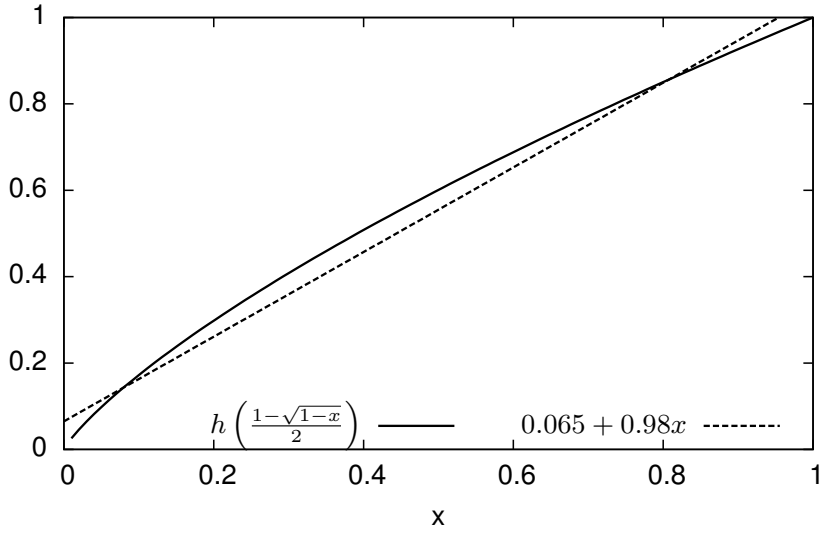

Figure 8: Comparison of $h\left(\frac{1-\sqrt{1-x}}{2}\right)$ with a fitted line. The absolute error is smaller than 0.05.

Using this approximation we get for the entanglement of formation $E(\rho)$ the following approximation (for $\Delta > n$)

$$E(\rho) \approx 0.065 + \frac{0.98\left(4\Delta^2-1\right)^2\left(n^2-\Delta^2\right)^2}{\left(2n^2+(1+4n(3+n))\Delta^2+8\Delta^4\right)^2}.$$

We can further approximate this expression by

$$E(\rho) \approx 0.065 + \frac{0.98\left(n^2-\Delta^2\right)^2}{\left(2n^2+(1+12n)\Delta^2+8\Delta^4\right)^2},$$

where we have used that $\left(4\Delta^4-1\right)\left(n^2-\Delta^2\right)^2 \approx \left(n^2-\Delta^2\right)^2$ and $n^2\Delta^2 \ll n\Delta^2$. The absolute error of this approximation is smaller than 0.063. Thus, we have found an approximation to the entanglement of formation that captures the qualitative (and to some extent the quantitative) behavior observed in Figure 6 and 7.

2.7 Polariton dispersion in a double cavity

We turn our attention now to the double cavity case; that is, two cavities stacked on top of each other where each cavity contains a single quantum well. A schematic illustration is given in Figure (9).

[1]For better accuracy we could also employ a polynomial of higher degree. However, since our goal is to derive a simple representation that captures the essential qualitative features of the solution, a first degree approximation is a good compromise between accuracy and simplicity.

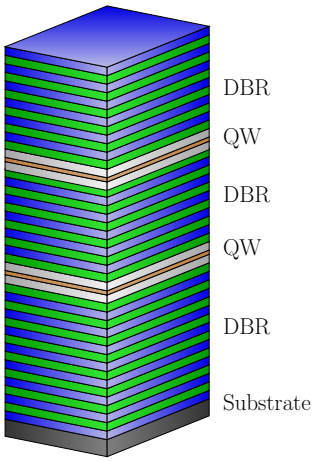

Figure 9: Schematic description of a double cavity. The distributed Bragg reflectors separate the two cavities; each includes a single quantum well.

In this situation we have a trapped photon in cavity 1 and in cavity 2 as well as an exciton in quantum well 1 and in quantum well 2 (as illustrated in Figure).

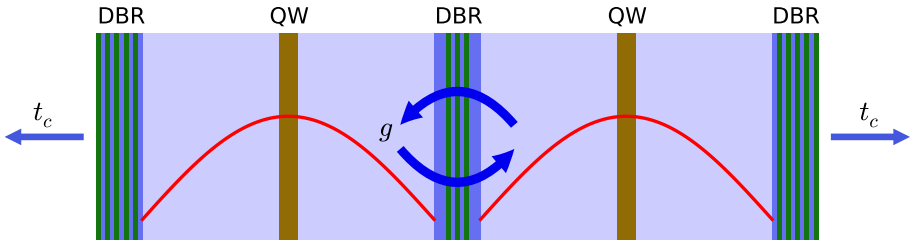

Figure 10: A sketch of the photon mode is shown alongside the structure of a double cavity. The cavity-cavity coupling coefficient g and the transmission coefficient t_c are indicated.

The Hamiltonian in the basis of the excitons/photons located in the first/second cavity/quantum well then takes the form

$$H_{12} = \begin{pmatrix} E_{e_1}(\mathbf{k}) & \hbar\Omega_1 & 0 & 0 \\ \hbar\Omega_1 & E_{c_1}(\mathbf{k}) & 0 & -g \\ 0 & 0 & E_{e_2}(\mathbf{k}) & \hbar\Omega_2 \\ 0 & -g & \hbar\Omega_2 & E_{c_2}(\mathbf{k}) \end{pmatrix}, \tag{26}$$

where g is the coupling constant between the two cavities and the subscripts denote the cavity/quantum well index. In general we can consider $\Omega_1 \neq \Omega_2$; however, to simplify the notations as well as the computations significantly we will assume that the two cavities have the same Rabi splitting (which we denote by Ω in the subsequent discussion) as well as the same photon and exciton dispersion.

First, we will transform the above Hamiltonian in a block diagonal form

$$H_{sa} = UH_{12}U^{-1} = \begin{pmatrix} E_e(\mathbf{k}) & \hbar\Omega_1 & 0 & 0 \\ \hbar\Omega_1 & E_c(\mathbf{k}) - g & 0 & 0 \\ 0 & 0 & E_e(\mathbf{k}) & \hbar\Omega_2 \\ 0 & 0 & \hbar\Omega_2 & E_c(\mathbf{k}) + g \end{pmatrix},$$

where

$$U = U^{-1} = \frac{1}{\sqrt{2}} \begin{pmatrix} 1 & 0 & 1 & 0 \\ 0 & 1 & 0 & 1 \\ 1 & 0 & -1 & 0 \\ 0 & 1 & 0 & -1 \end{pmatrix}. \tag{27}$$

Physically speaking we can interpret the transformation U as a change of basis to the symmetric and antisymmetric combinations of excitons and photons. Mathematically speaking

$$\begin{pmatrix} |\mathrm{X_s}\rangle \\ |\mathrm{P_s}\rangle \\ |\mathrm{X_a}\rangle \\ |\mathrm{P_a}\rangle \end{pmatrix} = U \begin{pmatrix} |\mathrm{X}_1\rangle \\ |\mathrm{P}_1\rangle \\ |\mathrm{X}_2\rangle \\ |\mathrm{P}_2\rangle \end{pmatrix} = \begin{pmatrix} \frac{|\mathrm{X}_1\rangle + |\mathrm{X}_2\rangle}{\sqrt{2}} \\ \frac{|\mathrm{P}_1\rangle + |\mathrm{P}_1\rangle}{\sqrt{2}} \\ \frac{|\mathrm{X}_1\rangle - |\mathrm{X}_2\rangle}{\sqrt{2}} \\ \frac{|\mathrm{P}_1\rangle - |\mathrm{P}_2\rangle}{\sqrt{2}} \end{pmatrix},$$

where $|\mathrm{P}_1\rangle$, $|\mathrm{P}_2\rangle$ are the photon states (not to be confused with the lower case $|\mathrm{p}\rangle$ which is a polariton state) and $|\mathrm{X}_1\rangle$, $|\mathrm{X}_2\rangle$ are the exciton states of the cavity/quantum well specified by the subscript.

Since the matrix can now be decoupled into two systems that exhibit the same characteristics as a single cavity with the photon energy shifted by $-g$ and g respectively we can compute the polariton states easily. First, the dispersion relation of the four polariton branches are given by

$$E_1(\mathbf{k}) = \frac{E_c(\mathbf{k}) + E_e(\mathbf{k}) - g - \sqrt{(E_c(\mathbf{k}) - E_e(\mathbf{k}) - g)^2 + 4\hbar^2\Omega^2}}{2} \tag{28}$$

$$E_2(\mathbf{k}) = \frac{E_c(\mathbf{k}) + E_e(\mathbf{k}) + g - \sqrt{(E_c(\mathbf{k}) - E_e(\mathbf{k}) + g)^2 + 4\hbar^2\Omega^2}}{2} \tag{29}$$

$$E_3(\mathbf{k}) = \frac{E_c(\mathbf{k}) + E_e(\mathbf{k}) - g + \sqrt{(E_c(\mathbf{k}) - E_e(\mathbf{k}) - g)^2 + 4\hbar^2\Omega^2}}{2} \tag{30}$$

$$E_2(\mathbf{k}) = \frac{E_c(\mathbf{k}) + E_e(\mathbf{k}) + g + \sqrt{(E_c(\mathbf{k}) - E_e(\mathbf{k}) + g)^2 + 4\hbar^2\Omega^2}}{2} \tag{31}$$

where the corresponding eigenstates are

$$\begin{pmatrix} |\mathrm{p}_1\rangle \\ |\mathrm{p}_2\rangle \\ |\mathrm{p}_3\rangle \\ |\mathrm{p}_4\rangle \end{pmatrix} = \begin{pmatrix} c_1 & c_2 & 0 & 0 \\ 0 & 0 & c_3 & c_4 \\ -c_2 & c_1 & 0 & 0 \\ 0 & 0 & -c_4 & c_3 \end{pmatrix} \begin{pmatrix} |\mathrm{X_s}\rangle \\ |\mathrm{P_s}\rangle \\ |\mathrm{X_a}\rangle \\ |\mathrm{P_a}\rangle \end{pmatrix}. \tag{32}$$

The dispersion relation is illustrated in Figure (11). Note that we have now two branches that are below the bare exciton energy. In addition, the two lower branches are such that a pump on the ground state of the second branch, for example, would result in parametric scattering to the first branch. We will discuss the ramifications of this in more detail in the subsequent sections.

For now let us conclude this section by giving the Hopfield coefficients employed in the above relation

$$|c_1(\mathbf{k})|^2 = \frac{1}{2}\left(1 + \frac{E_c(\mathbf{k}) - g - E_x(\mathbf{k})}{\sqrt{(E_c(\mathbf{k}) - g - E_x(\mathbf{k}))^2 + 4\hbar^2\Omega^2}}\right)$$

$$|c_2(\mathbf{k})|^2 = \frac{1}{2}\left(1 - \frac{E_c(\mathbf{k}) - g - E_x(\mathbf{k})}{\sqrt{(E_c(\mathbf{k}) - g - E_x(\mathbf{k}))^2 + 4\hbar^2\Omega^2}}\right)$$

$$|c_3(\mathbf{k})|^2 = \frac{1}{2}\left(1 + \frac{E_c(\mathbf{k}) + g - E_x(\mathbf{k})}{\sqrt{(E_c(\mathbf{k}) + g - E_x(\mathbf{k}))^2 + 4\hbar^2\Omega^2}}\right)$$

$$|c_4(\mathbf{k})|^2 = \frac{1}{2}\left(1 - \frac{E_c(\mathbf{k}) + g - E_x(\mathbf{k})}{\sqrt{(E_c(\mathbf{k}) + g - E_x(\mathbf{k}))^2 + 4\hbar^2\Omega^2}}\right).$$

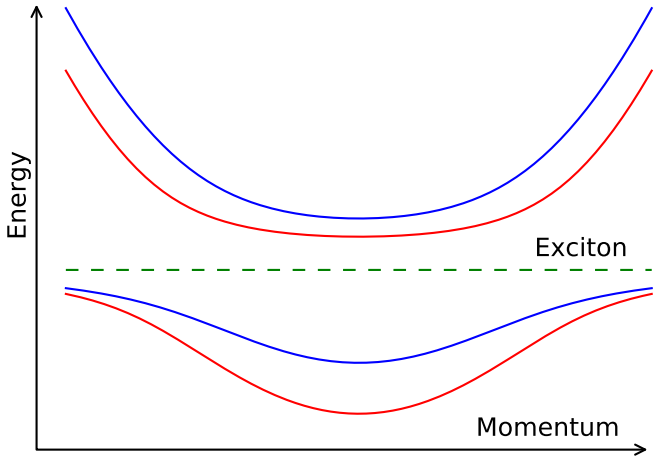

Figure 11: Illustration of the double cavity dispersion relation. The polariton branches are numbered from the bottom to the top (i.e. branch 1 is lowest in energy). The green line is the bare exciton energy.

2.8 Extensions of the equations of motion to the double cavity case

As can be seen in the previous section the double cavity is in some sense quite similar to the single cavity case. Thus we will, in this section, derive the equations of motion in the double cavity case. It will turn out that the form of those equations is the same as in equation (6). Thus, the only difference in this context will be in the coupling parameter.

Nevertheless, we should emphasize that there are two decisive advantages of the double cavity. First, as will be explained in this section the branch index will be conserved in polariton-phonon scattering processes which suppresses phonon induced photoluminescence on the second branch. Second, due to the modification of the dispersion of the two lowest branches there are a number of new pump schemes possible (this is explained in detail in section 3).

As before we will discuss the less complicated Hamiltonian based approach (Ciuti's model) first and then also extend Portolan's model to the double cavity case.

2.8.1 Ciuti's model

Hamiltonian The generalization of the exciton-exciton interaction Hamiltonian is straightforward as the excitons are localized in spatially separated quantum wells; thus, there is no exciton interaction between excitons located in different quantum wells. The Hamiltonian then reads

$$H_{XX} = \sum_{\mathbf{k}\mathbf{k}'\mathbf{q}} \frac{V_{xx}}{2} \left(B^\dagger_{1\mathbf{k}+\mathbf{q}} B^\dagger_{1\mathbf{k}'-\mathbf{q}} B_{1\mathbf{k}} B_{1\mathbf{k}'} + B^\dagger_{2\mathbf{k}+\mathbf{q}} B^\dagger_{2\mathbf{k}'-\mathbf{q}} B_{2\mathbf{k}} B_{2\mathbf{k}'} \right),$$

where $B_{j\boldsymbol{k}}$ is the annihilation operator of a exciton located in quantum well j. Along the same lines we can generalize the saturation Hamiltonian. In this case $a_{j\boldsymbol{k}}$ is the cavity-photon annihilation operator for a photon in cavity j.

$$H^{sat}_{XC} = \sum_{\mathbf{k}\mathbf{k}'\mathbf{q}} \frac{-V}{n_{sat}} \left(a^\dagger_{1\mathbf{k}+\mathbf{q}} B^\dagger_{1\mathbf{k}'-\mathbf{q}} B_{1\mathbf{k}} B_{1\mathbf{k}'} + a^\dagger_{2\mathbf{k}+\mathbf{q}} B^\dagger_{2\mathbf{k}'-\mathbf{q}} B_{2\mathbf{k}} B_{2\mathbf{k}'} + h.c. \right).$$

Now, let us combine equations (27) and (32) to get the transformation between the exciton-photon basis and the polariton basis

$$\begin{pmatrix} |\mathrm{p}_1\rangle \\ |\mathrm{p}_2\rangle \\ |\mathrm{p}_3\rangle \\ |\mathrm{p}_4\rangle \end{pmatrix} = \frac{1}{\sqrt{2}} \begin{pmatrix} c_1 & c_2 & c_1 & c_2 \\ c_3 & c_4 & -c_3 & -c_4 \\ -c_2 & c_1 & -c_2 & c_1 \\ -c_4 & c_3 & c_4 & -c_3 \end{pmatrix} \begin{pmatrix} |\mathrm{X}_1\rangle \\ |\mathrm{P}_1\rangle \\ |\mathrm{X}_2\rangle \\ |\mathrm{P}_2\rangle \end{pmatrix} \tag{33}$$

and

$$\begin{pmatrix} |\mathrm{X}_1\rangle \\ |\mathrm{P}_1\rangle \\ |\mathrm{X}_2\rangle \\ |\mathrm{P}_2\rangle \end{pmatrix} = \frac{1}{\sqrt{2}} \begin{pmatrix} c_1 & c_3 & -c_2 & -c_4 \\ c_2 & c_4 & c_1 & c_3 \\ c_1 & -c_3 & -c_2 & c_4 \\ c_2 & -c_4 & c_1 & -c_3 \end{pmatrix} \begin{pmatrix} |\mathrm{p}_1\rangle \\ |\mathrm{p}_2\rangle \\ |\mathrm{p}_3\rangle \\ |\mathrm{p}_4\rangle \end{pmatrix}, \tag{34}$$

where we have used that $c_1^2 + c_2^2 = c_3^2 + c_4^2 = 1$. Now writing out the relations for the exciton operators we get

$$\begin{aligned} B^\dagger_{1\mathbf{k}} &= \frac{1}{\sqrt{2}} \left(c_{1\mathbf{k}} p^\dagger_{1\mathbf{k}} + c_{3\mathbf{k}} p^\dagger_{2\mathbf{k}} - c_{2\mathbf{k}} p^\dagger_{3\mathbf{k}} - c_{4\mathbf{k}} p^\dagger_{4\mathbf{k}} \right) \\ B^\dagger_{2\mathbf{k}} &= \frac{1}{\sqrt{2}} \left(c_{1\mathbf{k}} p^\dagger_{1\mathbf{k}} - c_{3\mathbf{k}} p^\dagger_{2\mathbf{k}} - c_{2\mathbf{k}} p^\dagger_{3\mathbf{k}} + c_{4\mathbf{k}} p^\dagger_{4\mathbf{k}} \right), \end{aligned}$$

and hence the two terms of H_{XX} can be written as a product of the form

$$\begin{aligned} &\frac{1}{4} \left(\tilde{p}^\dagger_{1\mathbf{k}+\mathbf{q}} + \tilde{p}^\dagger_{4\mathbf{k}+\mathbf{q}} - \tilde{p}^\dagger_{2\mathbf{k}+\mathbf{q}} - \tilde{p}^\dagger_{4\mathbf{k}+\mathbf{q}} \right) \left(\tilde{p}^\dagger_{1\mathbf{k}'-\mathbf{q}} + \tilde{p}^\dagger_{3\mathbf{k}'-\mathbf{q}} - \tilde{p}^\dagger_{2\mathbf{k}'-\mathbf{q}} - \tilde{p}^\dagger_{4\mathbf{k}'-\mathbf{q}} \right) \times \\ &\quad \left(\tilde{p}_{1\mathbf{k}} + \tilde{p}_{3\mathbf{k}} - \tilde{p}_{2\mathbf{k}} - \tilde{p}_{4\mathbf{k}} \right) \left(\tilde{p}_{1\mathbf{k}'} + \tilde{p}_{3\mathbf{k}'} - \tilde{p}_{2\mathbf{k}'} - \tilde{p}_{4\mathbf{k}'} \right) \end{aligned}$$

and

$$\begin{aligned} &\frac{1}{4} \left(\tilde{p}^\dagger_{1\mathbf{k}+\mathbf{q}} - \tilde{p}^\dagger_{3\mathbf{k}+\mathbf{q}} - \tilde{p}^\dagger_{2\mathbf{k}+\mathbf{q}} + \tilde{p}^\dagger_{4\mathbf{k}+\mathbf{q}} \right) \left(\tilde{p}^\dagger_{1\mathbf{k}'-\mathbf{q}} - \tilde{p}^\dagger_{3\mathbf{k}'-\mathbf{q}} - \tilde{p}^\dagger_{2\mathbf{k}'-\mathbf{q}} + \tilde{p}^\dagger_{4\mathbf{k}'-\mathbf{q}} \right) \times \\ &\left(\tilde{p}_{1\mathbf{k}} - \tilde{p}_{3\mathbf{k}} - \tilde{p}_{2\mathbf{k}} + \tilde{p}_{4\mathbf{k}} \right) \left(\tilde{p}_{1\mathbf{k}'} - \tilde{p}_{3\mathbf{k}'} - \tilde{p}_{2\mathbf{k}'} + \tilde{p}_{4\mathbf{k}'} \right), \end{aligned}$$

respectively. Here we introduced the abbreviation $\tilde{p}_{i\boldsymbol{k}} = c_{\tilde{i}\mathbf{k}} p_{i\mathbf{k}}$ with

$$\tilde{i} = \begin{cases} i & i \in \{1, 4\} \\ 3 & i = 2 \\ 2 & i = 3 \end{cases}.$$

Then

$$\begin{aligned} H_{XX} &= \sum_{\mathbf{k}\mathbf{k}'\mathbf{q}} \frac{V_{xx}}{8} \sum_{i,j,k,l} \left\{ (-1)^{\lfloor \frac{i-1}{2} \rfloor + \lfloor \frac{j-1}{2} \rfloor + \lfloor \frac{k-1}{2} \rfloor + \lfloor \frac{l-1}{2} \rfloor} + (-1)^{\lfloor \frac{i}{2} \rfloor + \lfloor \frac{j}{2} \rfloor + \lfloor \frac{k}{2} \rfloor + \lfloor \frac{l}{2} \rfloor} \right\} \tilde{p}^\dagger_{i\mathbf{k}+\mathbf{q}} \tilde{p}^\dagger_{j\mathbf{k}'-\mathbf{q}} \tilde{p}_{k\mathbf{k}} \tilde{p}_{l\mathbf{k}'} \\ &= \sum_{\mathbf{k}\mathbf{k}'\mathbf{q}} \frac{V_{xx}}{8} \sum_{i,j,k,l} (-1)^{\lfloor \frac{i-1}{2} \rfloor + \lfloor \frac{j-1}{2} \rfloor + \lfloor \frac{k-1}{2} \rfloor + \lfloor \frac{l-1}{2} \rfloor} \left\{ 1 + (-1)^{i+j+k+l} \right\} \tilde{p}^\dagger_{i\mathbf{k}+\mathbf{q}} \tilde{p}^\dagger_{j\mathbf{k}'-\mathbf{q}} \tilde{p}_{k\mathbf{k}} \tilde{p}_{l\mathbf{k}'}, \end{aligned}$$

since

$$\left\lfloor \frac{i}{2} \right\rfloor - \left\lfloor \frac{i-1}{2} \right\rfloor = i + 1 \bmod 2.$$

Note that the above equation implies that the scattering amplitude is non-zero only if we require that $i+j+k+l \bmod 2 = 0$. Note that this condition is only satisfied if parity in the scattering process is conserved;

that is, $i+j \bmod 2 = k+l \bmod 2$. The origin of this behavior is the symmetrization/antisymmetrization of the excitons and cavity-photons and gives the double cavity a qualitative feature that is distinct from the single cavity case. Note, for example, that the original branch entanglement scheme devised in [2] for the single cavity violates parity[2]; that is, the scheme can not be implemented by employing the two lowest polariton branches in a double cavity.

In almost all schemes we are going to consider, we will exclusively use the two lower branches. In this case we can further simplify the expression above to get

$$H_{XX} = \sum_{\mathbf{k}\mathbf{k}'\mathbf{q}} \frac{V_{xx}}{8} \sum_{i,j,k,l} \left\{1 + (-1)^{i+j+k+l}\right\} \tilde{p}^\dagger_{i\mathbf{k}+\mathbf{q}} \tilde{p}^\dagger_{j\mathbf{k}'-\mathbf{q}} \tilde{p}_{k\mathbf{k}} \tilde{p}_{l\mathbf{k}'}.$$

For the saturation term H^{sat}_{XC} we in addition have to employ the following relations

$$a^\dagger_{1\mathbf{k}} = \frac{1}{\sqrt{2}} \left(c_{2\mathbf{k}} p^\dagger_{1\mathbf{k}} + c_{4\mathbf{k}} p^\dagger_{2\mathbf{k}} + c_{1\mathbf{k}} p^\dagger_{3\mathbf{k}} + c_{3\mathbf{k}} p^\dagger_{4\mathbf{k}} \right)$$
$$a^\dagger_{2\mathbf{k}} = \frac{1}{\sqrt{2}} \left(c_{2\mathbf{k}} p^\dagger_{1\mathbf{k}} - c_{4\mathbf{k}} p^\dagger_{2\mathbf{k}} + c_{1\mathbf{k}} p^\dagger_{3\mathbf{k}} - c_{3\mathbf{k}} p^\dagger_{4\mathbf{k}} \right)$$

which gives us

$$H^{sat}_{XC} = \sum_{\mathbf{k}\mathbf{k}'\mathbf{q}} \frac{-V}{4n_{sat}} \sum_{i,j,k,l} (-1)^{\lfloor \frac{j-1}{2} \rfloor + \lfloor \frac{k-1}{2} \rfloor + \lfloor \frac{l-1}{2} \rfloor} \left\{1 + (-1)^{i+j+k+l}\right\} \overline{p}^\dagger{}_{i\mathbf{k}+\mathbf{q}} \tilde{p}^\dagger_{j\mathbf{k}'-\mathbf{q}} \tilde{p}_{k\mathbf{k}} \tilde{p}_{l\mathbf{k}'} + h.c,$$

where $\overline{p}_{i\boldsymbol{k}} = c_{\bar{i}\mathbf{k}} p_{i\mathbf{k}}$ with

$$\bar{i} = \begin{cases} 2 & i = 1 \\ 4 & i = 2 \\ 1 & i = 3 \\ 3 & i = 4 \end{cases}.$$

This once again gives a non-zero scattering rate only if $i+j+k+l \bmod 2 = 0$. Let us once again emphasize that if we stay within branch 1 and 2 (i.e. no scattering to branch 3 and 4) we can simplify this to

$$H^{sat}_{XC} = \sum_{\mathbf{k}\mathbf{k}'\mathbf{q}} \frac{-V}{4n_{sat}} \sum_{i,j,k,l} \left\{1 + (-1)^{i+j+k+l}\right\} \overline{p}^\dagger{}_{i\mathbf{k}+\mathbf{q}} \tilde{p}^\dagger_{j\mathbf{k}'-\mathbf{q}} \tilde{p}_{k\mathbf{k}} \tilde{p}_{l\mathbf{k}'} + h.c.$$

Equations of motion Now it remains (as before) to derive the equations of motion from the Hamiltonian. We proceed as in the single cavity case; that is, we start from the Heisenberg equation and simplify the necessary commutators by assuming bosonic commutation relations. To simplify the notation let us write

$$C_{ijkl} = (-1)^{\lfloor \frac{i-1}{2} \rfloor + \lfloor \frac{j-1}{2} \rfloor + \lfloor \frac{k-1}{2} \rfloor + \lfloor \frac{l-1}{2} \rfloor}$$

[2]For the quantum wire case, also discussed in [2], the parity has to be taken into account. The scheme proposed in this context employs three polariton branches. In the double cavity, however, only two polariton branches are available below the exciton reservoir.

and keep in mind that $C_{ijkl} = 1$ if $i, j, k, l \in \{1, 2\}$. We start with the exciton-exciton interaction and get

$$\begin{aligned}
-\left[H_{XX}, p_{m\mathbf{p}}\right] &= \sum_{\boldsymbol{kk'q}} \frac{-V_{xx}}{8} \sum_{ijkl} C_{ijkl} \left\{1 + (-1)^{i+j+k+l}\right\} c_{\tilde{i}\mathbf{k}+\mathbf{q}} c_{\tilde{j}\mathbf{k}'-\mathbf{q}} c_{\tilde{k}\mathbf{k}} c_{\tilde{l}\mathbf{k}'} \left[p^\dagger_{i\mathbf{k}+\mathbf{q}} p^\dagger_{j\mathbf{k}'-\mathbf{q}} p_{k\mathbf{k}} p_{l\mathbf{k}'}, p_{m\mathbf{p}}\right], \\
&= \sum_{\boldsymbol{kk'q}} \frac{V_{xx}}{8} \sum_{ijkl} C_{ijkl} \left\{1 + (-1)^{i+j+k+l}\right\} c_{\tilde{i}\mathbf{k}+\mathbf{q}} c_{\tilde{j}\mathbf{k}'-\mathbf{q}} c_{\tilde{k}\mathbf{k}} c_{\tilde{l}\mathbf{k}'} \\
&\qquad \left(p^\dagger_{i\mathbf{k}+\mathbf{q}} p_{k\mathbf{k}} p_{l\mathbf{k}'} \delta_{jm} \delta_{\mathbf{k}'-\mathbf{q},\mathbf{p}} + p^\dagger_{j\mathbf{k}'-\mathbf{q}} p_{k\mathbf{k}} p_{l\mathbf{k}'} \delta_{im} \delta_{\mathbf{k}+\mathbf{q},\mathbf{p}}\right) \\
&= \sum_{\boldsymbol{kk'}} \frac{V_{xx}}{4} \sum_{ikl} C_{mjkl} \left\{1 + (-1)^{i+m+k+l}\right\} c_{\tilde{m}\boldsymbol{p}} c_{\tilde{i}\mathbf{k}+\mathbf{k}'-\boldsymbol{p}} c_{\tilde{k}\mathbf{k}} c_{\tilde{l}\mathbf{k}'} p^\dagger_{i\mathbf{k}+\boldsymbol{k}'-\boldsymbol{p}} p_{k\mathbf{k}} p_{l\mathbf{k}'} \qquad (35)
\end{aligned}$$

since

$$\begin{aligned}
\left[p^\dagger_{i\mathbf{k}+\mathbf{q}} p^\dagger_{j\mathbf{k}'-\mathbf{q}} p_{k\mathbf{k}} p_{l\mathbf{k}'}, p_{m\mathbf{p}}\right] &= p^\dagger_{i\mathbf{k}+\mathbf{q}} \left[p^\dagger_{j\mathbf{k}'-\mathbf{q}}, p_{m\mathbf{p}}\right] p_{k\mathbf{k}} p_{l\mathbf{k}'} + \left[p^\dagger_{i\mathbf{k}+\mathbf{q}}, p_{m\mathbf{p}}\right] p^\dagger_{j\mathbf{k}'-\mathbf{q}} p_{k\mathbf{k}} p_{l\mathbf{k}'} \\
&= -p^\dagger_{i\mathbf{k}+\mathbf{q}} p_{k\mathbf{k}} p_{l\mathbf{k}'} \delta_{\mathbf{k}'-\mathbf{q},\mathbf{p}} \delta_{jm} - p^\dagger_{j\mathbf{k}'-\mathbf{q}} p_{k\mathbf{k}} p_{l\mathbf{k}'} \delta_{\mathbf{k}+\mathbf{q},\mathbf{p}} \delta_{im}.
\end{aligned}$$

Second, if we define

$$D_{jkl} = (-1)^{\lfloor \frac{j-1}{2} \rfloor + \lfloor \frac{k-1}{2} \rfloor + \lfloor \frac{l-1}{2} \rfloor}$$

and expand the Hermitian conjugate in the saturation Hamiltonian we get

$$\begin{aligned}
H^{sat}_{XC} &= \sum_{\mathbf{kk'q}} \frac{-V}{4n_{sat}} \sum_{i,j,k,l} \left\{1 + (-1)^{i+j+k+l}\right\} \left[\overline{p}^\dagger{}_{i\mathbf{k}+\mathbf{q}} \tilde{p}^\dagger_{j\mathbf{k}'-\mathbf{q}} \tilde{p}_{k\mathbf{k}} \tilde{p}_{l\mathbf{k}'} + \tilde{p}^\dagger_{l\boldsymbol{k}'} \tilde{p}^\dagger_{k\boldsymbol{k}} \tilde{p}_{j\boldsymbol{k}'-\boldsymbol{q}} \overline{p}_{i\boldsymbol{k}+\boldsymbol{q}}\right] \\
&= \sum_{\mathbf{kk'q}} \frac{-V}{4n_{sat}} \sum_{i,j,k,l} \left\{1 + (-1)^{i+j+k+l}\right\} \left[\overline{p}^\dagger{}_{i\mathbf{k}+\mathbf{q}} \tilde{p}^\dagger_{j\mathbf{k}'-\mathbf{q}} \tilde{p}_{k\mathbf{k}} \tilde{p}_{l\mathbf{k}'} + \tilde{p}^\dagger_{i\boldsymbol{k}+\boldsymbol{q}} \tilde{p}^\dagger_{j\boldsymbol{k}'-\boldsymbol{q}} \tilde{p}_{k\boldsymbol{k}} \overline{p}_{l\boldsymbol{k}'}\right]
\end{aligned}$$

and thus

$$\begin{aligned}
\left[H^{sat}_{XC}, p_{m\mathbf{p}}\right] &= \sum_{\boldsymbol{kk'q}} \frac{-V}{4n_{sat}} \sum_{ijkl} D_{jkl} \left\{1 + (-1)^{i+j+k+l}\right\} \left(c_{\tilde{i}\mathbf{k}+\mathbf{q}} c_{\tilde{j}\mathbf{k}'-\mathbf{q}} c_{\tilde{k}\mathbf{k}} c_{\tilde{l}\mathbf{k}'} + c_{\tilde{i}\mathbf{k}+\mathbf{q}} c_{\tilde{j}\mathbf{k}'-\mathbf{q}} c_{\tilde{k}\mathbf{k}} c_{\overline{l}\mathbf{k}'}\right) \times \\
&\qquad \left[p^\dagger{}_{i\mathbf{k}+\mathbf{q}} p^\dagger_{j\mathbf{k}'-\mathbf{q}} p_{k\mathbf{k}} p_{l\mathbf{k}'}, p_{m\mathbf{p}}\right] \qquad (36) \\
&= \sum_{\boldsymbol{kk'q}} \frac{V}{4n_{sat}} \sum_{ijkl} D_{jkl} \left\{1 + (-1)^{i+j+k+l}\right\} \left(c_{\tilde{i}\mathbf{k}+\mathbf{q}} c_{\tilde{j}\mathbf{k}'-\mathbf{q}} c_{\tilde{k}\mathbf{k}} c_{\tilde{l}\mathbf{k}'} + c_{\tilde{i}\mathbf{k}+\mathbf{q}} c_{\tilde{j}\mathbf{k}'-\mathbf{q}} c_{\tilde{k}\mathbf{k}} c_{\overline{l}\mathbf{k}'}\right) \\
&\qquad \left(p^\dagger_{i\mathbf{k}+\mathbf{q}} p_{k\mathbf{k}} p_{l\mathbf{k}'} \delta_{jm} \delta_{\mathbf{k}'-\mathbf{q},\mathbf{p}} + p^\dagger_{j\mathbf{k}'-\mathbf{q}} p_{k\mathbf{k}} p_{l\mathbf{k}'} \delta_{im} \delta_{\mathbf{k}+\mathbf{q},\mathbf{p}}\right) \\
&= \sum_{\boldsymbol{kk'}} \frac{V}{4n_{sat}} \sum_{ikl} p^\dagger_{i\mathbf{k}+\boldsymbol{k}'-\boldsymbol{p}} p_{k\mathbf{k}} p_{l\mathbf{k}'} \left\{1 + (-1)^{i+m+k+l}\right\} \\
&\left(c_{\tilde{k}\mathbf{k}} c_{\tilde{l}\mathbf{k}'} \left[D_{mkl} c_{\tilde{i}\mathbf{k}+\mathbf{k}'-\mathbf{p}} c_{\tilde{m}\mathbf{p}} + D_{ikl} c_{\overline{m}\boldsymbol{p}} c_{\tilde{i}\boldsymbol{k}+\mathbf{k}'\text{-}\mathbf{p}}\right] + c_{\tilde{k}\mathbf{k}} c_{\overline{l}\mathbf{k}'} c_{\tilde{m}\boldsymbol{p}} c_{\tilde{i}\boldsymbol{k}+\mathbf{k}'\text{-}\mathbf{p}} \left[D_{mkl} + D_{ikl}\right]\right). \qquad (37)
\end{aligned}$$

If we limit ourselves to scattering processes on the first and second polariton branches we can write (for a two pump scheme)

$$\boldsymbol{g}_{\boldsymbol{p}} = V^{ijkl}_{\boldsymbol{kk'p}} + V^{ijkl}_{\boldsymbol{kk'p}}$$

with

$$V^{ijkl}_{\boldsymbol{kk'p}} = \overline{V}^{ijkl}_{\boldsymbol{kk'p}} + \underline{V}^{ijkl}_{\boldsymbol{kk'p}},$$

where

$$\overline{V}^{ijkl}_{\boldsymbol{kk'p}} = \frac{V_{xx}}{4} \left\{1 + (-1)^{i+m+k+l}\right\} c_{\tilde{m}\boldsymbol{p}} c_{\tilde{i}\mathbf{k}+\mathbf{k}'-\boldsymbol{p}} c_{\tilde{k}\mathbf{k}} c_{\tilde{l}\mathbf{k}'} \qquad (38)$$

and thus

$$\underline{V}^{ijkl}_{\boldsymbol{kk'p}} = \frac{V}{4n_{sat}}\left\{1+(-1)^{i+m+k+l}\right\} \tag{39}$$

$$\left(c_{\tilde{k}\mathbf{k}}c_{\tilde{l}\mathbf{k'}}\left[D_{mkl}c_{\tilde{-i}\boldsymbol{k}+\mathbf{k'}-\mathbf{p}}c_{\tilde{m}\mathbf{p}}+D_{ikl}c_{\overline{m}\boldsymbol{p}}c_{\tilde{i}\boldsymbol{k}+\mathbf{k'}\text{-}\mathbf{p}}\right]+c_{\tilde{k}\mathbf{k}}c_{\tilde{l}\mathbf{k'}}c_{\tilde{m}\boldsymbol{p}}c_{\tilde{i}\boldsymbol{k}+\mathbf{k'}\text{-}\mathbf{p}}\left[D_{mkl}+D_{ikl}\right]\right). \tag{40}$$

2.8.2 Portolan's model

Equations of motion Let us now extend Portolan's model to the double cavity case. The extension of the equations given in [16] are straightforward to generalize to the double cavity case (we denote the transmission rate by t_c)

$$\frac{d}{dt}a_{1\boldsymbol{k}} = -iE_{c_1}(\boldsymbol{k})a_{1\boldsymbol{k}}+i\hbar\Omega_1 B_{1\boldsymbol{k}}+t_c\mathscr{E}^{in}_{\boldsymbol{k}}a_{1\boldsymbol{k}}-iga_{2\boldsymbol{k}} \tag{41}$$

$$\frac{d}{dt}B_{1\boldsymbol{k}} = -iE_{e_1}(\boldsymbol{k})B_{1\boldsymbol{k}}+i\hbar\Omega_1 a_{1\boldsymbol{k}}-iR^{NL,1}_{\boldsymbol{k}} \tag{42}$$

$$\frac{d}{dt}a_{2\boldsymbol{k}} = -iE_{c_1}(\boldsymbol{k})a_{2\boldsymbol{k}}+i\hbar\Omega_2 B_{2\boldsymbol{k}}+t_c\mathscr{E}^{in}_{\boldsymbol{k}}a_{2\boldsymbol{k}}-iga_{1\boldsymbol{k}} \tag{43}$$

$$\frac{d}{dt}B_{2\boldsymbol{k}} = -iE_{e_2}(\boldsymbol{k})b_{2\boldsymbol{k}}+i\hbar\Omega_2 B_{2\boldsymbol{k}}-iR^{NL,2}_{\boldsymbol{k}}. \tag{44}$$

Let us, as before, assume that both cavities as well as both quantum well are of the same design. In addition, we rewrite the equation in matrix form; this gives

$$\frac{d}{dt}\begin{pmatrix}B_{1\boldsymbol{k}}\\a_{1\boldsymbol{k}}\\B_{2\boldsymbol{k}}\\a_{2\boldsymbol{k}}\end{pmatrix} = -i\begin{pmatrix}E_e(\mathbf{k})&\hbar\Omega&0&0\\\hbar\Omega&E_c(\mathbf{k})&0&-g\\0&0&E_x(\mathbf{k})&\hbar\Omega\\0&-g&\hbar\Omega&E_c(\mathbf{k})\end{pmatrix}\begin{pmatrix}B_{1\boldsymbol{k}}\\a_{1\boldsymbol{k}}\\B_{2\boldsymbol{k}}\\a_{2\boldsymbol{k}}\end{pmatrix}+\begin{pmatrix}-iR^{NL,1}_{\mathbf{k}}\\0\\-iR^{NL,2}_{\mathbf{k}}\\0\end{pmatrix}+\begin{pmatrix}0\\t_c\mathscr{E}^{in}_{\boldsymbol{k}}a_{1\boldsymbol{k}}\\0\\t_c\mathscr{E}^{in}_{\boldsymbol{k}}a_{2\boldsymbol{k}}\end{pmatrix}. \tag{45}$$

As is readily seen from equation (45) the linear part is exactly the same as in equation (26). Thus, let us use equations (33) and (34) to perform the transformation to the polariton basis.

The nonlinear term gives

$$\frac{1}{\sqrt{2}}\begin{pmatrix}c_1&c_2&c_1&c_2\\c_3&c_4&-c_3&-c_4\\-c_2&c_1&-c_2&c_1\\-c_4&c_3&c_4&-c_3\end{pmatrix}\begin{pmatrix}-iR^{NL,1}_{\mathbf{k}}\\0\\-iR^{NL,2}_{\mathbf{k}}\\0\end{pmatrix} = -\frac{i}{\sqrt{2}}\begin{pmatrix}c_{1\boldsymbol{k}}\left(R^{NL,1}_{\mathbf{k}}+R^{NL,2}_{\mathbf{k}}\right)\\c_{3\boldsymbol{k}}\left(R^{NL,1}_{\mathbf{k}}-R^{NL,2}_{\mathbf{k}}\right)\\-c_{2\boldsymbol{k}}\left(R^{NL,1}_{\mathbf{k}}+R^{NL,2}_{\mathbf{k}}\right)\\c_{4\boldsymbol{k}}\left(-R^{NL,1}_{\mathbf{k}}+R^{NL,2}_{\mathbf{k}}\right)\end{pmatrix} \tag{46}$$

whereas transforming the (classical) source term gives

$$\frac{1}{\sqrt{2}}\begin{pmatrix}c_1&c_2&c_1&c_2\\c_3&c_4&-c_3&-c_4\\-c_2&c_1&-c_2&c_1\\-c_4&c_3&c_4&-c_3\end{pmatrix}\begin{pmatrix}0\\t_c\mathscr{E}^{in}_{\boldsymbol{k}}a_{1\boldsymbol{k}}\\0\\t_c\mathscr{E}^{in}_{\boldsymbol{k}}a_{2\boldsymbol{k}}\end{pmatrix} = t_c\mathscr{E}^{in}_{\boldsymbol{k}}\begin{pmatrix}c_{2\boldsymbol{k}}\left(a_{1\boldsymbol{k}}+a_{2\boldsymbol{k}}\right)\\c_{4\boldsymbol{k}}\left(a_{1\boldsymbol{k}}-a_{2\boldsymbol{k}}\right)\\c_{1\boldsymbol{k}}\left(a_{1\boldsymbol{k}}-a_{2\boldsymbol{k}}\right)\\c_{3\boldsymbol{k}}\left(a_{1\boldsymbol{k}}-a_{2\boldsymbol{k}}\right)\end{pmatrix}. \tag{47}$$

Obviously we still have to express the nonlinearities ($R^{NL,1}_{\boldsymbol{k}}$ and $R^{NL,2}_{\boldsymbol{k}}$) in the polariton basis. To that end we write out the expressions for the exciton/photon operators as a function of the polariton operators. This

yields

$$B_{1\boldsymbol{k}} = \frac{1}{\sqrt{2}}\left(c_{1\boldsymbol{k}}p_{1\boldsymbol{k}} + c_{3\boldsymbol{k}}p_{2\boldsymbol{k}} - c_{2\boldsymbol{k}}p_{3\boldsymbol{k}} - c_{4\boldsymbol{k}}p_{4\boldsymbol{k}}\right) \tag{48}$$

$$B_{2\boldsymbol{k}} = \frac{1}{\sqrt{2}}\left(c_{1\boldsymbol{k}}p_{1\boldsymbol{k}} - c_{3\boldsymbol{k}}p_{2\boldsymbol{k}} - c_{2\boldsymbol{k}}p_{3\boldsymbol{k}} + c_{4\boldsymbol{k}}p_{4\boldsymbol{k}}\right) \tag{49}$$

$$a_{1\boldsymbol{k}} = \frac{1}{\sqrt{2}}\left(c_{2\boldsymbol{k}}p_{1\boldsymbol{k}} + c_{4\boldsymbol{k}}p_{2\boldsymbol{k}} + c_{1\boldsymbol{k}}p_{3\boldsymbol{k}} + c_{3\boldsymbol{k}}p_{4\boldsymbol{k}}\right) \tag{50}$$

$$a_{2\boldsymbol{k}} = \frac{1}{\sqrt{2}}\left(c_{2\boldsymbol{k}}p_{1\boldsymbol{k}} - c_{4\boldsymbol{k}}p_{2\boldsymbol{k}} + c_{1\boldsymbol{k}}p_{3\boldsymbol{k}} - c_{3\boldsymbol{k}}p_{4\boldsymbol{k}}\right) \tag{51}$$

Now we have to rewrite the nonlinearities

$$R_{\boldsymbol{k}}^{NL,1} = R_{\boldsymbol{k}}^{1,xx} + R_{\boldsymbol{k}}^{1,sat}$$
$$R_{\boldsymbol{k}}^{NL,2} = R_{\boldsymbol{k}}^{2,xx} + R_{\boldsymbol{k}}^{2,sat}$$

in terms of the polariton operators as

$$\begin{aligned} R_{\mathbf{k}}^{1,\mathrm{xx}} &= V_{\mathrm{xx}} \sum_{\mathbf{k}_1,\mathbf{k}_2} B^{\dagger}_{1\mathbf{k}_1+\mathbf{k}_2-\mathbf{k}} B_{1\boldsymbol{k}_1} B_{1\boldsymbol{k}_2} \\ &= \frac{V_{\mathrm{xx}}}{2\sqrt{2}} \sum_{\mathbf{k}_1,\mathbf{k}_2} \Big\{ \left(c_{1\boldsymbol{k}_1}p_{1\boldsymbol{k}_1} + c_{3\boldsymbol{k}_1}p_{2\boldsymbol{k}_1} - c_{2\boldsymbol{k}_1}p_{3\boldsymbol{k}_1} - c_{4\boldsymbol{k}_1}p_{4\boldsymbol{k}_1}\right)\left(c_{1\boldsymbol{k}_2}p_{1\boldsymbol{k}_2} + c_{3\boldsymbol{k}_2}p_{2\boldsymbol{k}_2} - c_{2\boldsymbol{k}_2}p_{3\boldsymbol{k}_2} - c_{4\boldsymbol{k}_2}p_{4\boldsymbol{k}_2}\right) \\ &\quad \left(c_{1\mathbf{k}_1+\mathbf{k}_2-\mathbf{k}}p^{\dagger}_{1\mathbf{k}_1+\mathbf{k}_2-\mathbf{k}} + c_{3\mathbf{k}_1+\mathbf{k}_2-\mathbf{k}}p^{\dagger}_{2\mathbf{k}_1+\mathbf{k}_2-\mathbf{k}} - c_{2\mathbf{k}_1+\mathbf{k}_2-\mathbf{k}}p^{\dagger}_{3\mathbf{k}_1+\mathbf{k}_2-\mathbf{k}} - c_{4\mathbf{k}_1+\mathbf{k}_2-\mathbf{k}}p^{\dagger}_{4\mathbf{k}_1+\mathbf{k}_2-\mathbf{k}}\right) \Big\} \end{aligned} \tag{52}$$

and

$$\begin{aligned} R_{\mathbf{k}}^{2,\mathrm{xx}} &= V_{\mathrm{xx}} \sum_{\mathbf{k}_1,\mathbf{k}_2} B^{\dagger}_{2\mathbf{k}_1+\mathbf{k}_2-\mathbf{k}} B_{2\boldsymbol{k}_1} B_{2\boldsymbol{k}_2} \\ &= \frac{V_{\mathrm{xx}}}{2\sqrt{2}} \sum_{\mathbf{k}_1,\mathbf{k}_2} \Big\{ \left(c_{1\boldsymbol{k}_1}p_{1\boldsymbol{k}_1} - c_{3\boldsymbol{k}_1}p_{2\boldsymbol{k}_1} - c_{2\boldsymbol{k}_1}p_{3\boldsymbol{k}_1} + c_{4\boldsymbol{k}_1}p_{4\boldsymbol{k}_1}\right)\left(c_{1\boldsymbol{k}_2}p_{1\boldsymbol{k}_2} - c_{3\boldsymbol{k}_2}p_{2\boldsymbol{k}_2} - c_{2\boldsymbol{k}_2}p_{3\boldsymbol{k}_2} + c_{4\boldsymbol{k}_2}p_{4\boldsymbol{k}_2}\right) \\ &\quad \left(c_{1\mathbf{k}_1+\mathbf{k}_2-\mathbf{k}}p^{\dagger}_{1\mathbf{k}_1+\mathbf{k}_2-\mathbf{k}} - c_{3\mathbf{k}_1+\mathbf{k}_2-\mathbf{k}}p^{\dagger}_{2\mathbf{k}_1+\mathbf{k}_2-\mathbf{k}} - c_{2\mathbf{k}_1+\mathbf{k}_2-\mathbf{k}}p^{\dagger}_{3\mathbf{k}_1+\mathbf{k}_2-\mathbf{k}} + c_{4\mathbf{k}_1+\mathbf{k}_2-\mathbf{k}}p^{\dagger}_{4\mathbf{k}_1+\mathbf{k}_2-\mathbf{k}}\right) \Big\} \end{aligned} \tag{53}$$

and

$$\begin{aligned} R_{\boldsymbol{k}}^{1,\mathrm{sat}} &= \frac{V}{n_{\mathrm{sat}}} \sum_{\boldsymbol{k}_1,\boldsymbol{k}_2} B_{1\boldsymbol{k}_1} a_{1\boldsymbol{k}_2} B^{\dagger}_{1\mathbf{k}_1+\mathbf{k}_2-\mathbf{k}} \\ &= \frac{V}{2\sqrt{2}n_{\mathrm{sat}}} \sum_{\mathbf{k}_1,\mathbf{k}_2} \Big\{ \left(c_{1\boldsymbol{k}_1}p_{1\boldsymbol{k}_1} + c_{3\boldsymbol{k}_1}p_{2\boldsymbol{k}_1} - c_{2\boldsymbol{k}_1}p_{3\boldsymbol{k}_1} - c_{4\boldsymbol{k}_1}p_{4\boldsymbol{k}_1}\right)\left(c_{2\boldsymbol{k}_2}p_{1\boldsymbol{k}_2} + c_{4\boldsymbol{k}_2}p_{2\boldsymbol{k}_2} + c_{1\boldsymbol{k}_2}p_{3\boldsymbol{k}_2} + c_{4\boldsymbol{k}_2}p_{2\boldsymbol{k}_2}\right) \\ &\quad \left(c_{1\mathbf{k}_1+\mathbf{k}_2-\mathbf{k}}p^{\dagger}_{1\mathbf{k}_1+\mathbf{k}_2-\mathbf{k}} + c_{3\mathbf{k}_1+\mathbf{k}_2-\mathbf{k}}p^{\dagger}_{2\mathbf{k}_1+\mathbf{k}_2-\mathbf{k}} - c_{2\mathbf{k}_1+\mathbf{k}_2-\mathbf{k}}p^{\dagger}_{3\mathbf{k}_1+\mathbf{k}_2-\mathbf{k}} - c_{4\mathbf{k}_1+\mathbf{k}_2-\mathbf{k}}p^{\dagger}_{4\mathbf{k}_1+\mathbf{k}_2-\mathbf{k}}\right) \Big\} \end{aligned} \tag{54}$$

and

$$\begin{aligned} R_{\mathbf{k}}^{2,\mathrm{sat}} &= \frac{V}{n_{\mathrm{sat}}} \sum_{\mathbf{k}_1,\mathbf{k}_2} B_{2\boldsymbol{k}_1} a_{2\boldsymbol{k}_2} B^{\dagger}_{2\mathbf{k}_1+\mathbf{k}_2-\mathbf{k}} \\ &= \frac{V}{2\sqrt{2}n_{\mathrm{sat}}} \sum_{\mathbf{k}_1,\mathbf{k}_2} \Big\{ \left(c_{1\boldsymbol{k}_1}p_{1\boldsymbol{k}_1} - c_{3\boldsymbol{k}_1}p_{2\boldsymbol{k}_1} - c_{2\boldsymbol{k}_1}p_{3\boldsymbol{k}_1} + c_{4\boldsymbol{k}_1}p_{4\boldsymbol{k}_1}\right)\left(c_{2\boldsymbol{k}_2}p_{1\boldsymbol{k}_2} - c_{4\boldsymbol{k}_2}p_{2\boldsymbol{k}_2} + c_{1\boldsymbol{k}_2}p_{3\boldsymbol{k}_2} - c_{4\boldsymbol{k}_2}p_{2\boldsymbol{k}_2}\right) \\ &\quad \left(c_{1\mathbf{k}_1+\mathbf{k}_2-\mathbf{k}}p^{\dagger}_{1\mathbf{k}_1+\mathbf{k}_2-\mathbf{k}} - c_{3\mathbf{k}_1+\mathbf{k}_2-\mathbf{k}}p^{\dagger}_{2\mathbf{k}_1+\mathbf{k}_2-\mathbf{k}} - c_{2\mathbf{k}_1+\mathbf{k}_2-\mathbf{k}}p^{\dagger}_{3\mathbf{k}_1+\mathbf{k}_2-\mathbf{k}} + c_{4\mathbf{k}_1+\mathbf{k}_2-\mathbf{k}}p^{\dagger}_{4\mathbf{k}_1+\mathbf{k}_2-\mathbf{k}}\right) \Big\}. \end{aligned} \tag{55}$$

In principle we could combine equation (46) with equations (52)-(55) to get a closed formula for the equations of motion as before. However, in what follows we will always focus on a single scattering process and therefore it is more convenient to leave the equations in the current form and derive the coupling rate for a given scheme as needed.

2.9 Polariton dispersion in a triple cavity

We consider a triple cavity where all cavities are of the same design and the coupling between the cavities is equal to g. The Hamiltonian is given by (a straightforward extension of the double cavity case)

$$H_{13} = \begin{pmatrix} E_x(\mathbf{k}) & \hbar\Omega & 0 & 0 & 0 & 0 \\ \hbar\Omega & E_c(\mathbf{k}) & 0 & g & 0 & 0 \\ 0 & 0 & E_x(\mathbf{k}) & \hbar\Omega & 0 & 0 \\ 0 & g & \hbar\Omega & E_c(\mathbf{k}) & 0 & g \\ 0 & 0 & 0 & 0 & E_x & \hbar\Omega \\ 0 & 0 & 0 & g & \hbar\Omega & E_c \end{pmatrix}.$$

If we consider only the photonic part we have

$$H_p = \begin{pmatrix} E_c & g & 0 \\ g & E_c & g \\ 0 & g & E_c \end{pmatrix}$$

with the following eigenvectors

$$\begin{pmatrix} 1 \\ \sqrt{2} \\ 1 \end{pmatrix}, \begin{pmatrix} 1 \\ 0 \\ -1 \end{pmatrix}, \begin{pmatrix} 1 \\ -\sqrt{2} \\ 1 \end{pmatrix} \tag{56}$$

corresponding to the energies

$$E_c - \sqrt{2}g, E_c, E_c + \sqrt{2}g.$$

The difference to the single and double cavity case is illustrated in Figure 12.

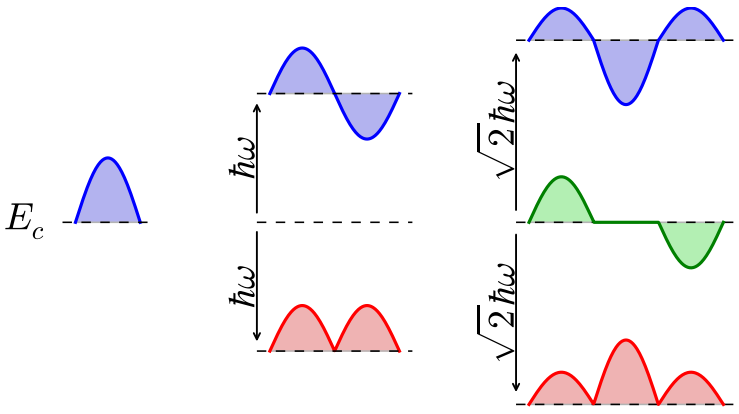

Figure 12: Symmetry of the cavity photons in a single, double, and triple cavity. The splitting of the energy levels is shown.

The discussion above suggests the introduction of one antisymmetric and two symmetric states (compare that to the double cavity case where there is only a single symmetric state) that are related to the bare states by

$$\begin{pmatrix} |\mathrm{X_{as}}\rangle \\ |\mathrm{P_{as}}\rangle \\ |\mathrm{X_{s_1}}\rangle \\ |\mathrm{P_{s_1}}\rangle \\ |\mathrm{X_{s_2}}\rangle \\ |\mathrm{P_{s_2}}\rangle \end{pmatrix} = U \begin{pmatrix} |\mathrm{X_1}\rangle \\ |\mathrm{P_1}\rangle \\ |\mathrm{X_2}\rangle \\ |\mathrm{P_2}\rangle \\ |\mathrm{X_3}\rangle \\ |\mathrm{P_3}\rangle \end{pmatrix},$$

where

$$U = \frac{1}{\sqrt{2}} \begin{pmatrix} 1 & 0 & 0 & 0 & -1 & 0 \\ 0 & 1 & 0 & 0 & 0 & -1 \\ \frac{1}{\sqrt{2}} & 0 & 1 & 0 & \frac{1}{\sqrt{2}} & 0 \\ 0 & \frac{1}{\sqrt{2}} & 0 & 1 & 0 & \frac{1}{\sqrt{2}} \\ \frac{1}{\sqrt{2}} & 0 & -1 & 0 & \frac{1}{\sqrt{2}} & 0 \\ 0 & \frac{1}{\sqrt{2}} & 0 & -1 & 0 & \frac{1}{\sqrt{2}} \end{pmatrix}$$

$$U^{-1} = \begin{pmatrix} \frac{1}{\sqrt{2}} & 0 & \frac{1}{2} & 0 & \frac{1}{2} & 0 \\ 0 & \frac{1}{\sqrt{2}} & 0 & \frac{1}{2} & 0 & \frac{1}{2} \\ 0 & 0 & \frac{1}{\sqrt{2}} & 0 & -\frac{1}{\sqrt{2}} & 0 \\ 0 & 0 & 0 & \frac{1}{\sqrt{2}} & 0 & -\frac{1}{\sqrt{2}} \\ -\frac{1}{\sqrt{2}} & 0 & \frac{1}{2} & 0 & \frac{1}{2} & 0 \\ 0 & -\frac{1}{\sqrt{2}} & 0 & \frac{1}{2} & 0 & \frac{1}{2} \end{pmatrix}.$$

This transformation gives us a block-diagonal form if applied to the Hamiltonian of the combined system, i.e.

$$H_{sa} = U H_{13} U^{-1} = \begin{pmatrix} E_x & \hbar\Omega & 0 & 0 & 0 & 0 \\ \hbar\Omega & E_c & 0 & 0 & 0 & 0 \\ 0 & 0 & E_x & \hbar\Omega & 0 & 0 \\ 0 & 0 & \hbar\Omega & E_c + \sqrt{2}g & 0 & 0 \\ 0 & 0 & 0 & 0 & E_x & \hbar\Omega \\ 0 & 0 & 0 & 0 & \hbar\Omega & E_c - \sqrt{2}g \end{pmatrix},$$

from which we can readily derive the energy of the six branches

$$E_1(\mathbf{k}) = \frac{E_p(\mathbf{k}) + E_x(\mathbf{k}) - \sqrt{2}g - \sqrt{(E_p(\mathbf{k}) - E_x(\mathbf{k}) - \sqrt{2}g)^2 + 4\hbar^2\Omega^2}}{2} \tag{57}$$

$$E_2(\mathbf{k}) = \frac{E_p(\mathbf{k}) + E_x(\mathbf{k}) - \sqrt{(E_p(\mathbf{k}) - E_x(\mathbf{k})) + 4\hbar^2\Omega^2}}{2} \tag{58}$$

$$E_3(\mathbf{k}) = \frac{E_p(\mathbf{k}) + E_x(\mathbf{k}) + \sqrt{2}g - \sqrt{(E_p(\mathbf{k}) - E_x(\mathbf{k}) + \sqrt{2}g)^2 + 4\hbar^2\Omega^2}}{2} \tag{59}$$

$$E_4(\mathbf{k}) = \frac{E_p(\mathbf{k}) + E_x(\mathbf{k}) - \sqrt{2}g + \sqrt{(E_p(\mathbf{k}) - E_x(\mathbf{k}) - \sqrt{2}g)^2 + 4\hbar^2\Omega^2}}{2} \tag{60}$$

$$E_5(\mathbf{k}) = \frac{E_p(\mathbf{k}) + E_x(\mathbf{k}) + \sqrt{(E_p(\mathbf{k}) - E_x(\mathbf{k}))^2 + 4\hbar^2\Omega^2}}{2} \tag{61}$$

$$E_6(\mathbf{k}) = \frac{E_p(\mathbf{k}) + E_x(\mathbf{k}) + \sqrt{2}g + \sqrt{(E_p(\mathbf{k}) - E_x(\mathbf{k}) + \sqrt{2}g)^2 + 4\hbar^2\Omega^2}}{2}. \tag{62}$$

The polariton states are then given by

$$\begin{pmatrix} |\mathrm{p}_1\rangle \\ |\mathrm{p}_2\rangle \\ |\mathrm{p}_3\rangle \\ |\mathrm{p}_4\rangle \\ |\mathrm{p}_5\rangle \\ |\mathrm{p}_6\rangle \end{pmatrix} = \tilde{U} \begin{pmatrix} |\mathrm{X}_1\rangle \\ |\mathrm{P}_1\rangle \\ |\mathrm{X}_2\rangle \\ |\mathrm{P}_2\rangle \\ |\mathrm{X}_3\rangle \\ |\mathrm{P}_3\rangle \end{pmatrix},$$

where the transformation matrix is

$$\tilde{U} = \begin{pmatrix} \frac{c_1}{\sqrt{2}} & \frac{c_2}{\sqrt{2}} & 0 & 0 & -\frac{c_1}{\sqrt{2}} & -\frac{c_2}{\sqrt{2}} \\ -\frac{c_2}{\sqrt{2}} & \frac{c_1}{\sqrt{2}} & 0 & 0 & \frac{c_2}{\sqrt{2}} & -\frac{c_1}{\sqrt{2}} \\ \frac{c_3}{2} & \frac{c_4}{2} & \frac{c_3}{\sqrt{2}} & \frac{c_4}{\sqrt{2}} & \frac{c_3}{2} & \frac{c_4}{2} \\ -\frac{c_4}{2} & \frac{c_3}{2} & -\frac{c_4}{\sqrt{2}} & \frac{c_3}{\sqrt{2}} & -\frac{c_4}{2} & \frac{c_3}{2} \\ \frac{c_5}{2} & \frac{c_6}{2} & -\frac{c_5}{\sqrt{2}} & -\frac{c_6}{\sqrt{2}} & \frac{c_5}{2} & \frac{c_6}{2} \\ -\frac{c_6}{2} & \frac{c_5}{2} & \frac{c_6}{\sqrt{2}} & -\frac{c_5}{\sqrt{2}} & -\frac{c_6}{2} & \frac{c_5}{2} \end{pmatrix}.$$

The Hopfield coefficients can be succinctly expressed by

$$|c_i|^2 = \frac{1}{2}\left(1 + (-1)^i \frac{E_c(\mathbf{k}) - 2g\cos\left\lfloor\frac{i+1}{2}\right\rfloor\frac{\pi}{4} - E_x(\mathbf{k})}{\sqrt{\left(E_c(\mathbf{k}) - 2g\cos\left\lfloor\frac{i+1}{2}\right\rfloor\frac{\pi}{4} - E_x(\mathbf{k})\right)^2 + (2\hbar\Omega)^2}}\right).$$

By employing the relation $c_1^2 + c_2^2 = c_3^2 + c_4^2 = c_5^2 + c_6^2 = 1$ the inverse of the transformation matrix can be written as

$$\tilde{U}^{-1} = \frac{1}{2}\begin{pmatrix} \sqrt{2}c_1 & -\sqrt{2}c_2 & c_3 & -c_4 & c_5 & c_6 \\ \sqrt{2}c_2 & \sqrt{2}c_1 & c_4 & c_3 & c_6 & c_5 \\ 0 & 0 & \sqrt{2}c_3 & -\sqrt{2}c_4 & -\sqrt{2}c_5 & \sqrt{2}c_6 \\ 0 & 0 & \sqrt{2}c_4 & \sqrt{2}c_3 & -\sqrt{2}c_6 & -\sqrt{2}c_5 \\ -\sqrt{2}c_1 & \sqrt{2}c_2 & c_3 & -c_4 & c_5 & -c_6 \\ -\sqrt{2}c_2 & -\sqrt{2}c_1 & c_4 & c_3 & c_6 & c_5 \end{pmatrix}.$$

To conclude this section let us compare the dispersion relations for the different cavity configurations (see Figure 13 for an illustration). In case of the triple cavity we now have three polariton states below the exciton reservoir. This potentially enables us to implement the branch entanglement scheme suggested by Ciuti in the context of quantum wires (see e.g. [2]). The possibility of implementing such a scheme touches on symmetry and thus we will postpone the discussion to the next section.

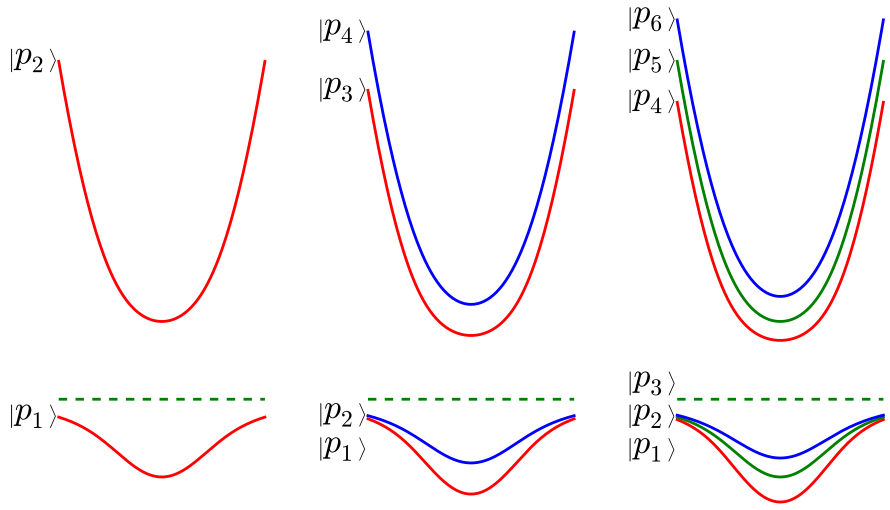

Figure 13: The dispersion relations labeled by polariton states for a single cavity (left), double cavity (middle), and triple cavity (right). The x-axis corresponds to the wavevector and the y-axis to energy. The green-dotted line represents the exciton reservoir.

2.10 Parity conservation in the triple cavity

We have already discussed in section 2.8 that parity is conserved in parametric scattering processes. It is thus expected that a similar selection rule prevents us from implementing arbitrary schemes in the triple cavity case. However, in case of the triple cavity it is rather tedious to work out all the scattering amplitudes in detail. Thus, in this section we will give a more elegant argument that is based on Fermi's golden rule.

First, let us consider a scattering processes with a single polariton particle only and a Hamiltonian that can be decomposed as a (tensor) product of a polariton operator and an operator in some orthogonal subspace. In this case the matrix element in Fermi's golden rule can be rewritten as

$$\langle p_i|H|p_j\rangle = \left(\vec{a}^{(i)}\cdot\vec{a}^{(j)}\right)\langle x_1|H|x_1\rangle,$$

where x_k is the wavefunction of the exciton in the k-th quantum well (we have assumed that all quantum wells give the same matrix element) and the coefficients $\vec{a}^{(i)},\vec{a}^{(j)}$ are given by (these are actually the eigenvectors described in equation (56))

$$\vec{a}^{(1)} = \begin{bmatrix} 1/2 \\ 1/\sqrt{2} \\ 1/2 \end{bmatrix}, \qquad \vec{a}^{(2)} = \begin{bmatrix} 1/\sqrt{2} \\ 0 \\ -1/\sqrt{2} \end{bmatrix}, \qquad \vec{a}^{(3)} = \begin{bmatrix} 1/2 \\ -1/\sqrt{2} \\ 1/2 \end{bmatrix}.$$

However, since these vectors are orthogonal only scattering processes that preserve the branch index give a contribution to the matrix element above. Thus, scattering from $|\mathrm{p_i}\rangle$ to $|\mathrm{p_{i+3}}\rangle$ is possible but all other scattering processes are forbidden.

For scattering processes involving two polaritons (parametric scattering, for example) we can rewrite the matrix element as

$$\langle p_ip_j|H|p_kp_l\rangle = \sum_n a_n^{(i)}a_n^{(j)}a_n^{(k)}a_n^{(l)}\langle x_1x_1|H|x_1x_1\rangle + \sum_{\substack{mn\\ m\neq n}} a_n^{(i)}a_m^{(j)}a_n^{(k)}a_m^{(l)}\langle x_1x_2|H|x_1x_2\rangle.$$

In light of the first term it is instructive to compute the pointwise multiplication of two vectors drawn from $\vec{a}^{(2)}$ (the antisymmetric branch) and $\vec{a}^{(1)}$, $\vec{a}^{(3)}$ (the symmetric branches). The non-trivial products yield

$$\begin{aligned}\left(\vec{a}^{(1)} * \vec{a}^{(3)}\right) \cdot \left(\vec{a}^{(2)} * \vec{a}^{(m)}\right) &= 0, \qquad m \in \{1,3\} \\ \left(\vec{a}^{(1)} * \vec{a}^{(2)}\right) \cdot \left(\vec{a}^{(3)} * \vec{a}^{(2)}\right) &\neq 0,\end{aligned}$$

where we have denoted the pointwise multiplication by $*$. Now if we put this in terms of wavefunction symmetry we actually have used the relation

$$\vec{a}^{(1)} * \vec{a}^{(2)} \begin{bmatrix} \frac{1}{4} \\ -\frac{1}{2} \\ \frac{1}{4} \end{bmatrix}, \qquad \vec{a}^{(1)} * \vec{a}^{(3)} = \begin{bmatrix} \frac{1}{2\sqrt{2}} \\ 0 \\ -\frac{1}{2\sqrt{2}} \end{bmatrix}, \qquad \vec{a}^{(1)} * \vec{a}^{(2)} = \begin{bmatrix} \frac{1}{2\sqrt{2}} \\ 0 \\ -\frac{1}{2\sqrt{2}} \end{bmatrix}$$

or to put it another way

$$\begin{aligned}\text{symmetric} * \text{symmetric} &= \text{symmetric} \\ \text{symmetric} * \text{antisymmetric} &= \text{antisymmetric}\end{aligned}$$

and

$$\begin{aligned}\text{symmetric} \cdot \text{antisymmetric} &= 0 \\ \text{antisymmetric} \cdot \text{antisymmetric} &\neq 0.\end{aligned}$$

From this, it is clear that once again we have a parity condition. More precisely, a process $|p_k p_l\rangle \to |p_i p_j\rangle$ (on the lower polariton branch) is allowed if and only if

$$q_k + q_l = q_i + q_j \bmod 2, \tag{63}$$

where

$$q_1 = 0, \qquad q_2 = 1, \qquad q_3 = 0.$$

Strictly speaking we still have to show that if this condition is **not** satisfied the second term of the matrix element vanishes. However, it is a straightforward computation (for a computer algebra system) to show the desired result; that is,

$$\sum_{\substack{mn \\ m \neq n}} a_n^{(i)} a_m^{(j)} a_n^{(k)} a_m^{(l)} = 0,$$

holds for all i, j, kl that violate condition (63).

Nevertheless, it should be duly noted that even though we arrive once again at a form of parity conservation the result is qualitatively quite different from the double cavity case. For example, we can have two pumps in the second polariton branch and investigate scattering to the first and third polariton branch. This is in fact similar to the quantum wire scheme discussed in [2].

2.11 The coherent pump

In the computations done so far we have treated all polariton states as full quantum variables[3] described by creation and annihilation operators. However, as we will excite polaritons by using a coherent pump laser at a given wavevector, it is convenient to describe those pump generated polaritons by the expectation value of the polariton operator $\mathcal{P}(t) = \langle P(t) \rangle$; that is, we we do not take quantum fluctuations into account.

[3]With the exception of the discussion of the quantum Langevin approach in section 2.4.

Thus, our goal in this section is to compute the coherent polariton operator $\mathcal{P}(t)$ from the pump intensity $I(t)$. This is done by taking the expected value of the following equation

$$P'(t) = -\gamma P(t) + t_c c E_{cl}(t)$$

where t_c is the cavity transmission coefficient and c the appropriate Hopfield coefficient. Note that this is just equation (17) with energy renormalized to zero and neglected polariton-polariton scattering (i.e. we assume that we do not deplete the pump). The latter assumption is certainly plausible as the scattering back into the pump state will be negligible compared to the pump induced polariton occupation. The expected value of this equation then reads

$$\begin{aligned}\mathcal{P}'(t) &= -\gamma \mathcal{P}(t) + t_c c E_{cl}(t)\\ \mathcal{P}(0) &= 0,\end{aligned}$$

where E_{cl} describes the classical light field. The initial condition follows easily from the fact that in the coherent case the polariton population is given by

$$N(t) = \langle P(t) P^\dagger(t)\rangle = \langle P(t)\rangle^2 =: \mathcal{P}(t)^2.$$

Now since at $t = 0$ there are no pump induced polaritons we have $N(0) = 0$ and thus $\mathcal{P}(t) = 0$.

We can represent the solution of this equation by an integral

$$\mathcal{P}(t) = c t_c e^{-\frac{1}{2}\gamma t} \int_{t_i}^{t} e^{\frac{1}{2}\gamma \tau} E_{cl}(\tau)\, d\tau, \tag{64}$$

where t_i is the initial value of the simulation (usually taken to be $t_i = 0$).

For some specific intensity distribution in time this integral can be solved exactly. We will do this for a Gaussian pulse and a CW pump in the next two sections. Usually we will not specify the (classical) electric field $E_{\mathrm{cl}}(t)$ but the intensity distribution $I(t)$. We know from classical electrodynamics that $I(t) = |E_{cl}(t)|^2$; for our purpose, however, we can average over the period of the electric field and use $E_{cl}(t) = \sqrt{I(t)}$.

2.11.1 Gaussian pulse

A Gaussian shaped pulse in time is described by the intensity function

$$I(t) = n \frac{\pi \lambda_x^2}{\tau_p \sqrt{2\pi}} e^{-\frac{(t-t_0)^2}{2\tau_p^2}},$$

where τ_p is the pulse width (standard deviation) and t_0 the time at which the intensity is maximal; n is the number of photons per μm^{-2} in a single pulse. We will (as before) assume that our area of quantization is the circle of radius λ_x, where λ_x is the Bohr radius of the exciton. Taking the relation between the intensity and the electric field from the previous section and inserting it into equation (64) we get

$$\mathcal{P}(t) = c t_c \sqrt{n \sqrt{\frac{\pi}{2}} \tau_p \pi \lambda_x^2}\, e^{-\frac{\gamma}{2}(t-t_0)} e^{\frac{\gamma^2 \tau_p^2}{4}} \left[\operatorname{erf}\left(\frac{t - t_0 - \gamma \tau_p^2}{2\tau_p} \right) - \operatorname{erf}\left(\frac{t_i - t_0 - \gamma \tau_p^2}{2\tau_p} \right) \right].$$

This is in fact the equation for $\mathcal{P}(t)$ that will be used in almost all simulations in section (4). We will discuss the ramifications of the shape of this function in section 4.4.

2.11.2 Continuous wave

In addition we also consider a quasi-CW (continuous wave) pump. In this case we have a time independent density distribution; that is,

$$I(t) = \frac{n\pi\lambda_x^2}{\tau_p},$$

where τ_p is the duration of the pump (which is taken long enough to reach a steady state for the coherent polariton population, approximately on the order of a ns) and n is the number of photons per μm^{-2} in a time frame of duration τ_p. Inserting this into equation (64) we get

$$\mathcal{P}(t) = \frac{2ct_c}{\gamma}\sqrt{\frac{n\pi\lambda_x^2}{\tau_p}}\left(1 - e^{-\frac{\gamma}{2}(t-t_i)}\right).$$

For the steady state (i.e. for $(t - t_i)\,\gamma \gg 1$) we have

$$\mathcal{P}(t) \approx \frac{2ct_c}{\gamma}\sqrt{\frac{n\pi\lambda_x^2}{\tau_p}}.$$

Therefore, the only reason for simulating the full time interval τ_p is to consider effects such as phonon induced photoluminescence. It should also be duly noted that a CW pump is only practical for pumping at the polariton ground state (i.e. where no decay channels are available that would introduce excessive noise into the system). If we neglect pump-induced photoluminescence and assume no or a constant noise background a connection between n, as defined in this section, and the parameter Δ as defined in section 2.6 must exists. We will explore this relationship in some detail in section 4.3.

3 Proposals for entanglement generation

In this section our goal is to investigate if there are any double and triple cavity schemes that are feasible and potentially advantageous compared to the single cavity case. Clearly, such a scheme has to fulfill the selection rules derived in section 2; we are mainly interested in schemes that are, to some extend, protected from decoherence due to pump induced photoluminescence by these selection rules. Before we discuss the double and triple cavity case we will revisit the single cavity schemes that have been proposed in the literature.

3.1 The single cavity case

In the literature a number of single cavity schemes for entanglement generation can be found. In this section we will describe some of them and classify them consistently for later comparison. In [2] Ciuti proposed a scheme for branch entangled polaritons that results in frequency entangled photons. We will call this scheme Cs2[4].

An experimentally more advantageous scheme that employs only the lower polariton branch has been proposed in [15]. This scheme (which we call Ps1) does not suffer from the additional decay channels present in Cs2 as only the branch lowest in energy is used. In addition, it employs a linear cross-polarization pump as described in section (2.3.2). Thus, the result of a scattering process are polaritons entangled in the spin degree of freedom. In this scheme the signal and idler photons have the same wavelength but are different with respect to the angle of emission.

Huang also proposed a scheme that results in polarization entanglement. However, as the idler is located on the ground state of the second branch it too suffers from the possible decay to the exciton reservoir. In addition, as there is no momentum difference between the signal and idler polaritons we have to differentiate the two photons either by setting up the cavity in such a way that (with some probability) one photon leaves to the front while the other leaves to the back of the cavity or by differentiating the emitted photons based on wavelength. We will call this scheme Hs2.

All the schemes listed above are illustrated in Figure 14.

3.2 Proposals for the double cavity case

First of all let us emphasize that we can easily generalize all single cavity schemes that employ only a single branch to the double cavity case. For example, Portolan's scheme in this context in denoted by Pd1. Even though quantitative differences are possible (due to the different dispersion relation, Hopfield coefficients, and scattering rates of the lowest polariton branch) qualitatively these schemes are equivalent to the corresponding single cavity scheme. That is, the only difference between the Ps1 and Pd1 schemes is the numbers we use for the coupling strength and the Hopfield coefficients.

However, since we have two polariton branches available that are below the exciton reservoir the double cavity schemes potentially have an advantage in schemes where two polariton branches are used. However, it is not possible to extend any single cavity two-branch scheme to the double cavity case (where we assume that only the two lowest polariton branches are used) as the scattering process needs to conserve parity (as was found in section 2.8). Neither Ciuti's scheme in the context of a double cavity (Cd2) nor Huang's scheme (Hd2) do preserve parity and are thus not possible in a double cavity.

3.2.1 The Gd2 and Gd2r schemes

As discussed in the previous section, at first sight, it might be rather difficult to find two-branch schemes that conserve parity. However, if we compare the dispersion relation of the double cavity (see Figure 11)

[4]Let us briefly explain our nomenclature for classifying entanglement schemes. We will use a two-letter and one-number combination. The first letter specifies the scheme (C stands for Ciuti, for example). The second letter will specify if we have a single (s), double (d), or triple (t) cavity, whereas the last number gives the number of branches employed in the scattering processes. For the variation of a given pump scheme we will also, on occasion, add a fourth identifier.

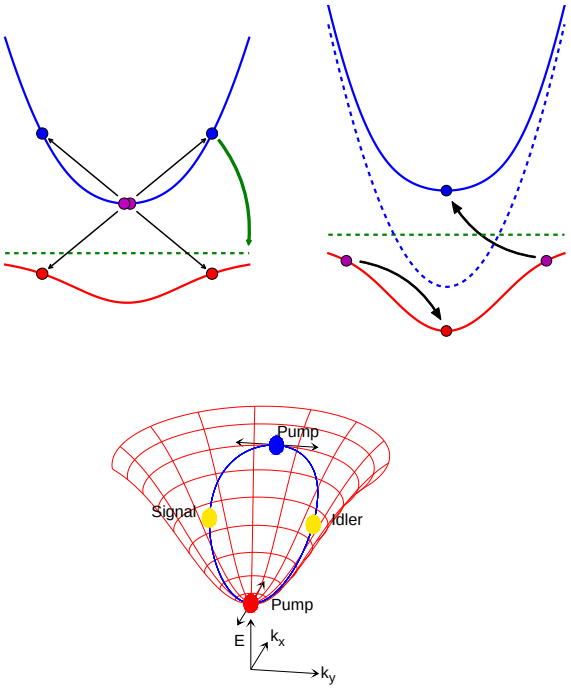

Figure 14: Ciutis scheme for branch entanglement (Cs2) on the top left; the pumps are located at the violet dots. The green dotted line represents the exciton dispersion. The green arrow illustrates the possible decay channel to the exciton reservoir. Huang's scheme for polarization entanglement (Hs2) is on the top right; we pump with circularly polarized light at the violet dots. Portolan's scheme (Ps1) is shown at the bottom (a 3d graph of the lower polariton branch is shown); we pump with cross-linearly polarized light at the red and blue dot as indicated in the figure. The signal and idler are degenerate in energy but can be differentiated in the angle of emission.

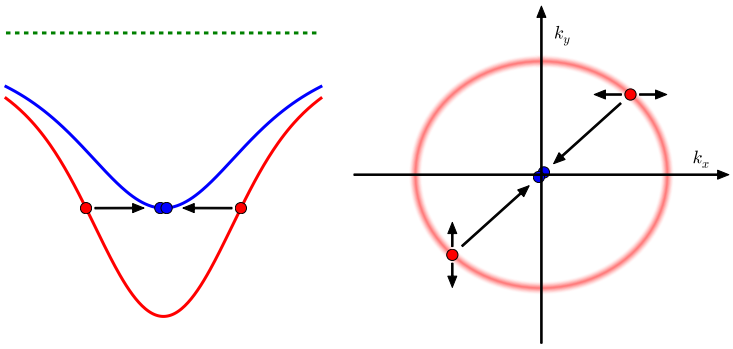

Figure 15: Due to the modified dispersion curve for the double cavity, we can either pump at the ground state or at two opposite directions . The latter scheme (Gd2r) is shown in the figure.

with the dispersion relation of the single cavity (see Figure 4) we immediately recognize that the two lower polariton branches degenerate (for large wavevectors) in the double cavity case while this is not true in the single cavity case.

This fact is at the heart of the scheme we now propose. To conserve parity we pump on a single branch while signal and idler are located on a different branch. For example, signal and idler are both on branch 1 while both pumps are on branch 2. It is then most convenient to choose the pump at the ground state of the second branch (we will denote this scheme by Gd2, the G stands for ground state). The signal and idler can then be picked up at different angles. However, the reverse (i.e. we pump on branch 1 and signal and idler are at branch 2) is just as easy to achieve (we call this scheme Gd2r). As discussed before it is advantageous to pump with linearly cross-polarized light (as indicated in Figure 15).

At first sight the Gd2r scheme seems unnecessarily complex from an experimental standpoint as we have to distinguish the signal and idler which both have the same wavevector and frequency. However, since experimentally it is preferable to have one photon leave to the back and one photon leave to the front of the cavity this is of not much consequence. The same situation arises, from a practical point of view, if we only pick up photons from a single side of the cavity (even if the photons can be differentiated by angle).

The advantage of Gd2r is that since there is not as much leakage from the ground state of the branch 2 polaritons the pump polaritons are better protected against decay. On the other hand care has to be taken as the ground state of the first branch might become populated due to polariton-phonon scattering (this is unwanted noise that can only be distinguished from the signal/idler by filtering in the frequency degree of freedom). We will, however, see in the numerical simulations in section 4 that this noise is somewhat controlled by the well-known bottleneck effect.

In addition, a crucial disadvantage of the Gd2 scheme is that both pumps are located at the same point in momentum space. Thus, the assumption we made in section 2.3.2, i.e. that we can pump linearly cross-polarized at two points in momentum space, is no longer valid and we can not get rid easily of the $+-$ channel. Even if we would shift the two pumps a bit apart phonon scattering would still result in essentially the same problem.

3.2.2 The Sd2 scheme

Another possibility to guarantee parity conservation is to pump on both the first and the second branch. In this case then the signal and idler will also be on different branches (we will denote this scheme by Sd2, S for symmetric). This is illustrated in Figure16.

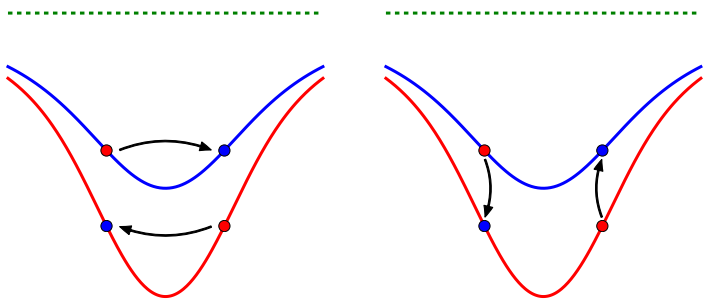

Figure 16: We pump at the red dots. The two possible scattering processes are shown on the left and right respectively. We can take signal as the left blue dot and idler as the right blue dot, for example.

Even though the signal and idler have different energies the scheme can still be constructed in such a way as to enable polarization entanglement. However, this scheme has a number of disadvantages. From an

experimental standpoint we have to pump with two different energies in a manner such that the pulses are synchronized. However, even if those difficulties can be overcome pump induced photoluminescence is likely to have an adverse effect on the generation of entanglement since the signal and idler share the energy with one of the pumps; note that due to the fast phonon scattering time for energy conserving channels there will be almost no angle dependence of the pump induced photoluminescence for timescales relevant to entanglement generation. Also Rayleigh scattering is definitely a concern for such a scheme. A discussion of Rayleigh scattering can be found in [9], for example.

3.3 Proposal for the triple cavity case

Due to the selection rules discussed in section 2.10 we are limited to the same pump schemes discussed in the previous section if we employ the first and second polariton branch or the second and third polariton branch. In this context we would call the schemes Gt2, Gt2r, and St2 respectively. In addition, all the single cavity pump schemes are still possible. However, such schemes (apart from a different scattering rate $g_{\boldsymbol{k}}$) offer nothing conceptually new. From an experimental standpoint, however, they decrease the potentially small splitting of the polariton levels by an additional factor of $\sqrt{2} \approx 1.4$ (see section 2.9).

Nevertheless, due to the fact that there are three polariton states below the exciton reservoir the selection rules permit one additional pump scheme that is of interest. If we put both pumps on the second polariton branch (which results in zero parity) scattering of one polariton to branch 1 and another polariton to branch 3 is allowed. With the usual condition of phase matching (i.e. energy and momentum conservation) we get, for example, the scheme illustrated in Figure 17.

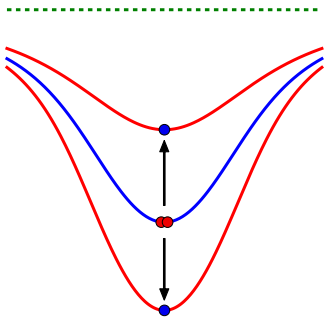

Figure 17: The two pumps are placed at the ground state of the second polariton branch. The phase matching condition is fulfilled if the parametric scattering results in polaritons at the ground state of the first and third polariton branch. Polariton branches with the same parity are illustrated in the same color.

As discussed in [2] such schemes are interesting for creating frequency entangled photon pairs. However, the scheme offers no discernible advantage if one considers polarization entanglement only.

3.4 Coupling coefficients

In order to simulate one of the schemes proposed we still have to compute the coupling coefficients. This is the goal of the present section. With the formulas derived in sections 2.8.1 and 2.8.2 we can get the desired coupling coefficients for all the pump schemes considered in the previous section. We will spell out the derivations for the Gd2, Gd2r, Ps1, and Pd1 schemes. Some of the single cavity result can be found in the literature (see e.g. [17] and [2]). A table that summarizes the coupling strength $g_{\boldsymbol{k}}$ for the schemes discussed can be found at the end of this section (Table 1).

Gd2r/Gd2 Let us start with the approach by Portolan (we will use the equations from section 2.8.2). Let us fix the pumps at $\boldsymbol{k}_{p_1}$ and $\boldsymbol{k}_{p_2}$ (both at branch 1). The signal and idler are then located at $\boldsymbol{k}$ and $\boldsymbol{k}_i$ (both at branch 2). In the actual Gd2r scheme it holds that $\boldsymbol{k} = \boldsymbol{k}_i = 0$ and $\boldsymbol{k}_{p_1} = -\boldsymbol{k}_{p_2}$where the remaining wavevector amplitude is determined such that the parametric scattering is consistent with the signal and idler given. This still leaves a rotational degree of freedom unspecified (which can be chosen without affecting the scheme). However, for the purpose of this derivation the specific values of the wavevectors do not result in any further simplification.

Now, let us select the corresponding scattering process from equation (54) to (53); this yields

$$\begin{aligned}
R_{\mathbf{k}}^{1,\mathrm{xx}} &= \left[\frac{V_{\mathrm{xx}}}{\sqrt{2}} c_{1\boldsymbol{k}_{p1}} c_{1\boldsymbol{k}_{p2}} c_{3\boldsymbol{k}_i}\right] p_{1\boldsymbol{k}_{p_1}} p_{1\boldsymbol{k}_{p_1}} p^{\dagger}_{2\boldsymbol{k}_i} \\
R_{\mathbf{k}}^{2,\mathrm{xx}} &= \left[\frac{-V_{\mathrm{xx}}}{\sqrt{2}} c_{1\boldsymbol{k}_{p1}} c_{1\boldsymbol{k}_{p2}} c_{3\boldsymbol{k}_i}\right] p_{1\boldsymbol{k}_{p_1}} p_{1\boldsymbol{k}_{p_1}} p^{\dagger}_{2\boldsymbol{k}_i} \\
R_{\mathbf{k}}^{1,\mathrm{sat}} &= \left[\frac{V}{2\sqrt{2} n_{\mathrm{sat}}} \left(c_{1\boldsymbol{k}_{p1}} c_{1\boldsymbol{k}_{p2}} + c_{1\boldsymbol{k}_{p2}} c_{2\boldsymbol{k}_{p1}}\right) c_{3\boldsymbol{k}_i}\right] p_{1\boldsymbol{k}_{p_1}} p_{1\boldsymbol{k}_{p_1}} p^{\dagger}_{2\boldsymbol{k}_i} \\
R_{\mathbf{k}}^{2,\mathrm{sat}} &= \left[\frac{-V}{2\sqrt{2} n_{\mathrm{sat}}} \left(c_{1\boldsymbol{k}_{p1}} c_{1\boldsymbol{k}_{p2}} + c_{1\boldsymbol{k}_{p2}} c_{2\boldsymbol{k}_{p1}}\right) c_{3\boldsymbol{k}_i}\right] p_{1\boldsymbol{k}_{p_1}} p_{1\boldsymbol{k}_{p_1}} p^{\dagger}_{2\boldsymbol{k}_i}.
\end{aligned}$$

Using the relation given in equation (46) we have

$$\begin{aligned}
g_{\mathbf{k}}^{\mathrm{xx}} &= \frac{c_{3\boldsymbol{k}}}{\sqrt{2}} \left(R_{\mathbf{k}}^{1,\mathrm{xx}} - R_{\mathbf{k}}^{2,\mathrm{xx}}\right) \\
g_{\boldsymbol{k}}^{sat} &= \frac{c_{3\boldsymbol{k}}}{\sqrt{2}} \left(R_{\mathbf{k}}^{1,\mathrm{sat}} - R_{\mathbf{k}}^{2,sat}\right)
\end{aligned}$$

and thus

$$g_{\boldsymbol{k}} = c_{3\boldsymbol{k}} \left[V_{xx} c_{1\boldsymbol{k}_{p1}} c_{1\boldsymbol{k}_{p2}} + \frac{V}{2n_{sat}} \left(c_{1\boldsymbol{k}_{p1}} c_{1\boldsymbol{k}_{p2}} + c_{1\boldsymbol{k}_{p2}} c_{2\boldsymbol{k}_{p1}}\right)\right] c_{3\boldsymbol{k}_i}.$$

Note that to compute $R_{\boldsymbol{k}}^{i,sat}$ it is important to take into account all combinations of $\boldsymbol{k}_{p_1}$ and $\boldsymbol{k}_{p_2}$ that occur in the summation. If this is not done properly we end up with a relation that is (contrary to what is expected) not invariant under the interchange of $\boldsymbol{k}_{p_1}$ and $\boldsymbol{k}_{p_2}$.

Now let us turn to the approach by Ciuti. In this case we start from equations (18) and (38); this yields

$$\overline{V}^{1111}_{\boldsymbol{k}_{p_1}\boldsymbol{k}_{p_2}\boldsymbol{k}} + \overline{V}^{1111}_{\boldsymbol{k}_{p_2}\boldsymbol{k}_{p_1}\boldsymbol{k}} = V_{xx} c_{3\boldsymbol{k}} c_{3\boldsymbol{k}_i} c_{1\boldsymbol{k}_{p_1}} c_{1\boldsymbol{k}_{p_2}}$$

and

$$\underline{V}^{1111}_{\boldsymbol{k}_{p_1}\boldsymbol{k}_{p_2}\boldsymbol{k}} + \underline{V}^{1111}_{\boldsymbol{k}_{p_2}\boldsymbol{k}_{p_1}\boldsymbol{k}} = \frac{V}{n_{sat}} \left[c_{1\boldsymbol{k}_{p_1}} c_{1\boldsymbol{k}_{p_2}} \left(c_{3\boldsymbol{k}} c_{4\boldsymbol{k}_i} + c_{4\boldsymbol{k}} c_{3\boldsymbol{k}_i}\right) + \left(c_{1\boldsymbol{k}_{p_1}} c_{2\boldsymbol{k}_{p_2}} + c_{2\boldsymbol{k}_{p_1}} c_{1\boldsymbol{k}_{p_2}}\right) c_{3\boldsymbol{k}} c_{3\boldsymbol{k}_i}\right].$$

Therefore, we get

$$g_{\boldsymbol{k}} = V_{xx} c_{3\boldsymbol{k}} c_{3\boldsymbol{k}_i} c_{1\boldsymbol{k}_{p_1}} c_{1\boldsymbol{k}_{p_2}} + \frac{V}{n_{sat}} \left[c_{1\boldsymbol{k}_{p_1}} c_{1\boldsymbol{k}_{p_2}} \left(c_{3\boldsymbol{k}} c_{4\boldsymbol{k}_i} + c_{4\boldsymbol{k}} c_{3\boldsymbol{k}_i}\right) + \left(c_{1\boldsymbol{k}_{p_1}} c_{2\boldsymbol{k}_{p_2}} + c_{2\boldsymbol{k}_{p_1}} c_{1\boldsymbol{k}_{p_2}}\right) c_{3\boldsymbol{k}} c_{3\boldsymbol{k}_i}\right].$$

Ps1 Starting with Portolan's approach we get from equations 18 and 10

$$\begin{aligned}
\overline{V}^{111}_{\boldsymbol{k}_{p_1}\boldsymbol{k}_{p_2}\boldsymbol{k}} + \overline{V}^{111}_{\boldsymbol{k}_{p_2}\boldsymbol{k}_{p_1}\boldsymbol{k}} &= 2V_{xx} \left[c_{1\boldsymbol{k}_{p_1}} c_{1\boldsymbol{k}_{p_2}}\right] c_{1\boldsymbol{k}_i} \\
\underline{V}^{111}_{\boldsymbol{k}_{p_1}\boldsymbol{k}_{p_2}\boldsymbol{k}} + \underline{V}^{111}_{\boldsymbol{k}_{p_2}\boldsymbol{k}_{p_1}\boldsymbol{k}} &= \frac{V}{n_{sat}} \left[c_{1\boldsymbol{k}_{p_1}} c_{2\boldsymbol{k}_2} + c_{2\boldsymbol{k}_{p_1}} c_{1\boldsymbol{k}_2}\right] c_{1\boldsymbol{k}_i}
\end{aligned}$$

and thus

$$g_{\boldsymbol{k}} = 2V_{xx} c_{1\boldsymbol{k}} c_{1\boldsymbol{k}_i} c_{1\boldsymbol{k}_{p_1}} c_{1\boldsymbol{k}_{p_2}} + \frac{V}{n_{sat}} c_{1\boldsymbol{k}} c_{1\boldsymbol{k}_i} \left[c_{1\boldsymbol{k}_{p_1}} c_{2\boldsymbol{k}_{p_2}} + c_{2\boldsymbol{k}_{p_1}} c_{1\boldsymbol{k}_{p_2}} \right].$$

Now let us consider the same situation in the context of Ciuti's approach; we have

$$\boldsymbol{g}_k = V^{1111}_{\boldsymbol{k}_{p_1}\boldsymbol{k}_{p_2},\boldsymbol{k}_{p_2}-\boldsymbol{k}} + V^{1111}_{\boldsymbol{k}_{p_1}\boldsymbol{k}_{p_2},\boldsymbol{k}-\boldsymbol{k}_{p_1}} + V^{1111}_{\boldsymbol{k}_{p_2}\boldsymbol{k}_{p_1},\boldsymbol{k}_{p_1}-\boldsymbol{k}} + V^{1111}_{\boldsymbol{k}_{p_2}\boldsymbol{k}_{p_1},\boldsymbol{k}-\boldsymbol{k}_{p_2}},$$

where

$$\overline{V}^{1111}_{\boldsymbol{k}_{p_1}\boldsymbol{k}_{p_2},\boldsymbol{k}_{p_2}-\boldsymbol{k}} + \overline{V}^{1111}_{\boldsymbol{k}_{p_1}\boldsymbol{k}_{p_2},\boldsymbol{k}-\boldsymbol{k}_{p_1}} + \overline{V}^{1111}_{\boldsymbol{k}_{p_2}\boldsymbol{k}_{p_1},\boldsymbol{k}_{p_1}-\boldsymbol{k}} + \overline{V}^{1111}_{\boldsymbol{k}_{p_2}\boldsymbol{k}_{p_1},\boldsymbol{k}-\boldsymbol{k}_{p_2}} = 2V_{xx} \left[c_{1\boldsymbol{k}_{p_1}} c_{1\boldsymbol{k}_{p_2}} \right] c_{1\boldsymbol{k}} c_{1\boldsymbol{k}_i}$$

and

$$\begin{aligned}
&\underline{V}^{1111}_{\boldsymbol{k}_{p_1}\boldsymbol{k}_{p_2},\boldsymbol{k}_{p_2}-\boldsymbol{k}} + \underline{V}^{1111}_{\boldsymbol{k}_{p_1}\boldsymbol{k}_{p_2},\boldsymbol{k}-\boldsymbol{k}_{p_1}} + \underline{V}^{1111}_{\boldsymbol{k}_{p_2}\boldsymbol{k}_{p_1},\boldsymbol{k}_{p_1}-\boldsymbol{k}} + \underline{V}^{1111}_{\boldsymbol{k}_{p_2}\boldsymbol{k}_{p_1},\boldsymbol{k}-\boldsymbol{k}_{p_2}} \\
&\quad = \frac{2V}{n_{sat}} \left[2 \left(c_{2\boldsymbol{k}_i} c_{1\boldsymbol{k}} + c_{2\boldsymbol{k}} c_{1\boldsymbol{k}_i} \right) c_{1\boldsymbol{k}_{p_1}} c_{1\boldsymbol{k}_{p_2}} + 2 \left(c_{1\boldsymbol{k}_{p_1}} c_{2\boldsymbol{k}_{p_2}} + c_{2\boldsymbol{k}_{p_1}} c_{1\boldsymbol{k}_{p_2}} \right) c_{1\boldsymbol{k}} c_{1\boldsymbol{k}_i} \right].
\end{aligned}$$

Finally, we get

$$g_{\boldsymbol{k}} = 2V_{xx} c_{1\boldsymbol{k}} c_{1\boldsymbol{k}_i} c_{1\boldsymbol{k}_{p_1}} c_{1\boldsymbol{k}_{p_2}} + \frac{2V}{n_{sat}} \left(\left[c_{2\boldsymbol{k}_i} c_{1\boldsymbol{k}} + c_{2\boldsymbol{k}} c_{1\boldsymbol{k}_i} \right] c_{1\boldsymbol{k}_{p_1}} c_{1\boldsymbol{k}_{p_2}} + c_{1\boldsymbol{k}} c_{1\boldsymbol{k}_i} \left[c_{1\boldsymbol{k}_{p_1}} c_{2\boldsymbol{k}_{p_2}} + c_{2\boldsymbol{k}_{p_1}} c_{1\boldsymbol{k}_{p_2}} \right] \right).$$

Pd1 Let us first consider the approach by Portolan. Using equations (52)-(55) we get

$$\begin{aligned}
R^{1,xx}_{\boldsymbol{k}} &= \frac{V_{xx}}{\sqrt{2}} \left[c_{1\boldsymbol{k}_i} c_{1\boldsymbol{k}_{p_1}} c_{1\boldsymbol{k}_{p_2}} \right] p^{\dagger}_{1\boldsymbol{k}_i} p_{1\boldsymbol{k}_{p_1}} p_{1\boldsymbol{k}_{p_2}} \\
R^{2,xx}_{\boldsymbol{k}} &= \frac{V_{xx}}{\sqrt{2}} \left[c_{1\boldsymbol{k}_i} c_{1\boldsymbol{k}_{p_1}} c_{1\boldsymbol{k}_{p_2}} \right] p^{\dagger}_{1\boldsymbol{k}_i} p_{1\boldsymbol{k}_{p_1}} p_{1\boldsymbol{k}_{p_2}}
\end{aligned}$$

and

$$\begin{aligned}
R^{1,sat}_{\boldsymbol{k}} &= \frac{V}{2\sqrt{2} n_{sat}} \left[c_{1\boldsymbol{k}_i} \left(c_{1\boldsymbol{k}_{p_1}} c_{2\boldsymbol{k}_{p_2}} + c_{1\boldsymbol{k}_{p_2}} c_{2\boldsymbol{k}_{p_1}} \right) \right] \\
R^{1,sat}_{\boldsymbol{k}} &= \frac{V}{2\sqrt{2} n_{sat}} \left[c_{1\boldsymbol{k}_i} \left(c_{1\boldsymbol{k}_{p_1}} c_{2\boldsymbol{k}_{p_2}} + c_{1\boldsymbol{k}_{p_2}} c_{2\boldsymbol{k}_{p_1}} \right) \right].
\end{aligned}$$

Therefore we get

$$g_{\boldsymbol{k}} = V_{xx} c_{1\boldsymbol{k}} c_{1\boldsymbol{k}_i} c_{1\boldsymbol{k}_{p_1}} c_{1\boldsymbol{k}_{p_2}} + \frac{V}{2n_{sat}} c_{1\boldsymbol{k}} c_{1\boldsymbol{k}_i} \left[c_{1\boldsymbol{k}_{p_1}} c_{2\boldsymbol{k}_{p_2}} + c_{1\boldsymbol{k}_{p_2}} c_{2\boldsymbol{k}_{p_1}} \right].$$

Now the approach by Ciuti starts from equation (38) and (39). This yields

$$\overline{V}^{1111}_{\boldsymbol{k}_{p_1}\boldsymbol{k}_{p_2}\boldsymbol{k}} + \overline{V}^{1111}_{\boldsymbol{k}_{p_2}\boldsymbol{k}_{p_1}\boldsymbol{k}} = V_{xx} c_{1\boldsymbol{k}} c_{1\boldsymbol{k}_i} c_{1\boldsymbol{k}_{p_1}} c_{1\boldsymbol{k}_{p_2}}$$

and

$$\underline{V}^{1111}_{\boldsymbol{k}_{p_1}\boldsymbol{k}_{p_2}\boldsymbol{k}} + \underline{V}^{1111}_{\boldsymbol{k}_{p_2}\boldsymbol{k}_{p_1}\boldsymbol{k}} = \frac{V}{n_{sat}} \left[c_{1\boldsymbol{k}_{p_1}} c_{2\boldsymbol{k}_{p_2}} \left(c_{2\boldsymbol{k}_i} c_{1\boldsymbol{k}} + c_{2\boldsymbol{k}_i} c_{1\boldsymbol{k}} \right) + 2 \left(c_{1\boldsymbol{k}_{p_1}} c_{2\boldsymbol{k}_{p_2}} + c_{2\boldsymbol{k}_{p_1}} c_{1\boldsymbol{k}_{p_2}} \right) c_{1\boldsymbol{k}} c_{1\boldsymbol{k}_i} \right].$$

Finally, we get

$$g_{\boldsymbol{k}} = V_{xx} c_{1\boldsymbol{k}} c_{1\boldsymbol{k}_i} c_{1\boldsymbol{k}_{p_1}} c_{1\boldsymbol{k}_{p_2}} + \frac{V}{n_{sat}} \left[c_{1\boldsymbol{k}_{p_1}} c_{2\boldsymbol{k}_{p_2}} \left(c_{1\boldsymbol{k}} c_{2\boldsymbol{k}_i} + c_{2\boldsymbol{k}} c_{1\boldsymbol{k}_i} \right) + \left(c_{1\boldsymbol{k}_{p_1}} c_{2\boldsymbol{k}_{p_2}} + c_{2\boldsymbol{k}_{p_1}} c_{1\boldsymbol{k}_{p_2}} \right) c_{1\boldsymbol{k}} c_{1\boldsymbol{k}_i} \right].$$

Further, the argument presented here can be used (with some obvious modifications) to derive the scattering rate for the Gd2 scheme. This results in the same expression except that c_1 and c_3 as well as c_2 and c_4 have to be interchanged. This, however, is to be expected as the pump is now on the second branch and signal and idler are picked up at the first branch.

Scheme	Model	coefficient of $2V_{xx}$	coefficient of $\frac{V}{n_{sat}}$
Ps1	Portolan	$c_{1\boldsymbol{k}}c_{1\boldsymbol{k}_i}c_{1\boldsymbol{k}_{p_1}}c_{1\boldsymbol{k}_{p_2}}$	$c_{1\boldsymbol{k}}c_{1\boldsymbol{k}_i}\left[c_{1\boldsymbol{k}_{p_1}}c_{2\boldsymbol{k}_{p_2}}+c_{2\boldsymbol{k}_{p_1}}c_{1\boldsymbol{k}_{p_2}}\right]$
	Ciuti	$c_{1\boldsymbol{k}}c_{1\boldsymbol{k}_i}c_{1\boldsymbol{k}_{p_1}}c_{1\boldsymbol{k}_{p_2}}$	$2\left[c_{2\boldsymbol{k}_i}c_{1\boldsymbol{k}}+c_{2\boldsymbol{k}}c_{1\boldsymbol{k}_i}\right]c_{1\boldsymbol{k}_{p_1}}c_{1\boldsymbol{k}_{p_2}}+2c_{1\boldsymbol{k}}c_{1\boldsymbol{k}_i}\left[c_{1\boldsymbol{k}_{p_1}}c_{2\boldsymbol{k}_{p_2}}+c_{2\boldsymbol{k}_{p_1}}c_{1\boldsymbol{k}_{p_2}}\right]$
Pd1	Portolan	$\frac{1}{2}c_{1\boldsymbol{k}}c_{1\boldsymbol{k}_i}c_{1\boldsymbol{k}_{p_1}}c_{1\boldsymbol{k}_{p_2}}$	$\frac{1}{2}c_{1\boldsymbol{k}}c_{1\boldsymbol{k}_i}\left[c_{1\boldsymbol{k}_{p_1}}c_{2\boldsymbol{k}_{p_2}}+c_{1\boldsymbol{k}_{p_2}}c_{2\boldsymbol{k}_{p_1}}\right]$
	Ciuti	$\frac{1}{2}c_{1\boldsymbol{k}}c_{1\boldsymbol{k}_i}c_{1\boldsymbol{k}_{p_1}}c_{1\boldsymbol{k}_{p_2}}$	$c_{1\boldsymbol{k}_{p_1}}c_{2\boldsymbol{k}_{p_2}}\left[c_{1\boldsymbol{k}}c_{2\boldsymbol{k}_i}+c_{2\boldsymbol{k}}c_{1\boldsymbol{k}_i}\right]+\left[c_{1\boldsymbol{k}_{p_1}}c_{2\boldsymbol{k}_{p_2}}+c_{2\boldsymbol{k}_{p_1}}c_{1\boldsymbol{k}_{p_2}}\right]c_{1\boldsymbol{k}}c_{1\boldsymbol{k}_i}$
Gd2r	Portolan	$\frac{1}{2}c_{3\boldsymbol{k}}c_{3\boldsymbol{k}_i}c_{1\boldsymbol{k}_{p1}}c_{1\boldsymbol{k}_{p2}}$	$\frac{1}{2}c_{3\boldsymbol{k}}c_{3\boldsymbol{k}_i}\left[c_{1\boldsymbol{k}_{p1}}c_{1\boldsymbol{k}_{p2}}+c_{1\boldsymbol{k}_{p2}}c_{2\boldsymbol{k}_{p1}}\right]$
	Ciuti	$\frac{1}{2}c_{3\boldsymbol{k}}c_{3\boldsymbol{k}_i}c_{1\boldsymbol{k}_{p_1}}c_{1\boldsymbol{k}_{p_2}}$	$c_{1\boldsymbol{k}_{p_1}}c_{1\boldsymbol{k}_{p_2}}\left[c_{3\boldsymbol{k}}c_{4\boldsymbol{k}_i}+c_{4\boldsymbol{k}}c_{3\boldsymbol{k}_i}\right]+\left[c_{1\boldsymbol{k}_{p_1}}c_{2\boldsymbol{k}_{p_2}}+c_{2\boldsymbol{k}_{p_1}}c_{1\boldsymbol{k}_{p_2}}\right]c_{3\boldsymbol{k}}c_{3\boldsymbol{k}_i}$
Gd2	Portolan	$\frac{1}{2}c_{1\boldsymbol{k}}c_{1\boldsymbol{k}_i}c_{3\boldsymbol{k}_{p1}}c_{3\boldsymbol{k}_{p2}}$	$\frac{1}{2}c_{1\boldsymbol{k}}c_{1\boldsymbol{k}_i}\left[c_{3\boldsymbol{k}_{p1}}c_{4\boldsymbol{k}_{p2}}+c_{3\boldsymbol{k}_{p2}}c_{4\boldsymbol{k}_{p1}}\right]$
	Ciuti	$\frac{1}{2}c_{1\boldsymbol{k}}c_{1\boldsymbol{k}_i}c_{3\boldsymbol{k}_{p_1}}c_{3\boldsymbol{k}_{p_2}}$	$c_{3\boldsymbol{k}_{p_1}}c_{3\boldsymbol{k}_{p_2}}\left[c_{1\boldsymbol{k}}c_{2\boldsymbol{k}_i}+c_{2\boldsymbol{k}}c_{1\boldsymbol{k}_i}\right]+\left[c_{3\boldsymbol{k}_{p_1}}c_{4\boldsymbol{k}_{p_2}}+c_{4\boldsymbol{k}_{p_1}}c_{3\boldsymbol{k}_{p_2}}\right]c_{1\boldsymbol{k}}c_{1\boldsymbol{k}_i}$

Table 1: Coupling coefficient $g_{\boldsymbol{k}}$ for the Gd2r, Gd2, Pd1, and Ps1 scheme with respect to both models.

4 Simulations

To conduct the simulation given in [14, 15] a `Fortran` code has been developed by Portolan. This code is divided into two different programs; the first program computes the pump-induced photoluminescence for phonon-polariton scattering. The output of this program is then used as an input to compute the populations and correlations in the context of parametric scattering.

However, the code is insufficient for our purpose as

- it includes only the single cavity case where the pump as well as the signal and idler are on the lower polariton branch. As indicated below a proper extension of the code is expected to be difficult.
- it is written in a fashion that uses global variables and other side-effects extensively. Even if one shows disregard for the criticism of such practices by the computer science community it becomes a problem as soon as one considers parallelization as a possibility of speeding up the computation. This, in our case, is vital as we want to compare different configurations and as such have to conduct a number of simulations.
- it is written neither with procedural nor with object oriented principles in mind. Thus, many computations are written out explicitly in the code at different places. As a consequence, to change such a computation the code has to be modified at many different places. To further worsen this situation, the state tomography code and the code to compute populations in k-space share almost no common code base (the state tomography code is about 2600 lines whereas the population code is about 1200 lines).

To remedy this situation we have developed a `C++` program that unifies the code that compute both the state tomography as well as the population in k-space. In fact, only about 250 lines are not shared between the two cases. In total about 1300 lines[5] are needed to implement the functionality of the above mentioned `Fortran` code (a reduction factor of about 2.5) and this already includes parallelization conducted with the help of the OpenMP library. The actual code base is a bit larger as there is some additional code to handle double cavity configurations, a continuous wave pump, as well as the conveniences to specify certain parameters directly on the command line.

Finally, let us discuss the performance characteristics of the code. The system under consideration is a dual socket system with two octa-core `Intel Xeon E5-2660` processors each clocked at `2.20GHz`. The state tomography takes about 2 minutes whereas the time integration of the population, depending on the grid size, takes from a couple of minutes to an hour. Relevant comparisons of the two codes are not possible as the NAG library employed in the `Fortran` code is not available on our system. However, the reported time scale is on the order of hours for the state tomography and about 2 days for the time integration of the population (note, however, that this computations have been conducted on hardware significantly older than ours).

In section 4.1 we will document our implementation both from a user perspective (configuration files, command line arguments, ...) and from a developers perspective (classes, cavity configurations, ...). In section 4.2 we will discuss the actual value of some coefficients used in the simulation (such as the exciton radius λ_x or the index of refraction n). This will equip us with the ability of comparing our simulation to the steady state model (as is done in section 4.3). In the subsequent sections we will show results obtained from simulations conducted for a number of cavity configurations of interest.

4.1 Documentation of the computer program

In this section we will explore the computer program used in all simulations. In section 4.1.1 we give a short introduction from a users perspective. In 4.1.2 we will supplement this treatment by a more detailed

[5] All line counts are computed by the command line toll cloc (which neither counts blank lines nor comments).

discussion of the configuration file. In the subsequent section we will turn our attention to a more detailed description of the source code and its organization. Specifically we will detail how extensions (i.e. new cavity configurations or pump schemes) can be added to the program.

4.1.1 Crash course

As every simulation includes a large number of parameters those are collected together in an xml encoded configuration file, with the `.inp` ending, that is placed in the input directory. The parameters given there determine both the cavity design (index of refraction, exciton radius, ...) as well as parameters specific to a mode of computation (detector window for the state tomography, maximal k vector for the population plot, ...). Before we discuss the input parameters in detail let us note that the following directory structure is assumed

```
- input
- output
- src
```

where the executable lives in the src directory (the name of this directory is in fact inconsequential; we can also use bin, for example). The program displays a help screen with the available command line parameters upon entering

```
$ ./parametric --help
```

Of those options we must specify the job name via `--job_name jobname`, which in turn determines the name of the input file, and the mode of the computation via setting on the following flags.

```
--diagnostic  # dispersion relation, Hopfield coefficients, and some other diagnostic values
--tomography  # state tomography
--signalidler # time evolution of the signal and idler only
--population  # a complete 2d population plot
```

All the output files are placed in the output directory and are named `jobname.ending`, where ending is the appropriate ending for the quantity computed as determined by the program. All data (except the state tomography) are formatted such that they can be easily visualized in gnuplot. For the state tomography a python script is included that produces the corresponding plots.

For concreteness' sake let us investigate a simple example. Let us enter

```
$ ./parametric --job_name test --tomography
```

Then the program will look for `../input/test.inp` as the configuration file to be read. Such a file must be provided. In addition, the program will read

```
../input/test.tstep
../input/test.Nkt
../input/test.srt
../input/test.Gin
```

to get the required data on pump-induced photoluminescence if needed for the simulation. These files must be provided and can, for example, be generated by Portolan's photoluminescence code. The output of the program can then be found in `../output/test.tomography` and includes the entries of the density matrix.

4.1.2 Configuration file

The configuration file must be located in `input/jobname.inp`. An example is given in Listing 1.

Listing 1 An example for a valid configuration file.

```
<?xml version="1.0" standalone=no>
<input>
        <cavity gamma='0.26e-3' exciton_bohr='10e-9' n='3.5' coupling='1.0e-3'/>
        <polariton rabi_splitting='5e-3' omega_exciton='1.52168'            detuning='-2.4e
            -3' binding_energy='6.6e-3' four_particle_correlation='0.75' />
        <model polariton="double_cavity" coupling="double_cavity_pump2" pl_enabled="true" />
        <pumps>
                <pump k_x='-1.37e6' k_y='0e6' pulse_width='1e-12' t0='4e-12' num_photons='42
                    ' branch_idx='1' />
                <pump k_x='1.37e6' k_y='0e6' pulse_width='1e-12' t0='4e-12' num_photons='42'
                     branch_idx='1'/>
        </pumps>

        <time   initial='0' final='1e-10' steps='602' />
        <space  kmax_x='2e6' kmax_y='2e6' n_x='120' n_y='120' n_input='100' />
        <signal k_x='0e6' k_y='0e6' branch_idx='2' />
        <detector detector_window='120e-12' />
</input>
```

The file is subdivided into 8 sections, where the first four define the characteristic of the cavity and the pumps whereas the remaining four give information specific to one or more computation modes. In the following we will detail the different options. A discussion about the specific values of some of these parameters can be found in section 4.2.

cavity Parameters related to the cavity and quantum wells. The decay rate (out of the cavity, also denoted by γ_c) `gamma` as well as the exciton Bohr radius `exciton_bohr` (in m) and the refractive index `n` of the quantum well (**not** of the surrounding cavity) have to be specified. If a double or triple cavity design is used `coupling` (in eV) specifies the inter-cavity coupling constant g. For a single cavity this parameter is optional.

polariton All the parameters in this section are mandatory. The Rabi splitting Ω is given by `rabi_splitting` (in eV). As mentioned before all our computations assume a constant dispersion for the exciton; the corresponding value is given in `omega_exciton` (in eV) and δ (the detuning at $\boldsymbol{k} = 0$) is given by `detuning` (in eV). The `four_particle_correlation` is a correction effect calculated in [14]. Finally, the binding energy of the exciton is specified by `binding_energy` (in eV).

model The model section specifies which polariton model is used (the allowed values are given in Table 2). The coupling model specifies the coupling constant $g_{\boldsymbol{k}}$ and is thus determined by a given pump scheme; the list of allowed values is given in Table 3. Finally, photoluminescence can be turned of by specifying `pl_enabled="false"`. If this parameter is omitted photoluminescence is turned on by default.

pumps We have to specify a pump tag for every pump used. In each pump tag we specify the in-plane wavevector (in m^{-1}) the pulse width τ_p and the time of maximum intensity t_0. The intensity is specified by `num_photons` (in units of $I_0 = 21$ photons/pulse). The parameter `branch_idx` gives a one-based index (i.e. 1 is the lowest branch) for the polariton branch the pump is on.

time We specify the initial and final time (in s). Those parameters are used in both the signal and idler as well as the population computations. The parameter `steps` specifies the number of time points in the externally loaded photoluminescence data.

space Used in population computations only. We specify the maximum value of the wavevectors considered (in 1/m) as well as the number of points computed in the simulation. The parameter `n_input` specifies the number of space points in the externally loaded photoluminescence data.

signal This tag is used in signal/idler and tomography calculations only. We have to specify the wavevector as well as the branch index (one-based indexing) of the signal (the idler is computed automatically from the pump data).

detector This tag is used in tomography calculations only. The detector window starts at $t = 0$ (there is no reason to shift the detector window, as we can set the initial time of the simulation arbitrarily) and ends at the value specified in `detector_window` (in s).

Values in the configuration file can be overridden on the command line. For example, by specifying

```
$ ./parametric --job_name test --tomography
          -p pumps/pump[0]/num_photons=120,detector/detector_window='60e-12'
```

we change the intensity of the first pump to $120I_0$ and the detector window to 60 ps. This changes take effect regardless of the values specified in the configuration file. As can be seen from the example, the notation uses traditional document object model path names.

value of `polariton` field	description
`single_cavity`	uses dispersion and Hopfield coefficients for a single cavity
`double_cavity`	uses dispersion and Hopfield coefficients for a double cavity

Table 2: Allowed values for the `polariton` field in the `model` tag.

value of the `coupling` field	description
Ps1_ciuti	Portolan's scheme in a single cavity (Ciuti's model)
Ps1	Portolan's scheme in a single cavity (Portolan's model)
Pd1_ciuti	Portolan's scheme in a double cavity (Ciuti's model)
Pd2	Portolan's scheme in a double cavity (Portolan's model)
Gd2	The Gd2 scheme (Portolan's model)
Gd2r	The Gd2r scheme (Portolan's model)
disabled	Disables parametric scattering effects (i.e. set $g_{\boldsymbol{k}} = 0$)

Table 3: Allowed values for the `coupling` field in the `model` tag.

4.1.3 General design

Our implementation is designed by keeping object oriented principles in mind. In that spirit the program is a collection of classes which can be extended if necessary. The main reason for preferring a class structure over a procedural approach is that often physical quantities are changed rarely but functions that employ them are invoked often. In this case one would significantly increase code complexity if such values have to be passed to every single function call.

The parsing of the command line arguments are performed in `main.cpp` with the help of the boost program options library. Then corresponding to the computation mode selected (either signalidler, population, tomography, or diagnostic) a class derived from `ParametricSolver` is instantiated and executed. The include dependency graph of main.cpp is illustrated in Figure 18; it gives a good overview of the general structure of the program.

As the `ParametricSolver` class is the main starting point for all computations, we will now describe that particular class in some detail. It is responsible for loading all the configuration from the input file as well as providing common functionality that is needed by all derived classes. The `ParametricSolver` class initializes the `Polariton` class (which is used to compute Hopfield coefficients and energy in a given cavity configuration), the `ScatteringRate` class (which is used to load the photoluminescence data and preprocesses it such that a performant usage in our simulations is possible), the `c_functions` class (which computes the

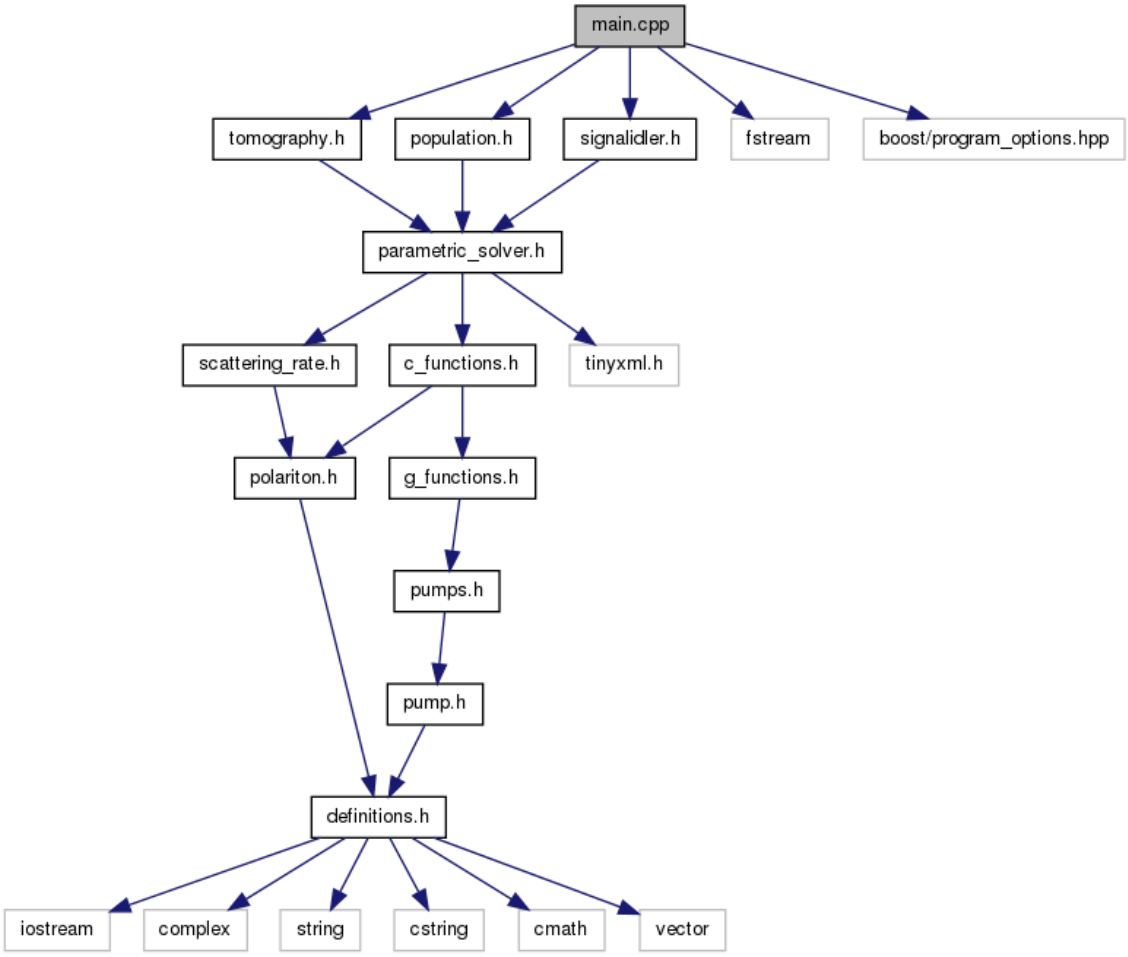

Figure 18: Include dependency graph for `main.cpp`. The arrows point from a header file to all the files that are included by that particular file. Note that this includes only classes that are needed in the definition, i.e. the header file. For example, the class `NumericalIntegration` is not included in this graph since it is only included by source files.

functions described in section 2.5), the appropriate superclass of the `g_function` class (which computes the coupling coefficient $g_{\boldsymbol{k}}$ for a given pump and cavity configuration), and finally the signal and idler member variables that are of the type `state` and combine the branch index with the in-plane wavevector $\boldsymbol{k}$. This is more succinctly illustrated in Figure 19 by a collaboration graph. In addition, the `ParametricSolver` class also provides a number of methods including the ability to compute both populations and correlations for a given state (called `get_population` and `get_correlation` respectively).

The `ParametricSolver` class is not an abstract type, i.e. it can be instantiated on its own. However, this is only done for the `--diagnostic` option. In the other three cases one of the classes `SignalIdlerSolver`, `PopulationSolver`, and `TomographySolver` is instantiated. All those three classes are derived from the `ParametricSolver` class.

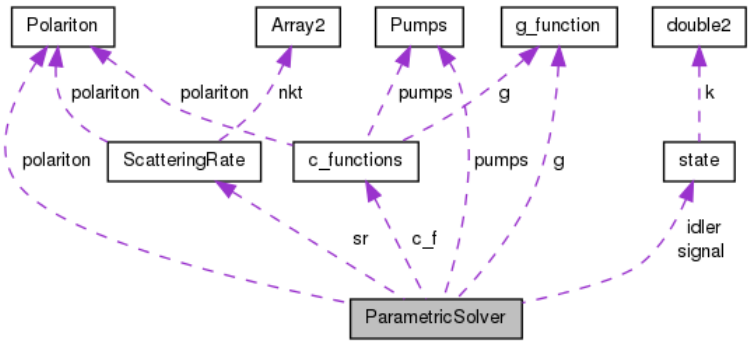

Figure 19: Collaboration graph of the class `ParametricSolver`. The arrows point to classes instantiated by the class at the base of the arrow. The labels indicate the name of the member variables.

4.1.4 How to add a new pump scheme

In the previous sections the general structure of the program has been elucidated; in addition, we have discussed the purpose of some classes and their relationship (including the all-important `ParametricSolver` class). Nevertheless, most of the time we will not change the internals of the `c_functions` or `ScatteringRate` class but extend our simulations to a new pump scheme or cavity configuration. Thus it is the purpose of this section to discuss the addition of another pump scheme (i.e. another coupling coefficient $g_{\boldsymbol{k}}$). Together with the addition of another cavity configuration (discussed in the next section) we are then in a position to extend the simulation to different configurations (for example, to quantum wires).

Let us first take a closer look at the (abstract) `g_functions` class[6]

```
struct g_function {
        virtual double  g(state) = 0;
};
```

As expected only a single function that depends on the wavevector and the state index has to be implemented. How this implementation is conducted is dependent on the model used for the cavity. For example for the Gd2r scheme we have

```
struct g_doublecav_Gd2r : g_function {
        double binding_energy, four_part_corr;
        Polariton* polariton;
        Pumps pumps;
        //
        // constructor
        //
        g_doublecav_Gd2r(double _binding_energy, double _four_part_corr,
            Polariton *_polariton, Pumps _pumps) {
                binding_energy  = _binding_energy;
                four_part_corr  = _four_part_corr;
                polariton       = _polariton;
                pumps           = _pumps;
        }
        //
        // coupling constant g_k
        //
        double  g(state s) {
                double BindingE = binding_energy;
                double FPC      = four_part_corr;
                double  f       = polariton->Rabi();
```

[6] In C++ the differences between a struct and class is that for a struct all member variables/methods are public by default while they are private by default for a class.

```
                state    si      = state(pumps.get_idler(s.k),s.branch_idx);

                // only for two pumps
                state s_p1 = pumps[0].s;
                state s_p2 = pumps[1].s;

                double sum1 = (16./7.) * f * 0.5*sqrt((c1(s_p1)*c2(s_p2)+c2(s_p1)*c1(s_p2)))
                    ;
                double sum2 = (6./M_PI) * BindingE * FPC * 0.5*sqrt((c1(s_p1)*c1(s_p2)));
                return sqrt(c3(s)*c3(si))*(sum1 + sum2);
        }
        //
        // helper functions
        //
        double c1(state s) {
                return polariton->HopfieldX(state(s.k,0));
        }
        double c2(state s) {
                return polariton->HopfieldX(state(s.k,1));
        }
        double c3(state s) {
                return polariton->HopfieldX(state(s.k,2));
        }
        double c4(state s) {
                return polariton->HopfieldX(state(s.k,3));
        }
};
```

where the definition of the `c1,...,c4` functions is purely to make the code more in line with the notation used in section 2. The value of the parameters will be discussed in section 4.2.

However, we are still missing an essential piece of the implementation. The class above defines a constructor that has to be filled with some values read from a configuration file. Not surprisingly that is the job of the `ParametricSolver` class; more precisely if we look at the constructor we discover the following code snippet

```
else if(model_coupling == "Gd2r")
                g = new g_doublecav_Gd2r(binding_energy, four_part_corr, polariton, pumps);
```

which has to be added for any new pump scheme. In fact `Gd2r` is just what we specify in the configuration file. Note that this also implies that different schemes can have different parameters. For example, in the actual implementation we can disable the coupling by specifying `model_coupling="disabled"` in the configuration file. In this case, obviously, no parameters at all have to be specified to the constructor of the `g_function_ps_disabled` class (the `g` function returns 0 for every wavevector and branch index).

4.1.5 How to add a new cavity configuration

We have already discussed in the last section how to adjust the coupling constant $g_{\boldsymbol{k}}$ for a given pump scheme. Now in this section we will go one step further. We will show how to add a new cavity configuration. If we look closely at the equations of motion we discover that (besides coefficients, such as the decay rate out of the cavity, that can be managed from the configuration file) the only quantities that are of interest are the dispersion as well as the Hopfield coefficients. It is thus no surprise that the abstract base class `Polariton` is given by

```
struct Polariton {
        virtual double E(state) = 0;
        virtual double HopfieldX(state) = 0;
        virtual double Rabi() = 0;

        double HopfieldC(state s) {
                return 1.0-HopfieldX(s);
        }
};
```

where the `E` functions defines the energy of a given state (in eV), `HopfieldX` gives the Hopfield coefficients (for example, in a double cavity that would be the functions $c_{1\boldsymbol{k}}, \ldots, c_{4\boldsymbol{k}}$ for branch indices 0 to 3) for a given state and `Rabi` returns the value of the Rabi splitting (in eV). The implementation is then quite straightforward. Let us once again take the example of a double cavity; in this case

```
class PolaritonDoubleCavity : public Polariton {
public:
        PolaritonDoubleCavity(double, double, double, double, double);
        double E(state);        double HopfieldX(state);
        double Rabi();

private:
        double photon, exciton, rabi, v_cavity, g;
        double Cavity(double2);
        double Exciton(double2);
};

PolaritonDoubleCavity::PolaritonDoubleCavity(double p, double e, double r, double v_cavity,
    double g) {
        photon          = p;
        exciton         = e;
        rabi            = r;
        this->v_cavity = v_cavity;
        this->g         = g;
}

double PolaritonDoubleCavity::E(state s) {
        double2 k      = s.k;
        double detun   = Exciton(k) - Cavity(k);
        double ave     = Cavity(k) + Exciton(k);

        if(s.branch_idx == 0)
                return 0.5*(ave - g - sqrt(pow(detun+g,2) + 4.0*pow(rabi,2)));
        else if(s.branch_idx == 1)
                return 0.5*(ave + g - sqrt(pow(detun-g,2) + 4.0*pow(rabi,2)));
        else if(s.branch_idx == 2)
                return 0.5*(ave + g + sqrt(pow(detun+g,2) + 4.0*pow(rabi,2)));
        else if(s.branch_idx == 3)
                return 0.5*(ave - g + sqrt(pow(detun-g,2) + 4.0*pow(rabi,2)));
}

double PolaritonDoubleCavity::HopfieldX(state s) {
        double2 k      = s.k;
        double detun   = Cavity(k) - Exciton(k);

        if(s.branch_idx == 0)
                return 0.5*(1.0 + (detun-g) / sqrt(pow(detun-g,2) + 4.0*pow(rabi,2)));
        else if(s.branch_idx == 1)
                return 0.5*(1.0 - (detun-g) / sqrt(pow(detun-g,2) + 4.0*pow(rabi,2)));
        else if(s.branch_idx == 2)
                return 0.5*(1.0 + (detun+g) / sqrt(pow(detun+g,2) + 4.0*pow(rabi,2)));
        else if(s.branch_idx == 3)
                return 0.5*(1.0 - (detun+g) / sqrt(pow(detun+g,2) + 4.0*pow(rabi,2)));
}

double PolaritonDoubleCavity::Rabi() {
        return rabi;
}

double PolaritonDoubleCavity::Cavity(double2 k) {
        double kk =  hbar*hbar*v_cavity*v_cavity*(k.x*k.x+k.y*k.y);
        return sqrt(photon*photon + kk);
}

double PolaritonDoubleCavity::Exciton(double2 k) {
```

```
        return exciton;
}
```

Note that in this case the constructor has an additional parameter, the cavity-cavity coupling g, as compared to the single cavity case. Once again we have to tweak the `ParametricSolver` class to account for that; more precisely, if we look at the constructor we see the following code snippet

```
else if(model_polariton == "double_cavity") {
                cavity_coupling = query_attribute(doc_handle,"cavity","coupling");
                polariton = new PolaritonDoubleCavity(omega_exciton + detuning,
                    omega_exciton,rabi_splitting,speed_of_light/n_cavity, cavity_coupling);
}
```

where the second line loads the additional parameter (that in the configuration file is located at `input/cavity` and is called `coupling`). In the third line the `PolaritonDoubleCavity` class is instantiated.

Thus, we can implement any configuration that admits an equation of motion as given in section 2.5 by simply extending the `Polariton` and `g_function` classes.

4.2 Value of the coefficients

In this section we will briefly discuss some physically relevant values for the quantities needed to conduct our simulations. Already in section 4.1.4 we plugged in some values without giving any further explanation. To provide this explanation is the purpose of this section. Let us emphasize that the formulas given here, consistent with most of the literature, are formulated in electrostatic cgs units.

First, let us recall from section 2.2.1 the following identity for the exciton-exciton scattering rate

$$V_{xx} = \frac{6e^2}{\pi\epsilon\lambda_x}.$$

An analytical expression for λ_x (the two dimensional exciton radius) is given, for example, in [3]; this formula reads[7]

$$\lambda_x = \frac{\epsilon\hbar^2}{2e^2\mu} = \frac{n^2}{2\mu}\frac{\hbar^2}{e^2 m_e}, \tag{65}$$

where μ represents the reduced mass of the exciton; we will use $\mu \approx 5 \cdot 10^{-2} m_e$ as given in [7] (as before we denote the mass of an electron by m_e). On the right hand side we have made the connection to the Bohr radius of the hydrogen atom. From this, as well as using $n = 3.6$ (which is approximately the index of refraction of GaAs at optical frequencies), and $\epsilon = \epsilon_0 n^2$ (which at optical frequencies is an excellent approximation) we get from equation (65) the exciton Bohr radius $\lambda_x \approx 10$ nm; this is consistent with the value given in [7].

We now have all the ingredients to compute the binding energy for the exciton-exciton interaction. In our simulations we will employ (consistent with the simulations conducted in [15])

$$E_b := \frac{\pi}{6} V_{xx} \approx 6.6 \text{ meV}.$$

Until now we only assumed that the exciton dispersion E_x is constant for wavevectors of interest but we did not specify a value for it. Let us take zero energy as the top of the valence band such that for GaAs

$$E_x \approx 1.52168 \text{ eV}.$$

This number is taken from [8].

[7] In [3] ϵ_0 is used for the permittivity of a given material in place of the more common and less confusing ϵ. We denote the permittivity of free space by ϵ_0 (which in cgs units is equal to 1).

Finally, we have to specify the linewidth of the cavity γ_c or equivalently the transmission rate t_c. These two quantities, for a symmetric cavity, are related by (see [14])

$$t_c = \sqrt{\frac{\gamma_c}{2\pi\hbar}}.$$

In an experimental setting it is more common to describe these parameters by a Q factor defined as

$$Q = \frac{\lambda_c}{\Delta\lambda_c},$$

where λ_c is the cavity resonance. The Q factor is related to the photon lifetime by (see e.g. [6])

$$\tau_c = \frac{2nLQ}{c},$$

where L is the cavity length. This, in turn gives a relation between the Q factor and γ_c

$$\gamma_c = \frac{\hbar c}{2nLQ}.$$

If we plug in $n = 3.6$, a cavity length of $L = 325$ nm, and $Q = 4000$ we get

$$\gamma_c \approx 0.26 \text{ meV}.$$

In terms of photon lifetime this gives $\tau_c \approx 1.3$ ps. The polariton lifetime is determined largely by the photon lifetime and is thus of the same order of magnitude.

4.3 Connection to the steady state model

In the steady state model we defined

$$\Delta = gP_1P_2,$$

where g is the scattering rate and P_1 and P_2 are the square roots of the polariton occupation at the two pumps, respectively. If we assume that both pumps are identical (usually this is a good approximation even if the pumps are not symmetric in $\boldsymbol{k}$ space)

$$\frac{\Delta}{\gamma} = \frac{gP^2}{\gamma} = \frac{4gc^2t_c^2nI_0\pi\lambda_x^2}{\gamma^3\tau_p}.$$

Note that, as before, we are only interested in the dimensionless quantity Δ/γ not in Δ itself. To make an appropriate comparison we have to plug in the values we use in our simulation. As discussed in the previous section we will use $\lambda_x \approx 10$ nm, $t_c \approx 2.5 \cdot 10^5$ s$^{-\frac{1}{2}}$, $\gamma \approx 1.5 \cdot 10^{11}$ s^{-1}, $c \approx \frac{1}{2}$, and $g \approx 2\,\text{meV} \approx 3 \cdot 10^{12}$ s^{-1}. In this case we get

$$\frac{\Delta}{\gamma} \approx 1.5 \cdot 10^{-12}\frac{nI_0}{\tau_p}.$$

If we take $\tau_p = 120$ ps, i.e. our detector window and use $I_0 = 21$, then

$$\frac{\Delta}{\gamma} \approx 3 \cdot 10^{-3}n.$$

Thus, a pump intensity of $n = 100$ corresponds to a $\Delta/\gamma \approx 0.3$. We have illustrated the result from the simulation as well as the steady state model in Figure 20.

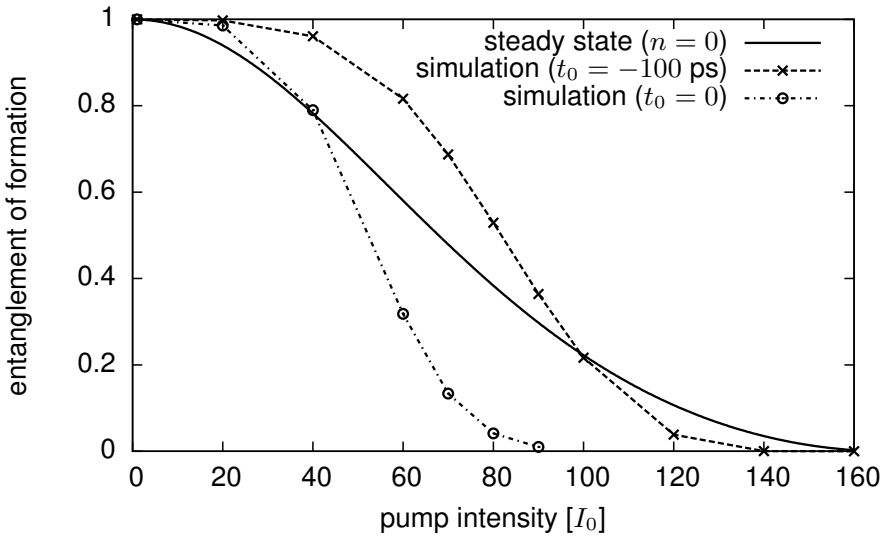

Figure 20: The steady state model is compared with two simulation results. We show both the case where the CW pump is switched on at the beginning of the detector window (i.e. at $t_0 = 0$) and the case where the CW pump is switched on 100 ps prior to the beginning of the detector window (i.e. $t_0 = -100$ ps).

We observe that while the steady state solution gives qualitatively a similar result, it does not agree particularly well with the simulation. Note, however, that even though we have neglected pump-induced photoluminescence in the simulation conducted there are still assumptions of the steady state computation in section 2.6 that are not made in the simulation. For example, it is not assumed that all decay rates are equal. In fact, the decay rates are weighted by the appropriate Hopfield coefficients, denoted by c. Since $c < 1$, it is no surprise that the initial decrease in the entanglement of formation is less pronounced in the simulation than it is in our steady state computation.

4.4 The dependence of the entanglement of formation on the pulse width

In section 2.11.1 we derived a formula that allows us to compute the coherent polariton population introduced by a given Gaussian pump. The formula for the population is given by

$$N_{pump} = c^2 t_c^2 n \sqrt{\frac{\pi}{2}} \tau_p \pi a \lambda_x^2 e^{-\gamma(t-t_0)} e^{\frac{\gamma^2 \tau_p^2}{2}} \left[\operatorname{erf}\left(\frac{t - t_0 - \gamma\tau_p^2}{2\tau_p} \right) - \operatorname{erf}\left(\frac{t_i - t_0 - \gamma\tau_p^2}{2\tau_p} \right) \right]^2, \tag{66}$$

where the parameter of interest in this section is the pulse width τ_p (all other parameters are assumed to be fixed in this section).

The schemes discussed in the literature always assumed a Gaussian pulse, as given above, with τ_p on the order of picoseconds. We have also seen that if no pump-induced photoluminescence has to be considered (as is the case in some double cavity schemes) a continuous wave pump can achieve highly entangled polariton states as well.

Therefore, we can argue that both $\tau_p \to 0$ as well as $\tau_p \to \infty$, for a fixed intensity, are possibilities to create photon pairs with sufficiently high entanglement. We have also learned that as we increase n (the pump intensity) the entanglement decreases quite rapidly above some threshold.

However, as can be inferred from the simulations we conducted it is not the pump intensity that is responsible for decoherence effects beyond what would be expected from noise alone; the correlation is even more pronounced if we consider the peak polariton population (as given in equation (66)) induced by the pump.

The peak polariton population induced by the pump $N_{pump,peak}$ is plotted as a function of τ_p in Figure (21).

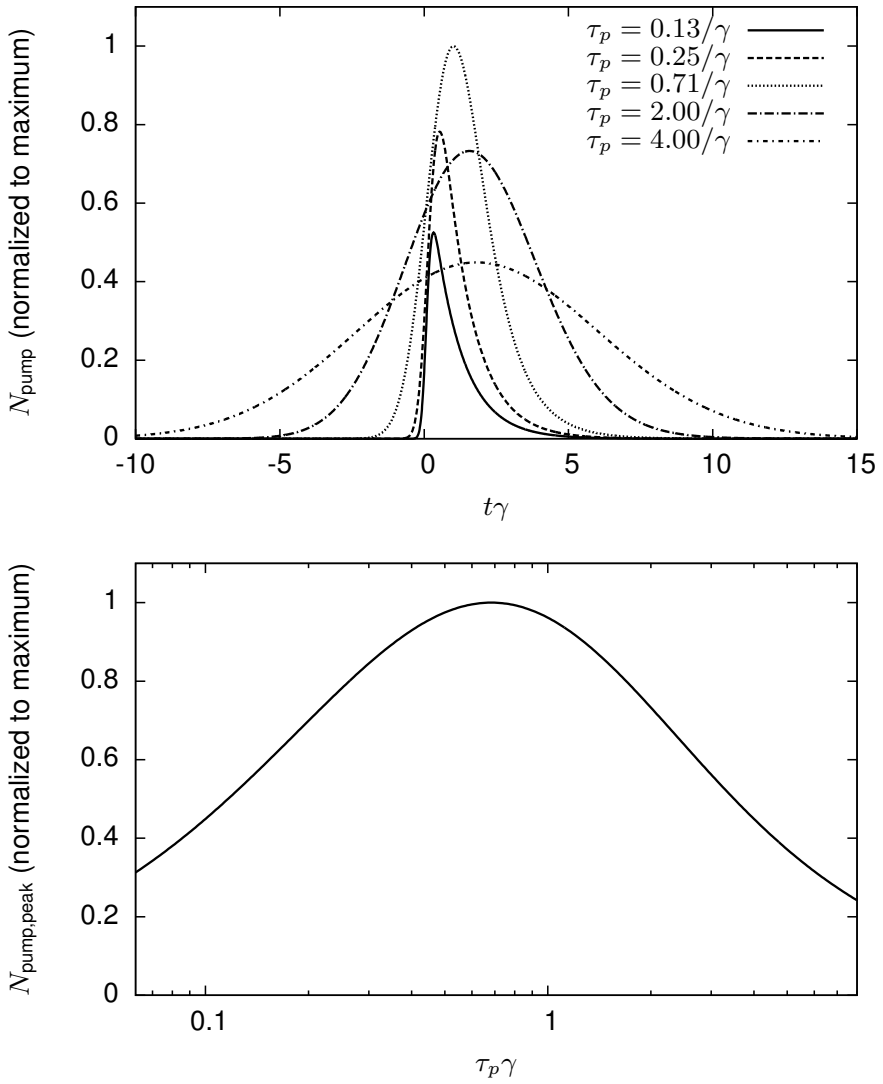

Figure 21: A plot of the pump induced polariton population as a function of time for five values of τ_p (top) and $N_{pump,peak}$ as a function of τ_p on a logarithmic scale (bottom) is shown. Both plots are normalized to the maximum intensity.

As this plot shows $N_{pump,peak}$ has a unique maximum at $\tau_p \approx 0.7/\gamma$. In the sense described above this is the worst pulse width we could possibly choose (as the instantaneous polariton population is maximized). Portolan's scheme has been simulated with $\tau_p = 1$ ps (see e.g. [15]) which corresponds to $\tau_p\gamma \approx 0.4$ (below the maximum). The steady case is, obviously, far below the maximum as well.

The same behavior can be observed by conducting a simulation of the achievable entanglement of formation as a function of the pulse width. The results are shown in Figure (22).

Thus, the behavior we discussed above manifests itself in a minimum for the entanglement of formation at approximately $\tau_p = 10$ ps (which is comparable in magnitude to the decay width, as expected). Therefore, it is advisable to either pump as fast as possible (in schemes were photoluminescence is a concern) or to employ

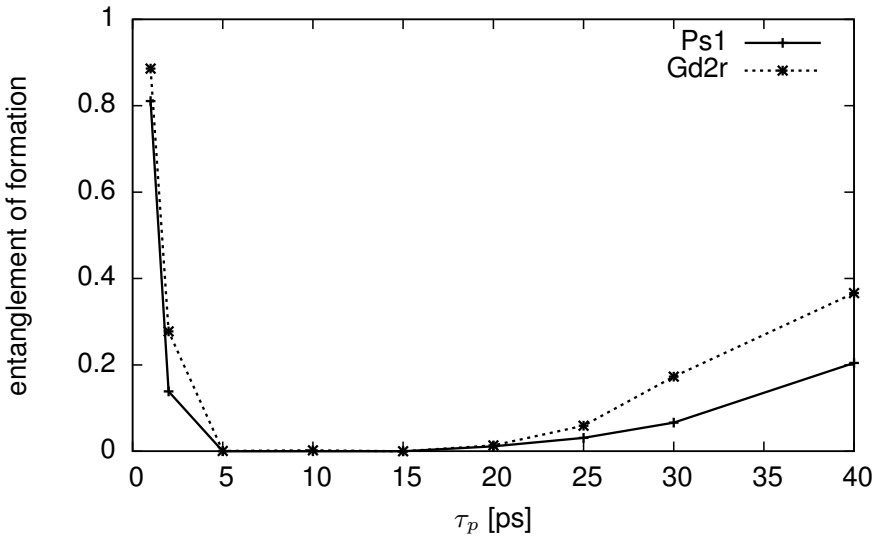

Figure 22: Entanglement of formation for a fixed pump intensity of $120I_0$ is shown as a function of the pulse width τ_p. Data for both the Gd2r and Ps1 schemes are shown. No photoluminescence effects are included in this simulation.

to the steady state case (which is only possible if a branch protected from pump induced photoluminescence is employed).

4.5 The Ps1 and Pd1 schemes

The Ps1 scheme (suggested by Portolan et. al. in [15]) has already been discussed in the literature as well as in the previous sections. The main purpose of this section is thus to compare it to the Pd1 scheme. Both schemes are designed in such a way that Rayleigh scattering is kept away from the signal/idler. This, in fact, is the major advantage of this configuration. If we plot the time integrated population in $\mathbf{k}$ space, it can be readily seen that signal and idler can be chosen in such a way that they are kept away from the circle formed by Rayleigh scattering from the second pump (see Figure 23). Note that all our simulations are performed with a pump induced photoluminescence computed at a temperature of 5 Kelvin.

From that figure we also observe that parametric scattering is lower in intensity in the Pd1 scheme, as compared to the Ps1 scheme. This behavior, however, is entirely expected if we look at Table 1 and observe that the scattering amplitude $g_{\mathbf{k}}$ is smaller by a factor of $\frac{1}{2}$ in the double cavity case. In principle we might expect that this allows us to pump twice as hard in the double cavity case and get the same entanglement of formation as in the single cavity case. However, for higher pump powers the pump-induced photoluminescence also increases. The simulation in Figure 24 show that this effect diminishes the increase in the entanglement of formation we might expect.

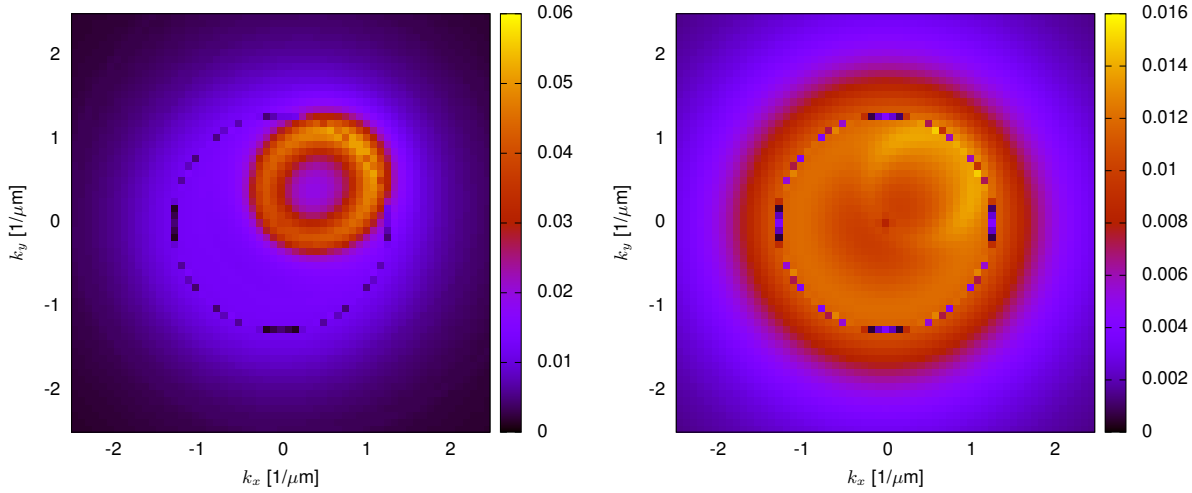

Figure 23: Time integrated population in **k** space for the Ps1 (left) and Pd1 (right) scheme. A Rabi splitting of $\Omega = 3$ meV and a detuning of 0.5 meV is used. In the double cavity case we use $g = 1$ meV. The pump intensity is set at $42\, I_0$ photons per pulse. The black dotted circle formed by elastic scattering is visible as this resonance is not computed properly by the photoluminescence code.

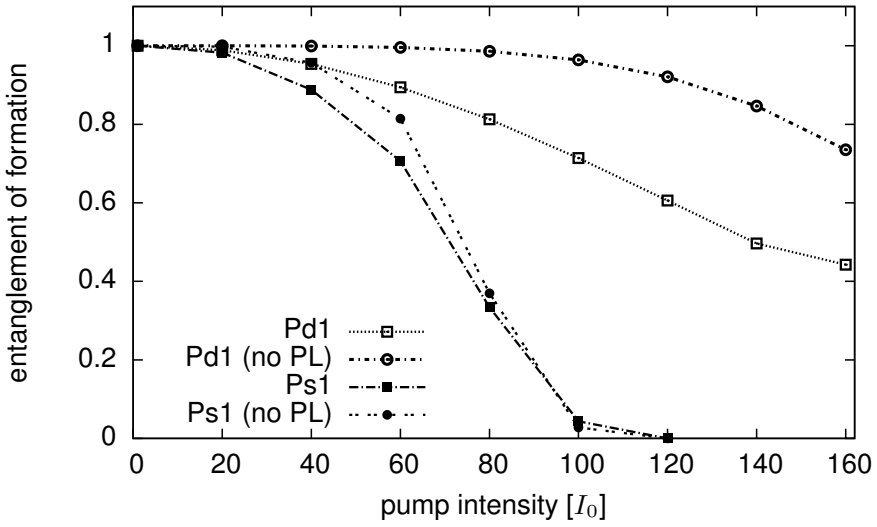

Figure 24: Entanglement of formation as a function of the pump intensity (in units of $I_0 = 21$ photons per pulse) for Rabi splitting $\Omega = 2$ meV and detuning $\delta = -2.4$ meV ($g = 1$ meV in the double cavity case).

Further, it is apparent in Figure 24 that both the Ps1 and Pd1 schemes are limited to a large extent by pump-induced photoluminescence. Before we discuss the Gd2r scheme, which offers protection from decoherence due to pump-induced photoluminescence, let us for a moment study the dependence of the photoluminescence on both detuning and Rabi splitting for a fixed pump intensity. As can be seen from Figure 25 there is only

a small difference in the achieved entanglement of formation. The simulation also shows that a small Rabi splitting and a moderate negative detuning gives the optimal entanglement of formation. However, as the difference is relatively small there is no need to have a sample where either δ or Ω are fine tuned.

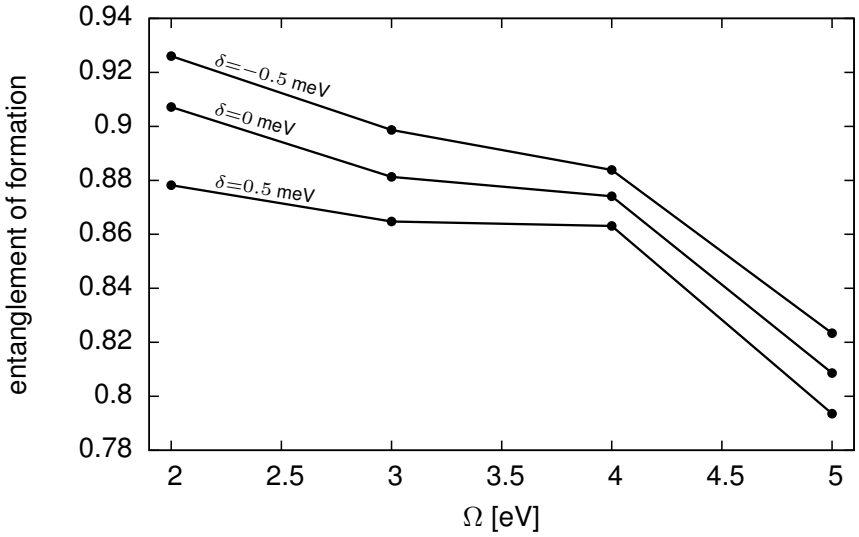

Figure 25: The entanglement of formation for the Ps1 scheme as a function of Rabi splitting Ω and detuning δ. A pump intensity of $n = 42I_0$ is used.

4.6 The Gd2r scheme

Let us now investigate a number of the properties of the Gd2r scheme numerically. As is spelled out in section 3.2.1, the second lowest polariton branch and thus the signal and idler are protected, to some extend, from the pump-induced photoluminescence that is created on the first branch.

For a first analysis we will focus on a negative detuning ($\delta = -2.4$ meV) and two Rabi splittings given by $\Omega = 3$ meV and $\Omega = 5$ meV respectively. We pump at $(1.37 \cdot 10^6, 0)$ m^{-1} and $(-1.37 \cdot 10^6)$ m^{-1}, i.e. just at the point where scattering to the ground state of the 2nd polariton branch is possible. Note that this value is only slightly different for different detunings and Rabi splittings and can be easily determined in the simulation by using the `--diagnostic` option and a simple `awk` script. The two pumps are (except for the wavevector $\boldsymbol{k}$) completely identical and are described by a Gaussian intensity profile. In addition, the pulse width (standard deviation) of the pump is taken to be 1 ps.

The corresponding time evolution for the signal and idler occupation is shown in Figure 26.

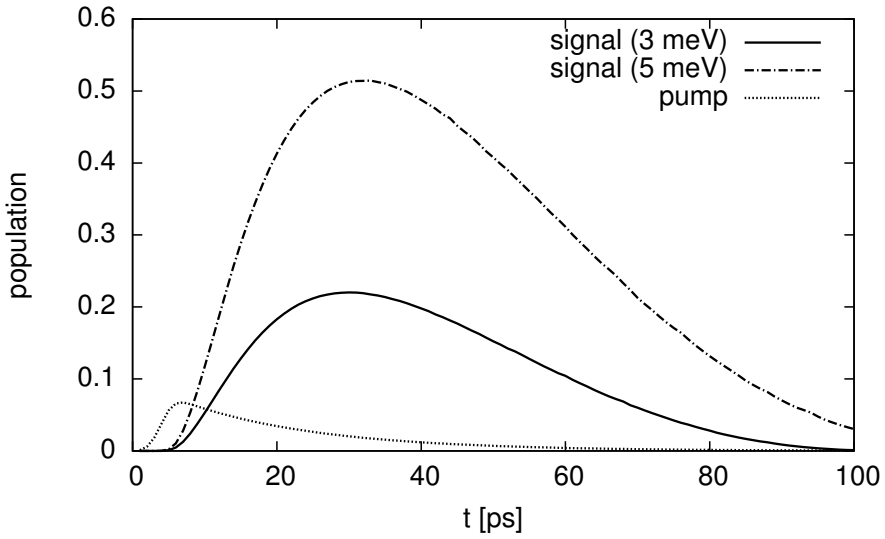

Figure 26: The polariton population at the signal wavevector is shown (both for $\Omega = 3$ meV and $\Omega = 5$ meV). It is unnecessary to show the idler as the scheme is completely symmetric. In both simulations $\delta = -2.4$ meV and $\gamma_c = 0.26$ meV is used. As a reference the shape of the pump-induced polariton population is shown as well. Note that no comparisons in value is possible, however, as the pump-induced population has been scaled in this plot.

Now let us look at the population in $\boldsymbol{k}$ space; this is illustrated for the lowest polariton branch in Figure 27. As expected the parametric scattering is concentrated on a ring of equal energy and takes over the pump-induced photoluminescence. In addition one can nicely observe the bottleneck effect that tends to keep polaritons from relaxing completely to the ground state. It is observed that a larger Rabi splitting reduces the effectiveness of this effect. However, we will see below that this is only true for negative detunings.

Now the discussion of the lower polariton branch is interesting on its own. Nevertheless, in the present scheme we are more interested in the second polariton branch (where signal and idler are located). As this branch is protected from pump-induced photoluminescence we only expect a broadening effect. This is indeed the outcome of our simulation as is shown in Figure 28.

However, as can be easily deduced from equations (28) to (31) the splitting of the two lowest polariton branches (at $\boldsymbol{k} = 0$) is of the order of the cavity coupling g. If a realistic value is substituted, for example $g \approx 1$ meV, we have to experimentally filter photons that differ in wavelength on the order of 0.1 nm. Thus, the question whether it is possible to minimize the pump-induced photoluminescence at $\boldsymbol{k} = 0$ by modifying either the Rabi splitting or the cavity detuning naturally arises.

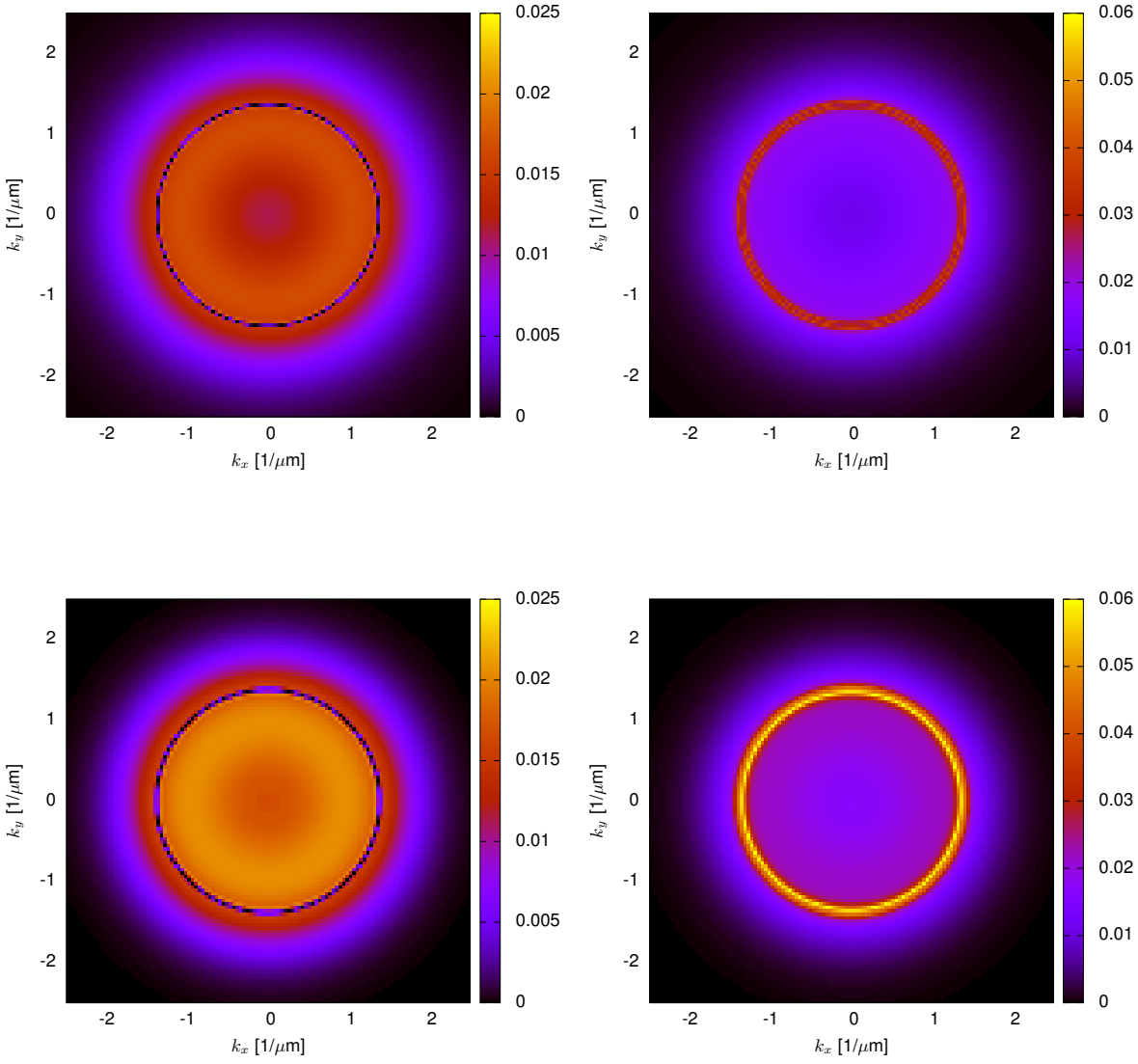

Figure 27: The population in $\boldsymbol{k}$ space of the first polariton branch for photoluminescence (left) and parametric scattering and photoluminescence (right) is shown. On the top $\Omega = 3$ meV and on the bottom $\Omega = 5$ meV is used. In both simulations a detuning of $\delta = -2.4$ meV is employed.

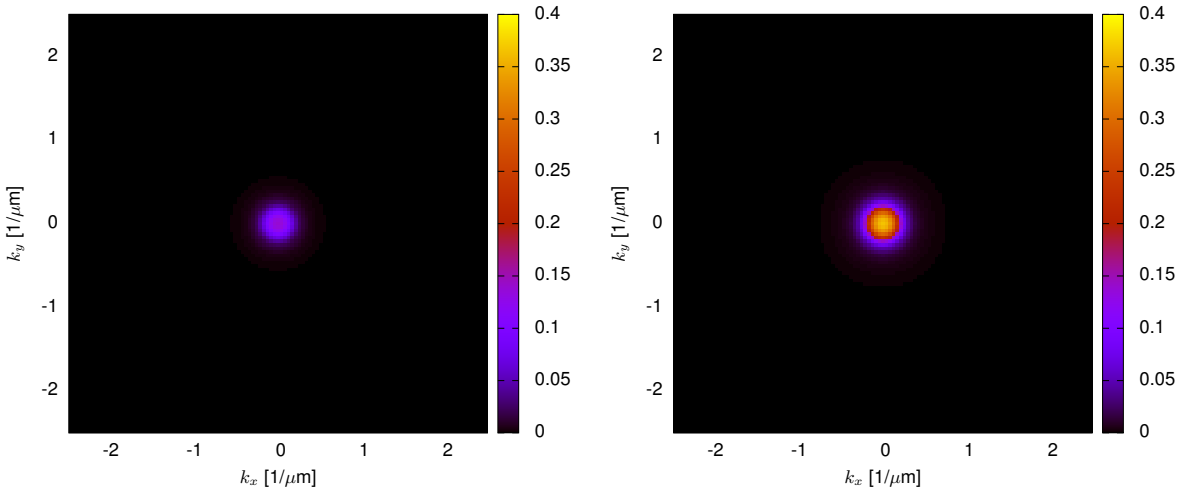

Figure 28: The population in $\boldsymbol{k}$ space of the second polariton branch is shown (for $\Omega = 3$ meV on the left and $\Omega = 5$ meV on the right).

In Figure 29 the photoluminescence at $\boldsymbol{k} = 0$ is shown as a function of the Rabi splitting for five different detunings. This is essentially an investigation of the bottleneck effect, which is well studied in the context of Bose–Einstein condensates (see e.g. [1]).

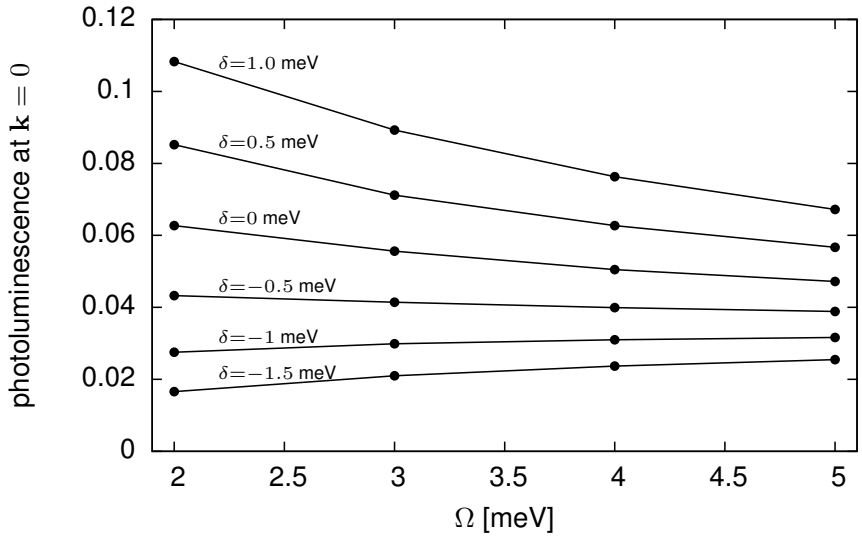

Figure 29: Plot of the time integrated photoluminescence at $\boldsymbol{k} = 0$ (y-axis) for different detunings δ as a function of the Rabi splitting Ω (x-axis) for the Gd2r scheme.

As is apparent from the plots the behavior is not influenced by detuning in a significant way. On the other hand it might be best (if possible) to use cavities with a relatively small Rabi splitting in order to minimize residual effects of the pump-induced photoluminescence.

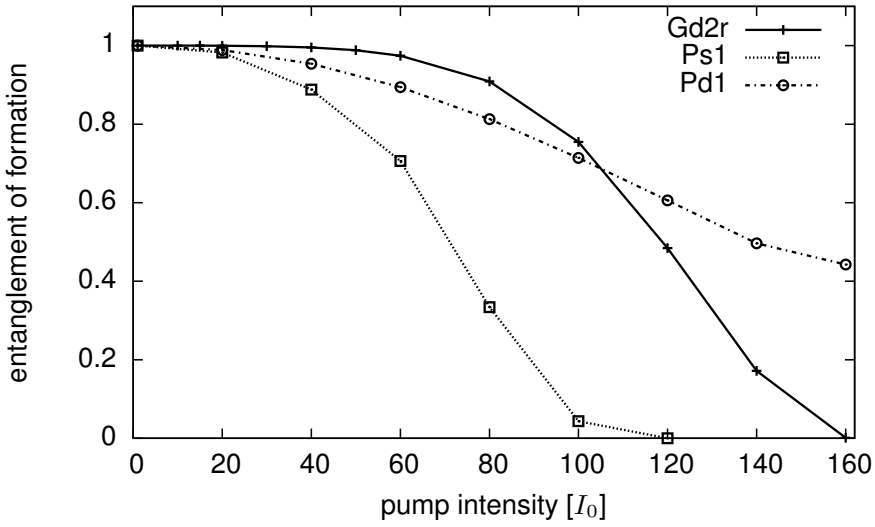

Figure 30: Entanglement of formation for the Gd2r pump scheme is plotted as a function of the pump intensity. The values for the Ps1 and Pd1 schemes are shown as a reference.

Our main goal is entanglement generation and to that end we will (as in section (6)) use the entanglement of formation as the metric of merit. First, we investigate the dependence of the entanglement of formation on the pump intensity. The results are shown in Figure 30.

Especially in the region of moderate pump intensities (that are promising for entanglement generation) the Gd2r scheme is superior to both the Ps1 as well as the Pd1 scheme. Although above this region the entanglement of formation is diminished rapidly (which is not as severe in case of the Pd1 scheme). This behavior is due to the fact that since signal and idler are located at the same wavevector, the effective population for stimulated polariton scattering is increased.

Second, let us investigate the dependence of the entanglement of formation on both Rabi splitting and detuning as we did in the single cavity case. The results are shown in Figure 31.

As in the case of the single cavity the detuning (and to some extent the Rabi splitting) has only a negligible effect on the achievable entanglement of formation.

To conclude the discussion of the Gd2r scheme, in Figure 33 the state tomography for two different values of θ (which share the same entanglement, as discussed before) is shown.

4.7 The Gd2 scheme

In the previous section we have discussed the Gd2r scheme at length. We have concluded that it is advantageous compared to the Ps1 as well the Pd2 scheme. Furthermore, we have given a handwaving argument to support the fact that the difference between the Gd2r scheme and the Pd1 scheme is not as large as one might expect purely from considerations involving pump-induced photoluminescence; namely that since signal and idler are located at the same wavevector, the polariton population is twice as large there which results in an increased scattering to that state. Therefore, as the population grows the entanglement is diminished more rapidly.

The Gd2 scheme, on the other hand, does not suffer from the problem described above. However, in this scheme signal and idler have to be picked up at two different wavevectors (as was illustrated in Figure 15). As expected this results in states with high entanglement of formation even for higher pump intensities. The result of the numerical simulations is given in Figure 32.

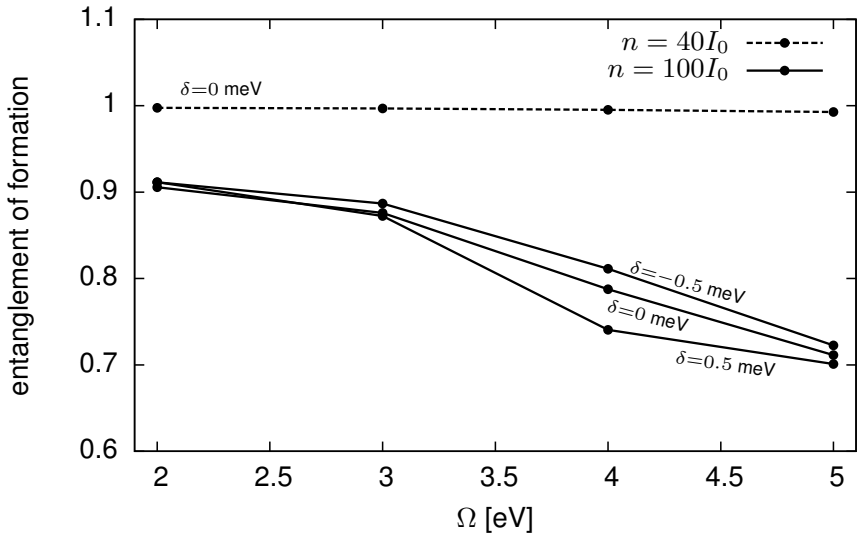

Figure 31: Entanglement of formation for different detunings δ as a function of the Rabi splitting Ω for the Gd2r scheme. The pump intensities employed are shown in the legend. For $n = 42I_0$ there is no discernible difference between different detunings; therefore, we have only shown the line corresponding to zero detuning.

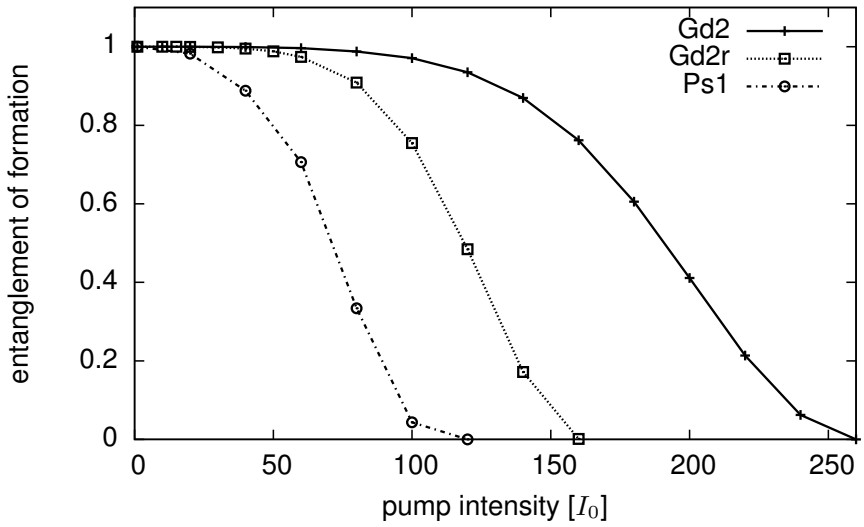

Figure 32: Entanglement of formation for the Gd2 scheme as a function of the pump intensity n. As a comparison the Gd2r and Ps1 scheme is shown.

However, the gain from an experimental point of view remains questionable as for the pump intensities we usually employ are on the order of $n = 40I_0$. In this region both the Gd2 and the Gd2r scheme are very close to the maximally achievable entanglement of formation.

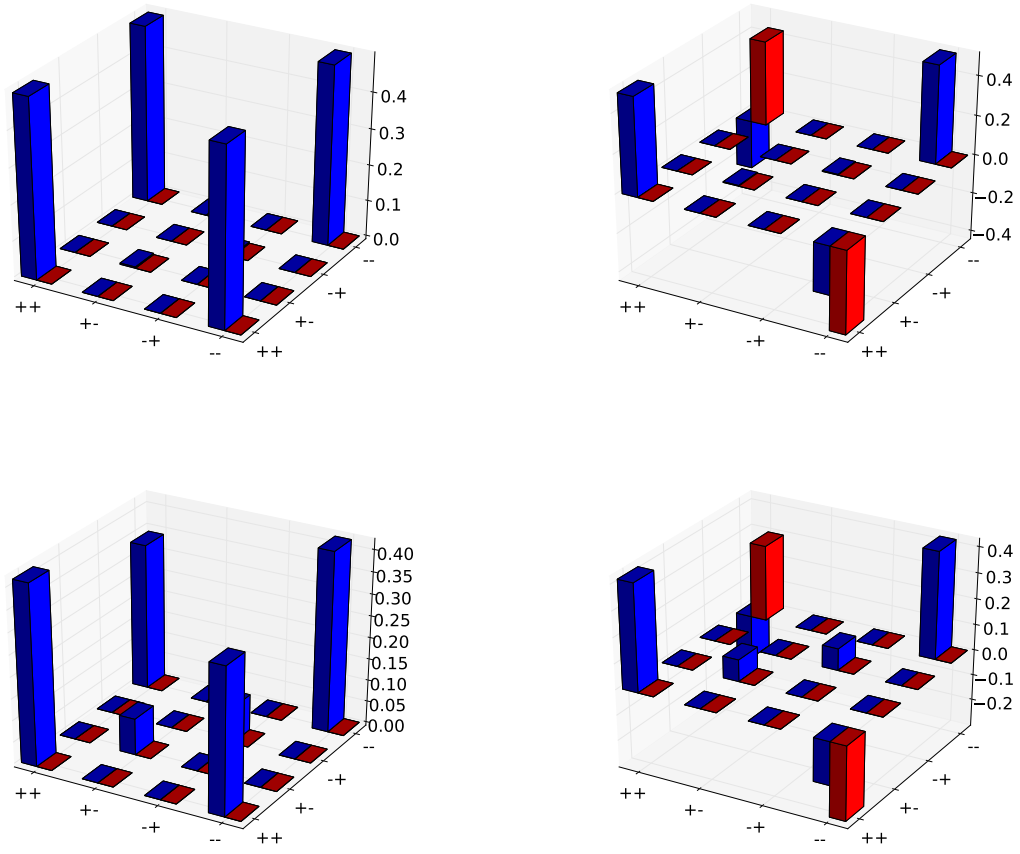

Figure 33: State tomography of a highly entangled state ($E(\rho) \approx 0.97$ computed with $n = 80I_0$) for $\theta = 0$ (left) and $\theta = \frac{\pi}{6}$ (bottom) is shown on the top. On the bottom we show a state with $E(\rho) \approx 0.36$ (computed with $n = 160I_0$). The real part is colored red while the imaginary part is colored blue.

5 Experiment

To conduct the experiment a GaAs double cavity is available. The cavity resonance is at approximately 768.8 nm and $\lambda/4$ mirrors have been used to implement the DBR. The sample was grown by Gottfried Strasser's group at the Vienna University of Technology.

First, let us use a white light source to excite the sample. Then, the reflection is measured for different wavelengths and angles of emission. This is done by adjusting a micrometer screw and collecting the light, that corresponds to a narrow angle, in an optical fiber (to elucidate the measurement setup a drawing is provided in Figure 34). The result is shown in Figure 35.

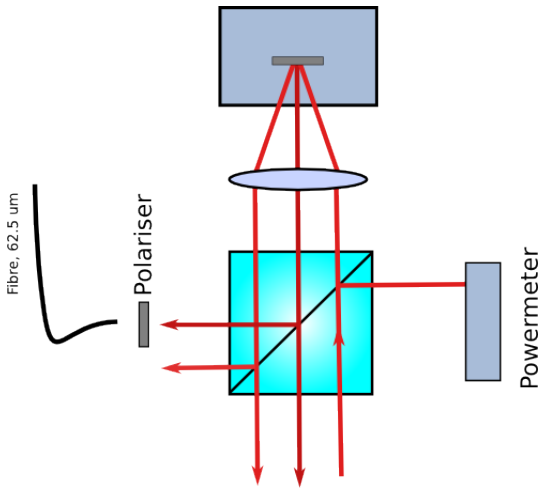

Figure 34: A single excitation beam and two beams exiting the cavity are shown. Due to the lens, angles are mapped to a position offset; we collect light in a fiber corresponding to such a specific offset in position.

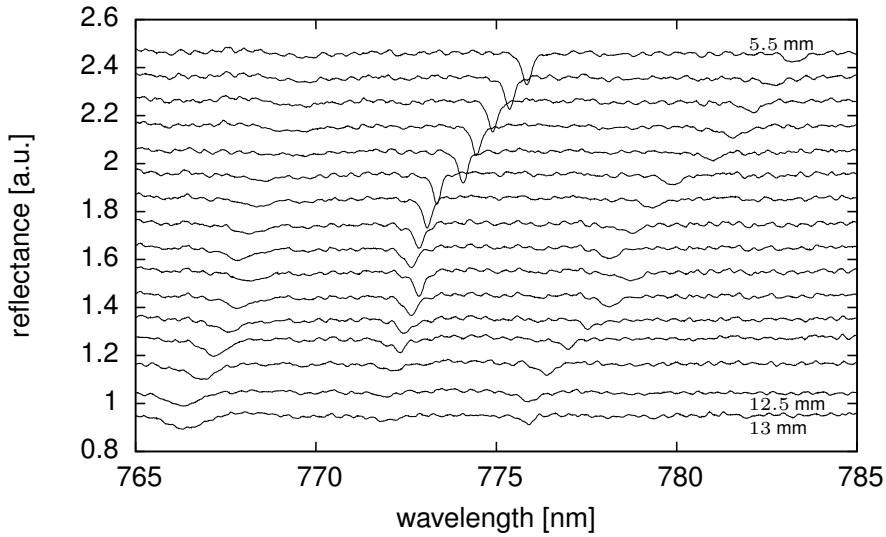

Figure 35: The reflectance is shown as a function of the wavelength and the position of the fiber (in 0.5mm steps as indicated in the figure) that collects the light for analysis.

We can clearly see three dips, corresponding to three polariton branches, in the spectrum. However, the fourth branch is not visible. If we excite the sample resonantly by using the Tekhnoscan laser (the angle is controlled with a piezo mirror) essentially the same behavior can be observed. In this instance we can map the dispersion relation of the polaritons by tuning the laser to the appropriate frequency and angle. The result is shown in Figure 36.

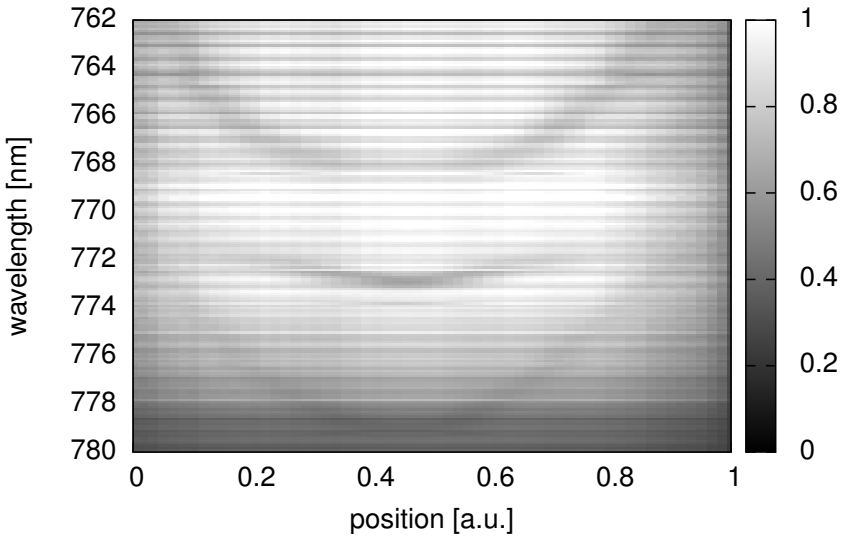

Figure 36: The intensity (normalized to 1) is shown as a function of the wavelength and the position of the piezo mirror.

The intensity observed is quite weak; especially the polariton branch lowest in energy is hardly distinguishable from background noise. The spacing in energy between the visible levels is on the order of a meV, as expected. As of now no parametric scattering has been observed in this sample.

6 Conclusion

From a theoretical point of view double and triple cavities certainly present interesting properties that go beyond the single cavity and the quantum wire case. This is mainly due to the selection rules discussed in section 2.

However, currently no experimental realization of such a scheme is available. In our case, only the spectrum of three polariton branches has been observed in an actual experiment. Therefore, it remains to be seen if cavities of sufficient quality can be constructed to enable entanglement generation as described in section 3.

In the triple cavity case one could also propose scattering schemes where the signal and idler are different in energy from the two pumps; such a scheme would have the obvious advantage that Rayleigh scattering would be of no concern. However, to produce a triple cavity of sufficient quality is believed to be significantly more challenging compared to a double or single cavity (due to the growth time).

References

[1] R.B. Balili. *Bose-Einstein condensation of microcavity polaritons*. PhD thesis, 2009.

[2] C Ciuti. Branch-entangled polariton pairs in planar microcavities and photonic wires. *Physical Review B*, 69(24):245304, 2004.

[3] C. Ciuti, V. Savona, C. Piermarocchi, A. Quattropani, and P. Schwendimann. Role of the exchange of carriers in elastic exciton-exciton scattering in quantum wells. *Physical Review B*, 58(12):7926–7933, 1998.

[4] C. Ciuti, P. Schwendimann, B. Deveaud, and A. Quattropani. Theory of the angle-resonant polariton amplifier. *Physical Review B*, 62(8):4825–4828, 2000.

[5] C. Ciuti, P. Schwendimann, and A. Quattropani. Theory of polariton parametric interactions in semiconductor microcavities. *Semiconductor science and technology*, 18(10):279, 2003.

[6] P. Cristofolini. Towards Entangled Photon Pairs in a Planar Microcavity, 2010.

[7] Y. Deng, H. and Haug, H. and Yamamoto. Exciton-polariton Bose-Einstein condensation. *Reviews of Modern Physics*, 82(2):1489, 2010.

[8] W. Langbein. Spontaneous parametric scattering of microcavity polaritons in momentum space. *Physical Review B*, 70(20):205301, November 2004.

[9] Wolfgang Langbein and Jørn M Hvam. Elastic Scattering Dynamics of Cavity Polaritons: Evidence for Time-Energy Uncertainty and Polariton Localization. *Physical Review Letters*, 88:47401, 2002.

[10] M.C. Nasr, M.B. and Saleh, B.E.A. and Sergienko, A.V. and Teich. Demonstration of Dispersion-Canceled Quantum-Optical Coherence Tomography. *Physical Review Letters*, 91(8):083601, August 2003.

[11] S. Portolan. Methods and explicit calculations, 2012.

[12] S. Portolan, O. Di Stefano, S. Savasta, F. Rossi, and R. Girlanda. Polariton entanglement in the self-stimulated regime. *physica status solidi (c)*, 3(7):2432–2435, 2006.

[13] S. Portolan, O. Di Stefano, S. Savasta, F. Rossi, and R. Girlanda. Dynamics-controlled truncation scheme for quantum optics and nonlinear dynamics in semiconductor microcavities. *Physical Review B*, 77(19):195305, 2008.

[14] S. Portolan, O. Di Stefano, S. Savasta, F. Rossi, and R. Girlanda. Nonequilibrium Langevin approach to quantum optics in semiconductor microcavities. *Physical Review B*, 77(3):035433, 2008.

[15] S. Portolan, O. Di Stefano, S. Savasta, and V. Savona. Emergence of entanglement out of a noisy environment : The case of microcavity polaritons. *EPL (Europhysics Letters)*, 88(2):20003, 2009.

[16] S. Portolan, O. Di Stefano, S. Savasta, and V. Savona. Emergent entanglement of microcavity polariton pairs. *Journal of Physics: Conference Series*, 210(1):012033, 2010.

[17] S. Portolan and S. Savasta. *Optical Generation and Control of Quantum Coherence in Semiconductor Nanostructures*. Springer, 1st edition, 2010.

[18] S. Savasta, O. Di Stefano, V. Savona, and W. Langbein. Quantum complementarity of microcavity polaritons. *Physical Review Letters*, 94(24):246401, 2005.

[19] F. Tassone and Y. Yamamoto. Exciton-exciton scattering dynamics in a semiconductor microcavity and stimulated scattering into polaritons. *Physical Review B*, 59(16):10830–10842, April 1999.

[20] W.K. Wootters. Entanglement of Formation of an Arbitrary State of Two Qubits. *Physical Review Letters*, 80(10):2245–2248, March 1998.

A A closed formula for the entanglement of formation

The entanglement of formation $E(\rho)$ of a density matrix ρ is given by (see for example [20])

$$E(\rho) = h\left(\frac{1+\sqrt{1-C(\rho)^2}}{2}\right)$$

with

$$h(x) = -x\log_2 x - (1-x)\log_2(1-x)$$

and

$$C(\rho) = \max\left(0, \lambda_1 - \sum_{i\geq 2}\lambda_i\right),$$

where $\lambda_1 > \lambda_2 > \cdots > \lambda_n$ are the eigenvalues of

$$\sqrt{\sqrt{\rho}\,(\sigma_y \otimes \sigma_y)\,\rho^*\,(\sigma_y \otimes \sigma_y)\,\sqrt{\rho}}$$

or equivalently the square roots of the eigenvalues of

$$\rho\,[(\sigma_y \otimes \sigma_y)\,\rho^*\,(\sigma_y \otimes \sigma_y)]\,.$$

Note that the complex conjugate of ρ is taken in the standard basis. In our implementation a Mathematica script is used to compute the entanglement of formation from a given density matrix (see Listing 2).

Listing 2 The Mathematica script reads a filename, where the density matrix is stored, from the command line and prints the entanglement of formation stdout.

```
#!/usr/local/bin/MathematicaScript -script

readdm[file_] := Partition[#[[3]] + I #[[4]] &
                                  /@ Partition[ReadList[file, Number], 4], 4]
EOF[\[Rho]_] := Module[{\[Rho]d, EV, C\[Rho], h},
  \[Rho]d =     KroneckerProduct[PauliMatrix[2], PauliMatrix[2]].Conjugate[\[Rho]].
      KroneckerProduct[PauliMatrix[2], PauliMatrix[2]];
  EV      = Sort[Sqrt@Eigenvalues[\[Rho].\[Rho]d], Greater];
  C\[Rho] = Max[0, First@EV - Plus @@ Drop[EV, 1]];
  h[x_]   =     If[x == 0, 0, -x Log[2, x]] - If[1 - x == 0, 0, (1 - x) Log[2, 1 - x]];
  h[(1 + Sqrt[1 - C\[Rho]^2])/2]
]

\[Rho] = readdm[$ScriptCommandLine[[2]]];
Print@EOF[\[Rho]]
```